Claudia Brauer

Modelling
rainfall-runoff processes
in lowland catchments

Modelling

rainfall-runoff processes

in lowland catchments

Claudia Brauer

Contents

1 | Introduction

A round the world, lowland areas are often densely populated and centers of economic activity and transportation. The lack of topography, however, makes them vulnerable to flooding, climate change, and deterioration of water quality. Hydrological models can be used by water managers as a tool for early warning, risk assessment and infrastructure design. However, the models that are commonly used in lowland areas are often high-dimensional (groundwater or hydraulic) models. Low-dimensional models have typically been designed for use in mountainous catchments. The title of this thesis reflects the two-part research question: (1) what are the dominant catchment processes determining a lowland river's response to rainfall and (2) how can these processes be represented in simple hydrological models? For both of these questions, I focussed on topics which are important for lowland areas: (1) the relation between catchment storage and discharge, (2) the coupling between shallow groundwater and unsaturated zone, (3) activation of flowroutes at different stages of wetness and (4) the feedback between groundwater and surface water.

1.1 Context and motivation

1.1.1 Lowlands around the world

Lowlands can be found all over the world, in different climates, geological settings and even altitudes. A universally accepted definition of lowlands does not exist, because people from different parts of the world have different views of this type of landscape. People from mountainous areas may call the lower river reaches at several hundreds of meters altitude lowlands (e.g. Kao et al., 2012, who classify areas below 1000 m as lowland in Taiwan). The Dutch, on the other hand, call the part of their country above sea level the "High Netherlands" (Witte et al., 2012). In this thesis, **lowlands are defined as areas in which hydrological processes are influenced by shallow groundwater**. This means that according to this definition, lowlands can also occur well above sea level and that low-lying arid areas are not considered in this thesis.

Shallow (phreatic) groundwater tables occur all over the world (often in river deltas): 16 % of world's land surface has groundwater tables shallower than 2 m, and 22 % shallower than 4 m (Fig. 1.1; data from Fan et al., 2013). Many of these areas have been reclaimed from sea or marshes by drainage and control of groundwater levels (and sometimes surface water levels). Reclaimed land can be found in coastal areas and river floodplains across different climate zones, from coastal wetlands in Indonesia and the Nile delta in Egypt to the Great Lakes in North-America (see Wandee, 2013, for an overview). This indicates that being able to understand and model lowland-specific hydrologic processes is beneficial for scientists and practitioners around the world.

Lowland catchments can be divided into freely draining ones and controlled ones, The latter are often called polders (Wandee, 2013). **Freely draining** lowland catchments have slightly sloping land surfaces and gravitational forces cause water to flow downhill naturally. **Polders** are flat and because their land surfaces are below their surroundings, water has to be removed by pumping. In reality, the distinction between the two types is less clear. In many freely draining areas, groundwater and surface water levels are controlled through the installation of drainpipes, ditches and weirs. In polder areas, water follows local (micro)topographical gradients to the surface water network.

1.1.2 Challenges in lowland areas

Lowlands areas, especially those in river deltas, are often densely populated and centers of agricultural production, economic activity and transportation. Therefore, socio-economic consequences of natural hazards are especially large in these areas (Day et al., 2007). In addition, the lack of topography increases their vulnerability to different threats:

1. *Floods* are a major hazard in lowland areas. Lowlands are often located in river deltas and are threatened simultaneously by high sea levels (coastal floods), high river discharges (fluvial floods) and large precipitation events (pluvial floods) (e.g. Zhang et al., 2008; Hidayat, 2013). Lowlands are not only more prone to flooding, but flood damage is also large due to the high density of population, infrastructure and economic activity (Jonkman et al., 2008). Flood risk, loosely defined as the product of probability and damage (e.g. Merz et al., 2004), is therefore extra large.

2. *Climate change* has a double effect on lowland catchments (Vellinga et al., 2009; Kwadijk et al., 2010). Firstly, temperature rise causes sea level rise, reducing drainage gradients in coastal lowlands (Bormann et al., 2012). Some areas will not be able to discharge water naturally anymore and surface water will have to be pumped out, or the land will be reclaimed by the
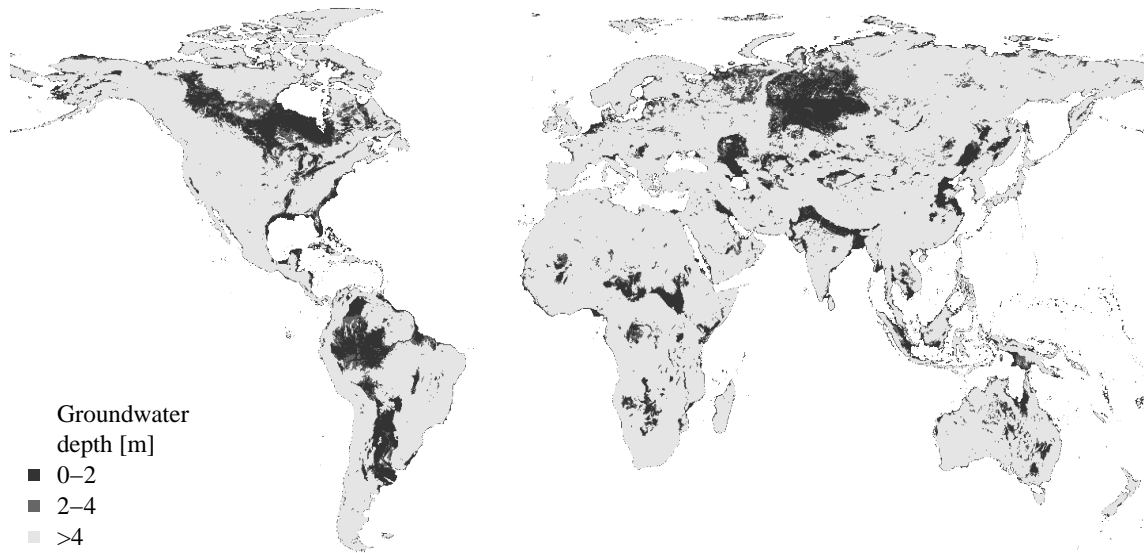
Figure 1.1: Lowland areas around the world: locations with shallow groundwater (based on data from Fan et al., 2013).

sea (Nicholls et al., 1999). In addition, upward (brackish) seepage will increase, leading to a decrease in agricultural production and food security (Oude Essink, 2001; Wassmann et al., 2004; Witte et al., 2012). More fresh water will have to be supplied upstream to flush the surface water network and reduce salt concentrations. Secondly, heavy precipitation events have become more frequent and intense in the past century in Europe and North America. This trend will very likely continue in the current century (Field et al., 2012; IPCC, 2013), leading to increased (flash) flood risk. The simultaneous occurrence of high river discharges and high sea levels poses an increased threat as rivers are unable to discharge to the sea (Kew et al., 2011).

3. *Land use change* is common in densely populated lowland areas (Bouwer et al., 2010). Rural areas are transformed into urban areas with more paved surfaces and less water storage capacity. In wetlands, a large fraction of the area is covered by surface water, which attenuates heavy precipitation events (Thompson et al., 2009). When wetlands are drained, peak discharges will increase (Azous and Horner, 2010). To increase food production, agricultural fields around the world are controlled more intensely to optimize groundwater levels and reduce crop yield loss caused by waterlogging and drought. This results in fields with more drain-pipes, channels, weirs, surface water supply installations and pumps (Elfert and Bormann,

2010).

4. *Water quality* deterioration is common in lowland areas because intensive agriculture causes a large influx of nutrients into the surface water (Lam et al., 2012; Neal et al., 2012). In addition, algal blooms may occur due to low flow velocities caused by the small topographic gradients. Legislation, such as the European Water Framework Directive, has been implemented to improve the ecological and chemical status of water systems (Howden et al., 2009). Numerous research projects have been carried out over the past decades to understand nutrient dynamics and the relation between nitrate and phosphate concentrations and flowpaths in intensively drained and managed lowland areas (e.g. Van den Eertwegh, 2002; Rozemeijer et al., 2010a; Van der Velde, 2011; Delsman et al., 2013).

5. *Land subsidence* is more common and more problematic in coastal lowland areas (Ericson et al., 2006). Peat is formed in waterlogged depressions in the landscape, but when old peat soils are drained for agricultural use, peat can oxidize and soils subside (Wösten et al., 1997). The threat of subsidence forces water managers to control groundwater levels to minimize oxidation (Gambolati et al., 2003). Low freely draining catchments may sink below the drainage base (the sea), and pumping may be required to remove excess water.

6. *Information demand* increases in the 21st cen-

tury (Montanari et al., 2013). Because lowland areas are densely populated, many water managers, governmental agencies, (re-)insurance companies and the general public benefit from accurate predictions of floods and droughts (Borga et al., 2011; Demeritt et al., 2013). In many countries, water managers have a legal obligation to investigate the hydrological effect of change in management, land use and climate in depth to reduce uncertainty about the future. The general public is increasingly aware of their surroundings, is more used to having access to data and predictions and is less willing to accept damage caused by natural hazards (Messner and Meyer, 2006).

To mitigate natural and human disasters, hydrological models can be used by water managers as a tool for risk assessment and infrastructure design.

1.2 Hydrological models

Many types of hydrological models exist, with different degrees of complexity. The appropriate degree of complexity depends on the objectives of the model study and the catchment the model is applied to (Wagener et al., 2001). **Black box** models are typically the least complex model type. They have hardly any physical background: relations between variables (often rainfall and discharge) are determined empirically, without predefining a model structure based on process understanding. Examples of black box models are the unit hydrograph (Clark, 1945) and artificial neural networks (Bishop, 1995; Reed and Marks, 1998). The most complex model type is usually described with the term **physically-based**, although this name is controversial because other model types are also based on physics (see e.g. Beven and Young, 2013). These models contain detailed, spatially distributed descriptions of measurable catchment properties (e.g. soil type, elevation, vegetation, channel dimensions). They are typically based on (partial) differential equations (e.g. Richards' equation for the unsaturated zone or the St. Venant equation for open water). Examples of this model type are SHE (Abbott et al., 1986) and MIKE-SHE (Refsgaard and Storm, 1995).

Between detailed, spatially distributed models and black box models lies the class of **parametric** rainfall-runoff models. This type of model simplifies hydrological systems into a collection of reservoirs and flowroutes, capturing the essence of the relevant hydrological processes, while restricting the number of parameters (Wagener and Wheater, 2004). Parametric models are spatially lumped: variables and parameters are effective catchment values (not necessarily the catchment average).

Widely used examples of parametric rainfall-runoff models are the Tank Model (Sugawara et al., 1974), PDM (Moore, 1985), HBV (Bergström and Forsman, 1973), the Sacramento Model (Burnash, 1995), ARNO (Todini, 1996), SWAT (Arnold et al., 1998) and GR4J (Edijatno et al., 1999; Perrin et al., 2003). However, these models have all been developed for mountainous catchments and errors may arise when applied to lowland catchments, because processes (e.g. capillary rise) are not accounted for and conditions (e.g. no influence of surface water on groundwater) are not met. Examples of the resulting problems are presented by Bormann and Elfert (2010), who used WaSiM-ETH (Schulla and Jasper, 2007) and Koch et al. (2013), who used SWAT, both in north-eastern Germany.

Water managers in lowland areas often use complex hydrological models. MIKE-SHE (Refsgaard and Storm, 1995), HEC-RAS (Brunner, 1995) and SOBEK (Deltares, 2013) have detailed schematisations of surface water networks to simulate the complex flow routing in intensively drained areas. HYDRUS (Simůnek et al., 2008) and SWAP (Van Dam et al., 2008) have detailed vertical schematisations to simulate unsaturated-saturated zone coupling. Regional groundwater models, such as MODFLOW (McDonald and Harbaugh, 1984), account for seepage and lateral groundwater flow. Combinations of several of these models can be used to account for groundwater-surface water feedbacks, such as SHE (Abbott et al., 1986), HydroGeoSphere (Therrien et al., 2006) SIMGRO (Querner, 1988; Van Walsum and Veldhuizen, 2011) or NHI (Prinsen and Becker, 2011). However, complex models have important disadvantages and simple models important advantages:

1. *Overparameterisation* – Model parameters account for differences in response times or recession shapes between catchments with the same dominant processes (represented by the model structure). With too many parameters, an inappropriate model structure can be compensated for by mathematically fitting the model to the calibration data (Kirchner, 2006). An overparameterised model may perform well during calibration, but unsatisfactorily during validation (Perrin et al., 2001) and in different (future) climate regimes (e.g. Seibert, 1999a).

2. *Parameter identification* – The risk of parameter dependence and equifinality (where different combinations of parameter values to lead to similar results, Beven and Binley, 1992; Uhlenbrook et al., 1999) increases with the number of parameters. With one objective function, typically only 3 to 5 parameters can be identified (Jakeman and Hornberger, 1993; Beven, 1989). Multi-objective calibration allows more param-

Figure 1.2: Discharge mechanisms at different scales in the Cabauw polder. Top row: animal burrow, soil cracks, gully, drainpipe. Bottom row: local ponding, field-scale ponding, surface water network.

eters to be calibrated (e.g. Gupta et al., 1998; Efstratiadis and Koutsoyiannis, 2010), but for many catchments only discharge data are available (Soulsby et al., 2008). It is therefore beneficial when the effect of each parameter on the discharge time series can be identified.

3. *Physical representation* – A simple, parametric model structure enables users to quickly grasp the process covered by each model element and the influence of each parameter. Values of effective model parameters cannot be determined with point measurements (Wagener, 2003; Vrugt et al., 2005), but model parameters do have physical connotations and can be explained qualitatively from catchment characteristics and field experience (Seibert and McDonnell, 2002). The effect of small-scale heterogeneity on catchment-scale processes is included implicitly in the model parameters (Beven, 1995; Kirchner, 2006; McDonnell et al., 2007).

4. *Practical applicability* – Computational efficiency facilitates operational forecasting and data assimilation (Liu et al., 2012; Rakovec et al., 2012). Ensembles can be generated for different forcing data or parameter sets to indicate predictive uncertainty (Krzysztofowicz, 2001). In addition, more complex and time-consuming algorithms can be used for calibra-

tion (e.g. DREAM by Vrugt et al., 2008) or parameter uncertainty estimation (e.g. GLUE by Beven and Binley, 1992). Avoiding the need to specify channel cross-sections and soil layers for each catchment can also be advantageous.

1.3 Characteristics of lowland catchments

In this section we discuss some characteristics which affect hydrological processes in lowland catchments and how they are represented in some widely used rainfall-runoff models.

1.3.1 Groundwater-unsaturated zone coupling

Whereas in most models percolation is assumed to be driven by downward gravitational forces only, the vertical profile of moisture content in lowland soils is influenced by capillary forces associated with the presence of a shallow groundwater table. Percolation is slower and evapotranspiration remains high in dry periods, because storage deficits are replenished by capillary rise (e.g. Hopmans and van Immerzeel, 1988; Stenitzer et al., 2007). Therefore, the vadose zone and the groundwater zone form a tightly coupled system and feedbacks should be in-

cluded in models for lowland catchments (Chen and Hu, 2004). In addition, when groundwater rises to the soil surface, the unsaturated zone shrinks and its storage capacity decreases. It is therefore important to include a dynamic unsaturated zone in the model, which is influenced by the surface fluxes precipitation and evapotranspiration as well as by the (dynamic) groundwater table below.

Many conceptual rainfall-runoff models, e.g. HBV, the Sacramento model and the Wageningen Model, contain separate reservoirs for soil moisture and groundwater, allowing only downward movement of groundwater without considering feedbacks. One version of PDM does reduce recharge when the soil ceases to be freely draining (Moore, 2007). Catchments can also be simplified to a single nonlinear reservoir, without discriminating between the saturated and unsaturated zone (Kirchner, 2009), which will be shown to yield limited success in the lowland Hupsel Brook catchment (Chapter 4). Quasi-steady state approaches have also been developed for implementation in distributed models e.g. by Koster et al. (2000), Bogaart et al. (2008) and Van Walsum and Groenendijk (2008).

1.3.2 Shallow groundwater and plant water stress

Vegetation in lowland catchments is hardly affected by water stress, which is one of the drivers for agricultural production. Water is not only made available through physical processes (capillary rise), but also through physiological ones: when plants have exhausted the readily available moisture in the top soil, deeper roots are used (Zencich et al., 2002), and vertical roots grow deeper (Canadell et al., 1996; Weir and Barraclough, 1986; Teuling et al., 2006) and more quickly (Zeng et al., 2013). Because plants adapt to spatial variability in moisture content, water uptake and its vertical distribution depend primarily on the availability of moisture in the whole root zone (Jarvis, 1989). As roots in lowlands often extend to close to the groundwater table, plants can adapt fully to dry periods and evapotranspiration reduction hardly occurs (Schenk and Jackson, 2002). This dynamic system of different plant species with varying stages of root development and spatially and temporally varying groundwater depths is complex, but not all complexity may be necessary to include in a model for runoff simulations (Van der Ploeg et al., 2012).

In some rainfall-runoff models for areas with deep water tables, a separate root zone is included, e.g. in SWAT and TOPMODEL, which exhibits a different behaviour than the unsaturated zone below. We assume that in lowlands, this distinction cannot be made because the whole unsaturated zone can be
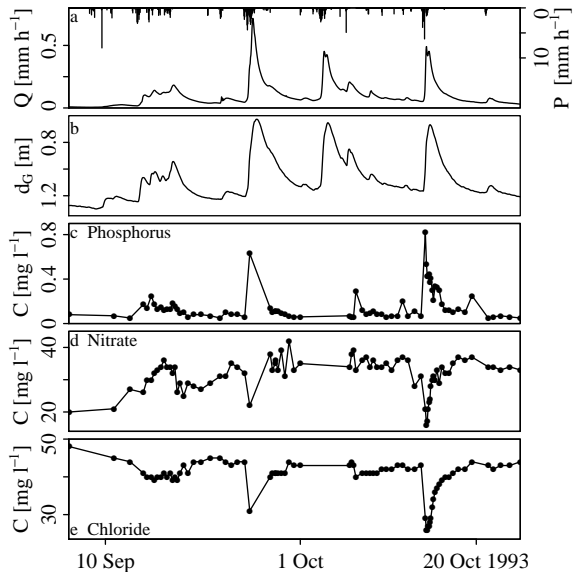
Figure 1.3: Activation of different flow paths revealed by water quality data measured at the outlet of the Hupsel Brook catchment. **(a)** Precipitation and discharge. **(b)** Groundwater depth at the meteorological station. **(c)** Phosphorus concentration (indicator for overland flow, Rozemeijer et al., 2010b), **(d)** Nitrate concentration (indicator for drainpipe flow, Van der Velde et al., 2010b). **(e)** Chloride concentration (indicator for groundwater flow, Van der Velde et al., 2010a).

used by plant roots. The variation of plant species within a catchment is sometimes represented by running a model for different vegetation types separately and multiplying the resulting discharge output with the fraction of that vegetation type (Van Dam et al., 2008).

1.3.3 Wetness-dependent flowroutes

When the soil wetness increases, different flowpaths are activated: from groundwater flow (Hall, 1968), to natural macropores (Mosley, 1979; Beven and Germann, 1982; McDonnell, 2003; Beven and Germann, 2013) and drainpipes (Tiemeyer et al., 2007; Rozemeijer et al., 2010a; Van der Velde et al., 2010b) and eventually to surface runoff (Dunne and Black, 1970; Brauer et al., 2011; Appels et al., 2011). Figure 1.2 provides examples of discharge mechanisms in lowland catchments at different scales.

Stream water chemistry is increasingly being used to detect hydrological flow paths (e.g. Soulsby et al., 2004; Tetzlaff et al., 2007; Delsman et al., 2013). Records of phosphorus, nitrate and chloride concentrations measured at the outlet of the Dutch Hupsel Brook catchment confirm the activation of different flow routes at different stages of catchment
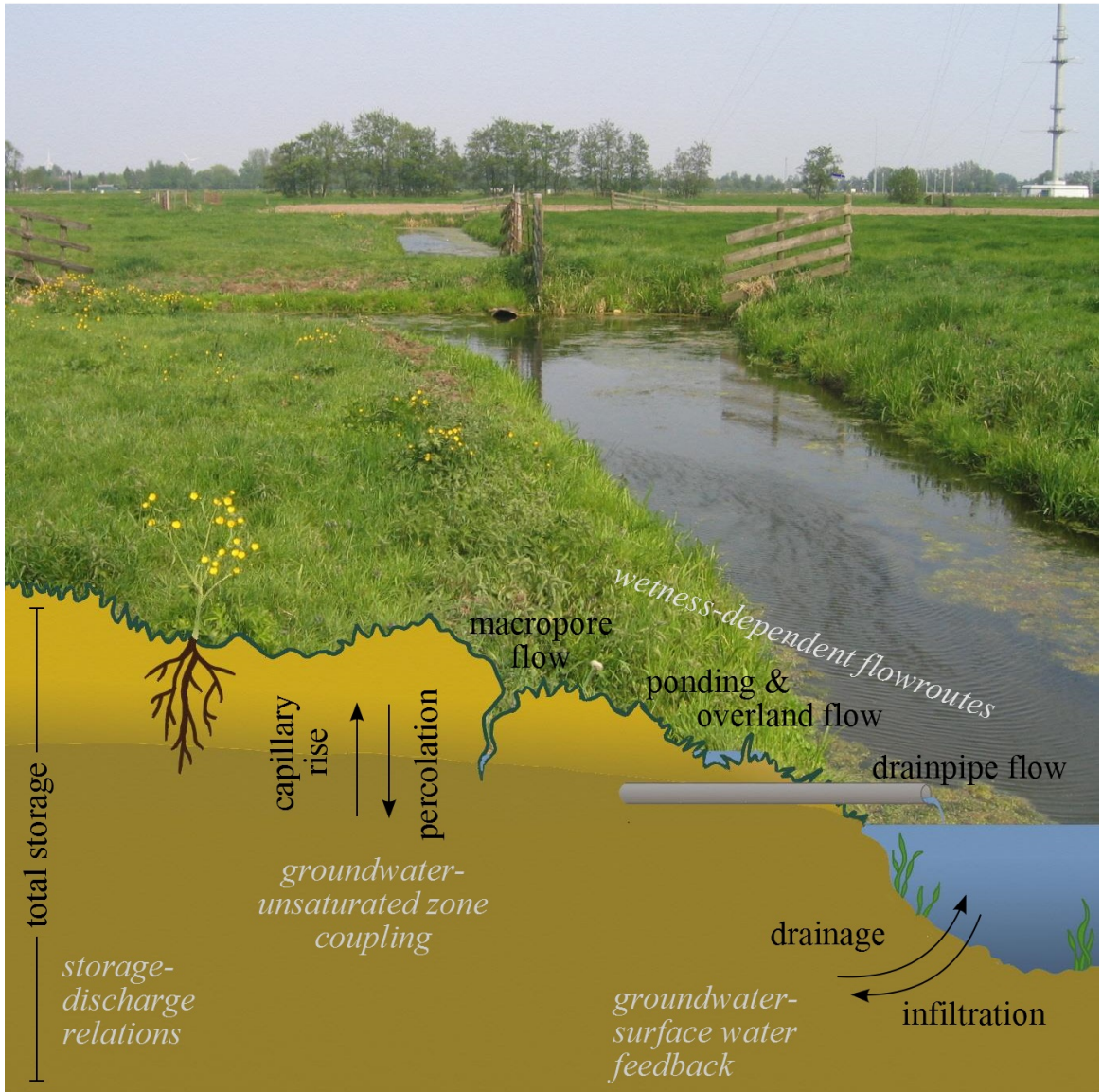
Figure 1.4: Schematic representation of the topics of this thesis: (1) storage-discharge relations, (2) groundwater-unsaturated zone coupling, (3) wetness-dependent flowroutes and (4) groundwater-surface water feedback. The large photo was taken in the Cabauw polder.

wetness (Fig. 1.3). The activation of drainpipes in September is indicated by increasing nitrate concentrations and overland flow during peaks by decreasing chloride and nitrate concentrations and increasing phosphorus concentrations.

The contribution of preferential flow and macropore flow can be considerable and needs to be accounted for in the model structure (Beven and Germann, 1982; Weiler and McDonnell, 2004; Hansen et al., 2013). Drainpipes can be viewed as man-made macropores (Herrmann and Duncker, 2008) and account for a large fraction (up to 80 %) of drainage in

lowlands (Van der Velde et al., 2011; Turunen et al., 2013). When local storage thresholds are exceeded and quick flowpaths are activated, a sudden increase in local discharge occurs (the fill and spill hypothesis by Tromp-van Meerveld and McDonnell, 2006), but at the catchment scale, sudden changes in discharge are hardly ever observed, because spatial variability in groundwater depth, drainpipe depth and microtopography cause these thresholds to be reached at different moments at different locations (Appels, 2013).

Parametric models often divide water between

fast and slow routes. In the GR4J model (Perrin et al., 2003) this division is fixed, the PDM model (Moore, 1985) uses a wetness-dependent probability distribution to express the spatial variability in quick-flow contribution, and in the Wageningen Model (Stricker and Warmerdam, 1982) the division depends on groundwater storage.

1.3.4 Groundwater-surface water feedbacks

Surface water is an important feature in lowland landscapes (Fig. 1.2). The aim of man-made drainage networks in controlled catchments is to optimize groundwater depths by adjusting surface water levels (Krause et al., 2007). During discharge peaks, backwater feedbacks can occur and high surface water levels reduce groundwater drainage or may even cause infiltration (Brauer et al., 2011).

Most parametric rainfall-runoff models do not simulate surface water levels, and therefore parametric models for vertical flow in the unsaturated zone are often coupled to a distributed groundwater model for studies on groundwater-surface water interactions (Krause and Bronstert, 2007; Sophocleous and Perkins, 2000; Lasserre et al., 1999; Van der Velde et al., 2009).

1.3.5 Seepage and surface water supply

Regional groundwater flow is common in lowland areas and upward or downward seepage can be a large term in the water budget. Surface water is often supplied to raise groundwater levels for optimal crop growth, to avoid algal blooms (by maintaining flow velocity), to reduce brackish seepage in coastal areas below sea level, or to prevent peat oxidation. In addition, the water can be removed from the catchment by pumping (Van den Eertwegh et al., 2006; Te Brake et al., 2013; Delsman et al., 2013).

Usually, distributed models are used for regional groundwater flow (MODFLOW), surface water supply and extraction (MIKE-SHE, SOBEK) and control operations (Van Andel et al., 2010) and the effect of changing surface water levels on runoff generation is not taken into account.

1.4 Aim and research questions

The aim of this thesis is to contribute to lowland hydrological science and practice by providing improved understanding of rainfall-runoff processes and a novel parametric model to simulate these processes. The title of this thesis reflects the two-part research question:

1. **what are the dominant rainfall-runoff processes in lowland catchments**
   and

2. **how can these processes be represented in parametric models**?

For both of these questions, I focused on topics which are important for lowland areas:

1. the relation between (catchment) storage and discharge,

2. the coupling between shallow groundwater and the unsaturated zone,

3. the activation of flowroutes at different stages of wetness, and

4. the feedback between groundwater and surface water.

The connection between the different topics and their position in the soil-water continuum are illustrated in Fig. 1.4. During model development, special attention was paid to limiting complexity and quantifying uncertainty.

1.5 Thesis outline

In Ch. 2, the freely draining Hupsel Brook catchment and the controlled Cabauw polder are described and characteristics and processes which are typical for lowland catchments are identified. Data and field experience from these catchments are used throughout the thesis. Ch. 3 contains the analysis of an extreme rainfall event and flash flood in August 2010 in the Hupsel Brook catchment. This event provided detailed information on a lowland catchment's behaviour during extremely wet conditions. In Ch. 4 storage-discharge relations are investigated through a simple dynamical systems approach, in which the catchment is represented by a single nonlinear reservoir. I use hydrograph fitting, recession analyses and soil moisture data to obtain the storage-discharge relation and used it to simulated discharge. Because this method did not yield satisfactory results, I used the field experience described in Chs. 2 and 3 to develop a new parametric rainfall-runoff model: the Wageningen Lowland Runoff Simulator (WALRUS). The model structure, mathematical relations and technical implementation are described in Ch. 5. In Ch. 6 WALRUS is tested with calibration, validation, sensitivity and uncertainty analyses using data and experience from the Hupsel Brook catchment and the Cabauw polder. Finally, in Ch. 7, I combine findings of all chapters to answer the research questions, provide recommendations for further research and identify the contribution of this thesis for water management.

2 | Two contrasting lowland catchments

owland catchments can be divided into mildly sloping, freely draining catchments and flat areas with managed surface water levels. In this thesis, data from two Dutch field sites are used. The mildly sloping, freely draining Hupsel Brook catchment is located in the east of The Netherlands, with elevations ranging from 22 to 35 m above sea level. This catchment has been an experimental catchment since the 1960s. The flat Cabauw polder is located in the west of The Netherlands at an "elevation" of 1 meter below sea level. This area is part of the Cabauw Experimental Site for Atmospheric Research (CESAR).

In The Netherlands, a distinction can be made between the freely draining High Netherlands (above mean sea level, although this can still be considered lowland) in the east and south of the country and the Low Netherlands with controlled water levels (below, or a few meters above, mean sea level) in the west and north (Fig. 2.1). Some areas with deep groundwater tables (> 10 m) exist in the far south (Limburg) and the old glacier ridges in the middle of the country (e.g. Veluwe). Two field sites are used in this thesis: the Hupsel Brook catchment is located in the relatively high eastern part of The Netherlands and the Cabauw polder in the low-lying western part (Fig. 2.1).

2.1 Hupsel Brook catchment

The Hupsel Brook catchment has been a well-known field site for hydrological studies since the 1960s. It has been used for studies on evapotranspiration (Stricker and Brutsaert, 1978), soil physical properties (Hopmans and van Immerzeel, 1988; Hopmans and Stricker, 1989), rainfall-runoff modelling (Stricker and Warmerdam, 1982; Bierkens and Puente, 1990) and relations between flow routes and water quality (Van den Eertwegh, 2002; Rozemeijer et al., 2010b; Van der Velde et al., 2012). The catchment of 6.5 km^2 is slightly sloping (0.8 %). Its soil consists of a loamy sand layer (with some clay, peat and gravel) of 0.2 to 10 m thickness on an impermeable clay layer of more than 20 m thickness (Table 2.1). A more detailed catchment description can be found in e.g. Van der Velde et al. (2010).

No surface water is supplied upstream in the Hupsel Brook catchment and the elevations of several weirs and flumes in the catchment are fixed. Some small water courses (large gullies) cross the catchment boundary (Fig.2.1), but these only carry water in winter. The catchment boundary is based on a steady state groundwater map simulated with MODFLOW (Van der Velde et al., 2012), but in reality the boundary is believed to shift slightly during the year, depending on the catchment wetness and slopes of the active flow paths (groundwater gradient, drainpipe slope or channel slope). There may

be some lateral groundwater flow across the catchment boundary, but this is assumed to be small in comparison with the other water balance terms.

In the Hupsel Brook catchment many hydrological variables have been measured since the 1960s, in different periods and with varying frequencies. Daily data of precipitation (P), potential evapotranspiration (ET_{pot}) and discharge (Q) are available since 1976 and hourly data since April 1979, with a gap between March 1987 and February 1992. For 8 % of the hours in the periods 1979–1987 and 1992-2013, at least one of the variables P, ET_{pot} or Q was missing.

Precipitation was measured with a rain gauge located at the meteorological station in the catchment (Fig. 2.1). Daily values of potential evapotranspiration (ET_{pot}) have been computed using data from the same meteorological station. Before 1988 the method of Thom and Oliver (1977) has been used and since 1989 the method of Makkink (1957). For our approach daily sums of ET_{pot} have been disaggregated to hourly sums by multiplication with the

Table 2.1: The main catchment characteristics and average annual water budget. f_{XS} denotes surface water supply and f_{XG} seepage (for all abbreviations, see Tab. 5.1).

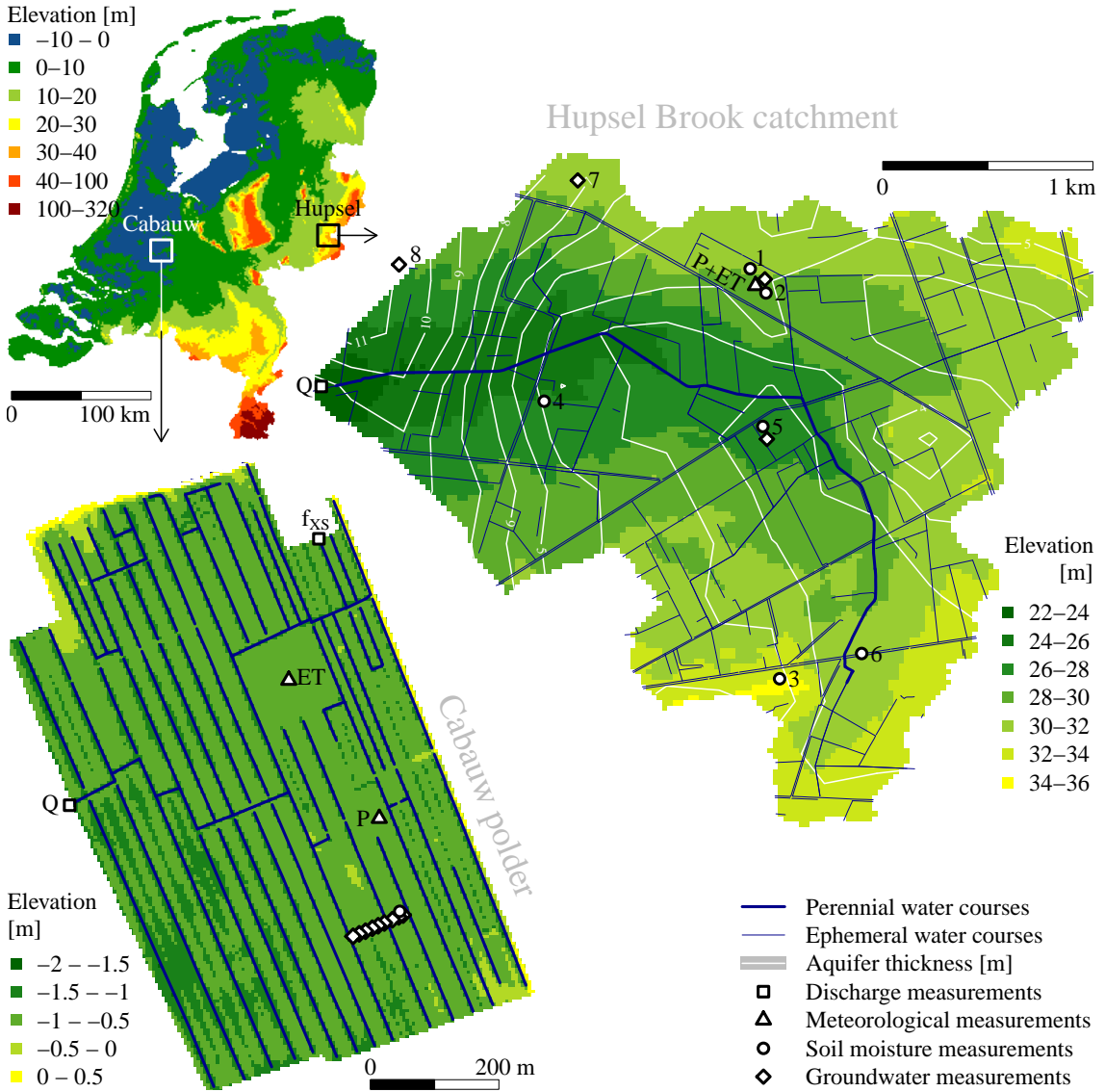|		Hupsel	Cabauw
Size	[km^2]	6.5	0.5
Elevation	[m a.s.l.]	22–35	−1
Slope	[%]	0.8	0
Soil type		0.2–11 m	0.7 m
		sand on	clay on
		clay	peat
Land use: grass	[%]	59	∼80
maize	[%]	33	∼15
forest	[%]	3	0
impervious	[%]	5	0
surface water	[%]	1	5
Annual P	[mm]	790	780
ET	[mm]	560	620
Q	[mm]	310	970
f_{XS}	[mm]	0	630
f_{XG}	[mm]	0	100

Figure 2.1: Elevation maps of the Cabauw polder (left), The Netherlands (middle) and the Hupsel Brook catchment (right) with measurement locations and surface water networks. Soil moisture measurements in the Cabauw polder (circles) consist of 4 arrays of TDR sensors; piezometers (diamonds) are ordered in a transect; f_{XS} denotes surface water supply. In the Hupsel Brook catchment, the numbered circles denote locations of the soil moisture and groundwater observations from the period 1976–1984 and the diamonds denote piezometers used after January 2012.

relative contribution of hourly global radiation sums to the daily global radiation sums. During the growing seasons (15 Apr–14 Sept) of 1979 through 1982 daily sums of actual evapotranspiration (ET_{act}) have been computed with the energy budget method: net radiation was measured and wind and temperature profile observations were used to estimate the sensible and ground heat fluxes. Evapotranspiration was then estimated as residual of the energy budget (for more information see Stricker and Brutsaert, 1978).

Discharge was measured by a type of H-flume at the catchment outlet (see for more information Section 3.2.3). Groundwater data were collected continuously at the meteorological station between 1976 and 2006. In addition, groundwater and soil moisture were measured intermittently at additional locations. From 1976 through 1984, soil moisture content and groundwater level were measured biweekly at 6 sites (circles in Fig. 2.1). Soil moisture content was measured with a neutron probe at 12 depths,

Figure 2.2: Some photos from the Hupsel Brook catchment. Top: (1) brook near the outlet, (2) ditch that has run dry and (3) headwater in a slightly sloping field. Bottom: (1) weather station, (2) dry H-flume near piezometer 5 (looking from upstream; note the standing water upstream of the flume and the culvert downstream) and (3) H-flume at the outlet.

ranging from 0.15 to 2.05 m. Since January 2012, groundwater levels were measured hourly at 4 locations (diamonds in Fig. 2.1). Additional groundwater and soil moisture data are available from a field next to the meteorological station for a period around an extreme rainfall and flood event in 2010.

2.2 Cabauw polder

The Cabauw polder area considered as a catchment in this study is 0.5 km^2 and part of a larger polder (Table 2.1). Its soil consists of heavy clay on peat and is characterized by an intensive drainage network of channels and drainpipes. Water is supplied upstream into the area from a more elevated water course through a variable inlet controlled by the water authority and through two small pipes with relatively constant discharge (Fig. 2.1). Surface water supply is necessary to raise groundwater levels for optimal crop growth and to prevent peat oxidization, while maintaining surface water flow velocity to avoid algal blooms in standing water. Downstream of the outlet is a larger water course, from which water is pumped into the river Lek (a large branch of the Rhine delta). It is important to note that there is no pumping station within the catchment and hence drainage is driven by gravity. The surface water levels are regulated by two weirs, which are set 10 cm higher in summer than in winter. The variable inlet is used to maintain these sur-

face water levels. Surface water levels vary to keep groundwater at an optimal depth: deep enough to avoid waterlogging and to provide a firm ground for tractors (wet clay and peat are too unstable) and high enough to avoid oxidization of peat and plant water stress. In winter, groundwater levels are convex between ditches because precipitation exceeds evapotranspiration and as a consequence groundwater flows towards the ditches. In summer, groundwater levels are concave between ditches because evapotranspiration exceeds precipitation and hence water infiltrates from ditches into the soil. The spatial and temporal variability in groundwater levels will be discussed in more detail in Sect. 2.4

The "catchment" is part of the Cabauw Experimental Site for Atmospheric Research (CESAR), which is well-known in the international meteorological community (Russchenberg et al., 2005; Van Ulden and Wieringa, 1996; Chen et al., 1997; Leijnse et al., 2010). The site is maintained by the Royal Netherlands Meteorological Institute (KNMI) and a consortium of 8 Dutch institutes (including Wageningen University). The site contains a 213 m high measurement tower, a separate flux tower for studies on land surface-atmosphere interaction (a FLUXNET location, Baldocchi et al., 2001), and many additional instruments. Extensive summaries can be found in Russchenberg et al. (2005) and Leijnse et al. (2010). Data from Cabauw have been used in hydro(meteoro)logical studies to estimate land-surface fluxes with SWAP (Gusev and

Figure 2.3: Some photos from the Cabauw polder. Top: (1) northern catchment boundary with elevated water course (between the houses) as seen from the tower, (2) variable inlet (water flows from right to left, under the road into the catchment), and (3) of one of the constant inlets (pipe). Middle: (1) V-notch weir to measure variable inlet, (2) trapezoidal weir to measure outflow and (3) piezometer transect. Bottom: (1) tower and meteorological station, (2) the river Lek as seen from the tower and (3) the southern half of the catchment (the road is the boundary) as seen from the tower, with locations of piezometers (yellow) and soil moisture sensors (black).

Nasonova, 1998), to investigate the effect of spatial variability in rainfall on soil moisture, groundwater and discharge with SIMGRO (Schuurmans and Bierkens, 2007), and to assess the transferability of land-surface hydrology models (Devonec and Barros, 2002).

Precipitation is measured with an automatic rain gauge, potential evapotranspiration is estimated with the approach of Makkink (1957) and actual evapotranspiration is determined by measuring net radiation, ground heat flux and Bowen ratio (with an eddy covariance set-up) and closing the energy balance (Beljaars and Bosveld, 1997; Foken, 2008). ET_{act} estimated with this method was on average 4 % higher than ET_{pot} during well-watered conditions (meaning that the storage deficit was below 100 mm). Overestimation of the daily evapotranspiration sum may be caused by an underestimation of dew formation at night (De Roode et al., 2010). As a quick fix, we divided ET_{act} by 1.04. Using ET_{act} estimated from the eddy covariance set-up directly was not an option due to the underestimation by eddy-covariance measurements which is often reported in the literature (e.g. Twine et al., 2000) and amounts to 18 % in the Cabauw polder.

Discharge is measured since May 2007 using a V-notch weir (downstream of the variable inlet) and trapezoidal Rossby weir (outlet), of which the stage-discharge relations have been obtained by laboratory calibration. The uncertainty associated with the discharge measurements of surface water supply is large because the V-notch weir was often submerged due to the small topographical gradient. In addition, the two small inlets (pipes) with relatively constant discharge were maintained by local residents and could not be measured continuously.
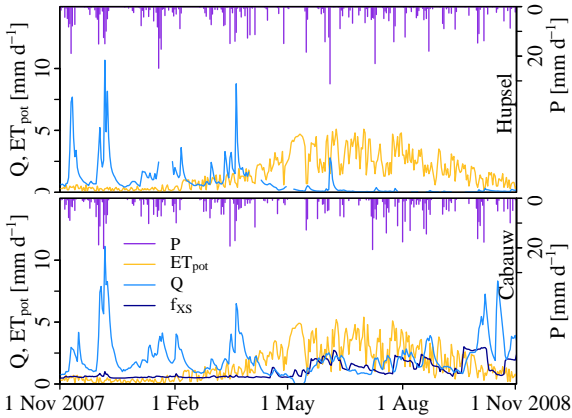
Figure 2.4: Example time series of the main water balance terms. Note the effect of surface water supply f_{XS} on the outflow in the Cabauw polder in summer.
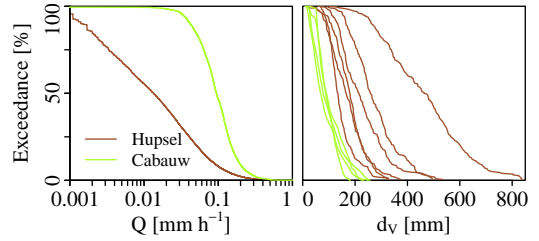

Figure 2.5: Regimes of discharge at the catchment outlet Q and storage deficit d_V (i.e. effective thickness of empty soil pores (volume per unit area) or the volume required to saturate the profile, see Fig. 2.11) for the two catchments. Note the effect of f_{XS} on the discharge regime of the Cabauw polder: discharge is relatively constant throughout the year. The different lines for d_V correspond to different measurement sites, which are well distributed over the Hupsel Brook catchment, but near each other in the Cabauw polder (circles in Fig. 2.1)

Groundwater levels have been measured since August 2003 with nine piezometers in the transect in the southeast corner of the catchment (Fig. 2.1): 5 automatically (4-hour resolution) and 4 manually (biweekly resolution). Soil moisture contents have been measured daily between November 2003 and August 2010 with a TDR set-up developed by Heimovaara and Bouten (1990), consisting of four arrays of six sensors between 5 and 73 cm below the soil surface.

There is likely groundwater flow into the catchment from the nearby river Lek (1 km to the south), of which the water level is variable and on average about 2 m higher than the water levels in the catchment (and 0.2–1.5 m above mean sea level). The top soil consists of a mixture of clay and peat and is not permeable enough for significant groundwater flow, but locally flow may occur through buried river sands (National Institute for Drinking Water Supply, 1982). Because no seepage data are available, we estimated the seepage as residual of the water budget of the year Nov. 2007–Oct. 2008 (also used for calibration, see Sec. 6.2) and assuming a constant seepage flux year-round. This seepage estimate amounts to about 7 % of the annual water budget.

2.3 Climatology

Since the Hupsel Brook catchment and Cabauw polder area are located only 120 km apart, the climate is quite similar: annual precipitation is around 800 mm and the annual potential evapotranspiration amounts to 600 mm (Tab. 2.1). The actual evapotranspiration (ET_{act}) in the Hupsel Brook catchment is usually within 5 % of ET_{pot} (based on 4 years of

combined observations). In the Cabauw polder, shallow groundwater tables prevent a strong soil moisture limitation on evapotranspiration (Brauer et al., 2014a). Precipitation occurs on 50 % of the days, but quantities are typically low: on 15 % of the days more than 5 mm was measured and on 5 % more than 10 mm. During 11 % of the hours precipitation was observed, of which 75 % with accumulations less than 1 mm. Hourly rainfall sums above 10 mm occur on average 3 times per year (at a given location and based on clock hours rather than a moving window).

Snow is of limited importance, even though freezing conditions are common. Sub-zero daily average temperatures occur on average on 28 (Hupsel) and 18 (Cabauw) days per year, leading to freezing of ponds on the land surface, water in soil cracks
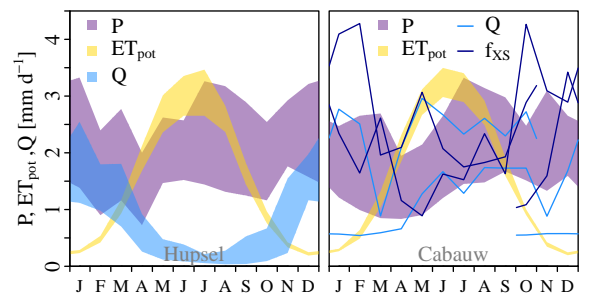

Figure 2.6: Regimes of the main water balance terms. The ranges show the 25th to 75th percentile of mean monthly values (divided by the length of the month to obtain mm d^{-1}). Percentiles for discharge and surface water supply in the Cabauw polder could not be computed because only two years of data were available.

and drainpipes, and the top layer of slowly flowing or standing surface water. On the majority of these days, the daily maximum temperature is above zero, leading to daily cycles of freezing and thawing. Cold winter conditions are often caused by persistent high pressure systems with little precipitation: on average 0.4 (Hupsel) and 0.3 (Cabauw) mm of precipitation on days with daily mean temperature below zero, leading to on average 12 (Hupsel – 1.5 % of total P) and 6 (Cabauw – 0.8 % of total P) mm of precipitation annually.

It should be noted that water input from dew can be considerable. Jacobs et al. (2006, 2010) estimated dew to amount to 4.5 % of the annual precipitation sum at Wageningen (located roughly halfway between the Hupsel Brook catchment and the Cabauw polder). Unfortunately, dew measurements were not available for either catchment. Therefore, dew is not considered separately in the water balance, but assumed to be included in the rain gauge measurements.

Water balance terms show seasonal variation (Figs. 2.4 and 2.6). Evapotranspiration exceeds precipitation between April and August, which means that excess water stored in winter and, in the case of the Cabauw polder, surface water supply f_{XS} and seepage f_{XG} are used in summer for both Q and ET. The influence of water management in the Cabauw polder is clearly visible: discharges remain high in summer due to surface water supply, on 6 May 2008 discharge suddenly dropped to zero as a result of the increase of weir elevation, and on 16 November 2007 and 15 October 2008, discharge increased because the weir was lowered. The surface water supply flux in the Cabauw polder is large and variable and can reach 800 mm in some years. As a consequence, discharge, groundwater level and soil moisture contents vary much less in the Cabauw polder than in the Hupsel Brook catchment (Fig. 2.5). In the Cabauw polder, there is always water in all branches of the surface water network, whereas the headwaters of the Hupsel Brook frequently run dry. Discharge at the outlet of the Hupsel Brook catchment dropped to zero during three months in 1976, a month in 1982 and several shorter periods in 1983, 1988 and 2011.

2.4 Soil moisture and groundwater variability

The spatial and temporal variation in soil moisture content and groundwater depth provide information about the catchment behaviour. At the meteorological station in the Hupsel Brook catchment, maximum groundwater depth was 1.8 m (Fig. 2.7), which occurred in 1976, a famous drought year in western Europe (Van Huijgevoort et al., 2013; Teuling et al., 2013). In the Cabauw polder, the maximum groundwater depth since the start of our measurements was 1.4 m, during the exceptionally dry summer of 2006. Because groundwater is always shallow, soil moisture contents measured at the same locations show similar fluctuations. This confirms that in these catchments groundwater and the unsaturated zone are coupled, as implied in Sect. 1.3.1. At both sites, the first tens of cm of soil above the groundwater table is saturated, indicating that a capillary fringe is present. In the Cabauw polder, enough water is always available for plant transpiration: soil moisture contents never drop below 40 % at 40 cm depth. At the meteorological station in the Hupsel Brook catchment, some stress and transpiration reduction may occur if volumetric soil moisture contents drop below 10 % in the top 40 cm during dry summers.

The horizontal bands in Fig. 2.7 are caused by vertical variation in soil characteristics. Organic matter increases towards the soil surface in both catchments. In the Cabauw polder, the transition between the clay top soil and peat underneath is visible at 0.7 m depth. The green stripe at 1.5 m depth in the Hupsel Brook catchment may be caused by a local clay or till layer or by instrumental errors. These results indicate that the soil is not homogeneous and that describing the vertical moisture profile with theoretical relations of e.g. Van Genuchten (1980) or Brooks and Corey (1964) may induce errors.

Groundwater does not only vary in time, but also in space. In the Cabauw polder, groundwater levels are mainly determined by the season (precipitation excess or deficit), distance from the surface water network and the surface water level. With the array of piezometers in the southeastern corner of the catchment (Fig. 2.1), we obtained text-book examples of water tables in areas with controlled surface water levels. In winter, surface water levels are low (because weirs are lowered) and excess rainfall is drained, showing a convex groundwater table (Fig. 2.8). In summer, surface water levels are higher because weirs are elevated and more surface water is supplied. Water is extracted from the soil through evapotranspiration, drawing the water table below the surface water level. Water then infiltrates from the surface water into the soil, creating a concave groundwater table. These examples show that groundwater-surface water interactions (Sect. 1.3.4) are very important in areas with controlled water tables, such as the Cabauw polder, especially when surface water is supplied upstream (Sect. 1.3.5).

Variation in groundwater tables in the Hupsel Brook catchment does not only depend on the dis-
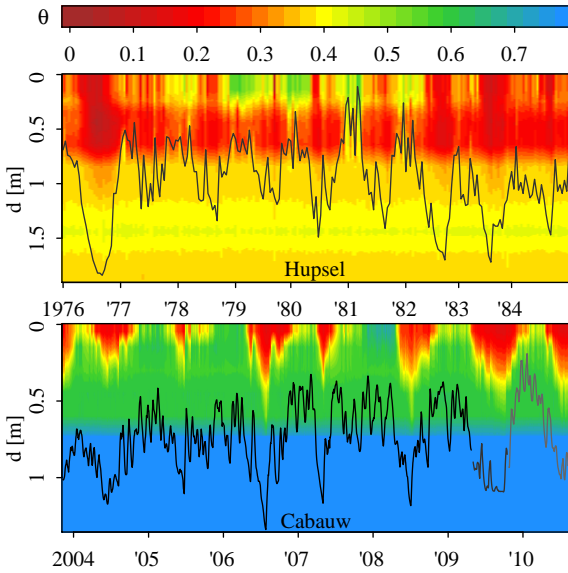
Figure 2.7: Temporal variation in volumetric soil moisture content at the meteorological station in the Hupsel Brook catchment and the mean of the sites in the Cabauw polder. The horizontal bands are caused by vertical variation in organic matter content. The black lines indicate groundwater depths. In the Cabauw polder, the piezometer at the soil moisture measurement site was moved twice, indicated by the different grey colours.

Figure 2.9: Temporal variation in groundwater depth in the Hupsel Brook catchment at different locations. The numbers correspond to the piezometers and soil moisture measurement locations in Fig. 2.1. Distance to the surface water network and aquifer thickness increase in the order of sites 5–2–7–8.

Figure 2.8: Cross-sections through a field between ditches (and a gully in the middle), showing the groundwater table on four days. Groundwater levels were obtained with the array of piezometers indicated in Fig. 2.1. August 2003 was exceptionally dry.
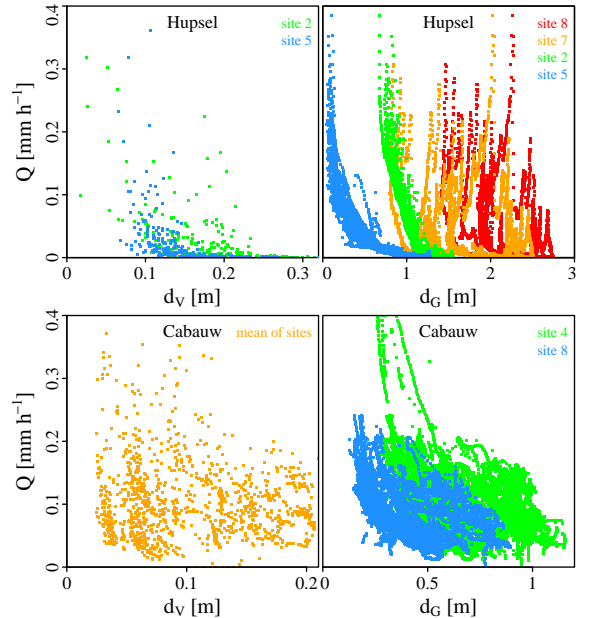
Figure 2.10: Relations between storage deficit and discharge (left panels) and groundwater depth and discharge (right panels). For clarity, not all sites are shown. Groundwater site 4 in the Cabauw polder is the site 10 m and site 8 50 m from the east ditch in Fig. 2.8.
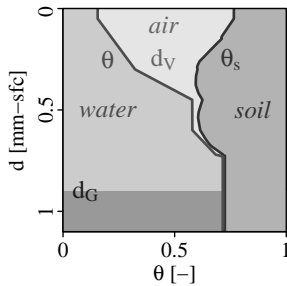
Figure 2.11: Computation of the storage deficit d_V (a case for the Cabauw polder): d_V (the air fraction) can be obtained by integrating the difference between the profiles of volumetric soil moisture content θ (the water fraction) and soil moisture content at saturation θ_s ($1 - \theta_s$ being the soil fraction).

tance from the surface water network, but also on the local hydrogeological conditions. Moving from southeast to northwest, the impermeable clay layer becomes deeper and thus the aquifer becomes thicker (Fig. 2.1). In addition, the soil contains more gravel, leading to a higher conductivity. Both increasing aquifer thickness and increasing conductivity lead to increasing transmissivity towards the northwest. Piezometers located in the northwest (i.e. number 7 and 8 in Fig. 2.1) show little temporal variation in groundwater depth (Fig. 2.9). Groundwater is deep because water can easily be transported to the surface water network. Infiltrating rainfall is attenuated in the unsa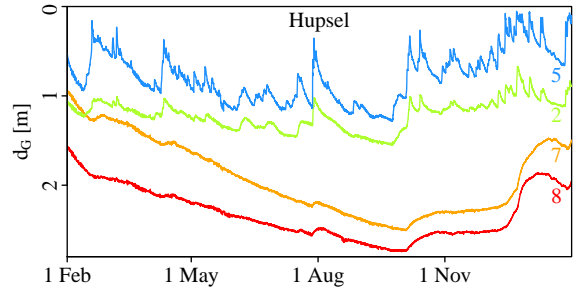turated zone. Piezometers in areas with a thinner aquifer and closer to the surface water network (site 5 and, to a lesser extent, site 2) respond more directly to rainfall events. Around site 5, ponding is observed frequently. At site 2, Van der Velde et al. (2011) measured drainpipe flow, which transported approximately 80 % of the water from this field. This shows that the contribution of quick flowroutes such as drainpipe and overland flow to the total drainage varies both in space and in time (Sect. 1.3.3). Although the high-frequency groundwater dynamics is more pronounced in sites 5 and 2, the seasonal amplitude is larger in sites 7 and 8, because they are located further away from the surface water network, allowing for a higher groundwater table. This can be compared to the situations in Fig. 2.8: in the middle of the field, the seasonal variation is larger than near the ditches. In the Cabauw polder, however, all piezometers show as much temporal variation as at

site 5 in the Hupsel Brook catchment, because they are all relatively close to the surface water network and storage capacity is low.

The relation between discharge and storage, be it groundwater storage or total storage (in the saturated zone, unsaturated zone, on the land surface and in the surface water network together), is in many catchments quite strong (e.g. Kirchner, 2009). In the Hupsel Brook catchment, this is also the case for areas relatively close to the surface water network (i.e. sites 5 and 2). In this Section, rather than using total storage, we focus on its complement: the storage deficit (assuming a limited contribution of storage on the land surface and as surface water). Storage deficit d_V is the amount of water necessary to saturate the soil completely (see Fig. 2.11 for an explanation). We plotted d_V measured at sites 5 and 2 against discharge in Fig. 2.10a and although there is a lot of scatter, a general pattern can be observed. The relation between groundwater depth d_G and discharge at these two locations is much clearer (Fig. 2.10b), indicating that discharge is more closely related to groundwater storage than to total storage at these sites. The relation between groundwater depth and discharge at sites 7 and 8 appears to be less clear. When zooming in, relations (with hysteresis loops) can be identified for single events, but when all data are lumped together, the relation is not unique (which will be explored further in the next Chapters). This also indicates that within one catchment, different piezometers represent different combinations of contributions from seasonal and event-related fluctuations.

As expected, the relation between storage (groundwater and total) and discharge is not clear at all in the Cabauw polder (Fig. 2.10cd). This is of course caused by the surface water supply, which increases discharge directly, but groundwater only indirectly and by changeable elevation of weirs. This shows that the Cabauw polder cannot be approximated by a simple storage-discharge relation.

2.5 Data use in next chapters

Data from the Hupsel Brook catchment are used for the analysis of the extreme rainfall and flood that occurred in August 2010 (Ch. 3) and to investigate storage-discharge relations in more detail (Ch. 4). Data from both catchments are used to develop (Ch. 5) and test (Ch. 6) a new rainfall-runoff model.

3 | Extreme rainfall and flash flood

O n 26 August 2010 the eastern part of The Netherlands and the bordering part of Germany were struck by a series of rainfall events lasting for more than a day. Over an area of $740\,km^2$ more than $120\,mm$ of rainfall was observed in $24\,h$. This extreme event resulted in local flooding of city centres, highways and agricultural fields, and considerable financial loss. In this Chapter we report on the unprecedented flash flood triggered by this exceptionally heavy rainfall event in the $6.5\,km^2$ Hupsel Brook catchment, which has been the experimental watershed employed by Wageningen University since the 1960s. This study aims to improve our understanding of the dynamics of such lowland flash floods. We present a detailed hydrometeorological analysis of this extreme event, focusing on its synoptic meteorological characteristics, its space-time rainfall dynamics as observed with rain gauges, weather radar and a microwave link, as well as the measured soil moisture, groundwater and discharge response of the catchment. At the Hupsel Brook catchment $160\,mm$ of rainfall was observed in $24\,h$, corresponding to an estimated return period of well over 1000 years. As a result, discharge at the catchment outlet increased from 4.4×10^{-3} to nearly $5\,m^3\,s^{-1}$. Within $7\,h$ discharge rose from 5×10^{-2} to $4.5\,m^3\,s^{-1}$. The catchment response can be divided into four phases: (1) soil moisture reservoir filling, (2) groundwater response, (3) surface depression filling and surface runoff and (4) backwater feedback. The first $35\,mm$ of rainfall were stored in the soil without a significant increase in discharge. Relatively dry initial conditions (in comparison to those for past discharge extremes) prevented an even faster and more extreme hydrological response.

3.1 Introduction

Flash floods, defined here as extreme floods generated by intense precipitation over rapidly responding catchments, have recently drawn increased attention, both from the scientific community and from the media. Their often devastating consequences, both in terms of material damage and loss of life, have triggered a number of European research projects (e.g. FLOODsite, HYDRATE, and IMPRINTS) to study the meteorological causes and hydrological effects of such events. These and other projects have lead to recent publications by e.g. Smith et al. (1996), Ogden et al. (2000), Gaume et al. (2003), Gaume et al. (2004), Delrieu et al. (2005) and Borga et al. (2007).

From the perspective of water management and early warning, one of the main challenges posed by the phenomenon of flash floods is the extremely rapid response times of many of the catchments involved (as short as $10\,min$ for certain small urban watersheds in mountainous environments). The consequence of this short lead time is that hydrological forecasting systems for regions with catchments prone to flash floods must rely heavily on meteorological forecasts, either from radar-based short-term precipitation forecasting (nowcasting) or from numerical weather prediction. Improved forecasting and early warning of flash floods is crucial, because the extreme discharges associated with such events (maximum specific discharges can reach tens of $m^3\,s^{-1}\,km^{-2}$) can have devastating societal consequences.

Typically, a timescale of a few hours is used to distinguish a flash flood from a regular flood. Since runoff generation is faster in mountainous catchments with steep slopes than in lowland catchments and since orography can impact the magnitude of rainfall extremes (Miglietta and Regano, 2008), most flash floods occur in mountainous areas. However in case of extreme rainfall, rapid runoff generation due to overland flow can also trigger flash floods in lowland catchments (Van der Velde et al., 2010).

Lowland areas, such as the densely populated delta region of The Netherlands, are typically associated with large-scale flooding of the Rhine and Meuse. These rivers have relatively slow response times (of the order of days to weeks). However, heavy rainfall events and the associated local flooding do occur in The Netherlands (Monincx et al., 2006). In addition, the magnitude of 24-h rainfall extremes that can trigger such flooding is expected to increase in a warmer climate (Kew et al., 2010). Thus, an improved understanding of the hydrological processes involved in the response of both natural and man made (polder) catchments to local heavy rainfall is needed to support water management in lowlands.

In this chapter we report on the flash flood triggered by an exceptionally heavy rainfall event on 26 August 2010 that occurred over the $6.5\,km^2$ Hupsel Brook catchment. The objective of this study is to understand the meteorological causes and hydrological effects of this event in order to improve process understanding and, eventually, flood fore-

casting models.

The available data will be described in Sect. 3.2, with special attention to the accuracy of the discharge measurements. We present a detailed analysis of the synoptic meteorological situation leading to the event (Sect. 3.3.1), the rainfall accumulations as measured by rain gauges, weather radar, and a microwave link (Sects. 3.3.2 and 3.3.3) and the extreme value statistics of the rainfall accumulation (Sect. 3.3.4). The soil moisture, groundwater and surface water response within the catchment will be described in Sects. 3.4.1–3.4.4. We present a dissection of the observed hydrological response into a sequence of contrasting regimes that characterize the storage and discharge dynamics of the catchment following this extraordinary rainfall event (Sect. 3.5). Finally we present conclusions (Sect. 3.6)

3.2 Observations

The Hupsel Brook catchment has already been introduced in detail in Sect. 2.1. This Section focusses on the observations used in this Chapter.

3.2.1 Rainfall observations

The Royal Netherlands Meteorological Institute (KNMI) operates a network of 32 automatic meteorological stations (with a density of about 1 station per $1000\,km^2$), where rainfall (measured with an automatic rain gauge), global radiation and air temperature are measured (10-min resolution). One of the meteorological stations (called Hupsel) is located within the Hupsel Brook catchment (Figs. 2.1 and 3.2). Unfortunately, the rain gauge stopped recording at 26 August, 21:00 UTC, apparently due to instrumental problems caused by the extreme rainfall.

The KNMI also operates a manual rain gauge network (with a density of about 1 gauge per $100\,km^2$) to collect daily (08:00–08:00 UTC) rainfall accumulations. One of these manual rain gauges is located within the catchment, less than 1 km southwest of the meteorological station (Fig. 3.2).

Weather radars are valuable in flash flood research, because they give quantitative information about both the spatial and the temporal variability of rainfall (e.g. Bonnifait et al., 2009; Younis et al., 2008). Two weather radars are operated by the KNMI in De Bilt and Den Helder. The weather radar in De Bilt is about 100 km west of the catchment. Since standard weather radar rainfall estimates are prone to large errors, a network of 326 manual and 32 automatic rain gauges was used to adjust radar-based accumulations. This adjustment method has been described in detail and verified in Overeem et al. (2009a,b).

This extreme rainfall event provided a test-case for a less well-known source of rainfall data, which could be valuable in data-sparse regions or during extreme events. As part of commercial networks for mobile telecommunication, many microwave links have been installed in The Netherlands. Microwaves are sent from a transmitting antenna to a receiving antenna. Rainfall attenuates the microwave signal and because of this, as a byproduct, such links can provide quantitative information about path-averaged rainfall intensities (Messer et al., 2006; Leijnse et al., 2007).

One of these microwave links has one antenna located within the Hupsel Brook catchment and the other 15.1 km to the southwest (see Fig. 3.2). From this link minimum and maximum received powers were available over 15-min intervals (with a resolution of 0.1 dB), based on 10-Hz sampling. The path-averaged rainfall intensity was estimated from the minimum and maximum received powers according to Overeem et al. (2011).

In the hydrological analysis 1-h rainfall data from the automatic rain gauge at the meteorological station in Hupsel have been used. When no automatic rain gauge data were available (between 26 August, 21:00 UTC and 27 August, 15:00 UTC) the gauge-adjusted 1-h radar rainfall depths at the same location have been used.

3.2.2 Groundwater and soil moisture observations

In a field (with drainpipes) located next to the meteorological station, 31 piezometers have been installed (Van der Velde et al., 2009). The surface has local elevations and depressions with height differences of about 50 cm. Here we use groundwater level data recorded with pressure sensors (resolution 15-min) from 2 representative piezometers: one in a local elevation and one in a local depression. A number of Echoprobe capacitance sensors (type Echoprobe EC-20) were also installed in this field to measure soil moisture content. Here we use data from one sensor at 40 cm depth situated in a local elevation.

We investigated the consequences of spatial variability in initial groundwater depths with the detailed groundwater model presented by Van der Velde et al. (2009). With this model a groundwater map was made for a day with similar measured groundwater levels at the piezometer field as on 25 August 2010 (namely 4 August 1994). With the groundwater depths from this map, potential saturation excess has been computed as the total rainfall depth minus groundwater depth times a specific storage of 10 %. These are potential values, because

during the rainfall event, water is discharged to the brook or local depressions through the soil or drain-pipes, leading to more saturation excess than computed near the brook and in local depressions. Spatial variation in rainfall and specific storage have not been taken into account when computing the potential saturation excess, but spatial variation in permeability and aquifer thickness have been incorporated in the model.

3.2.3 Discharge observations

Since 1968, discharge has been measured with a particular type of H-flume at the catchment outlet (see Hooghart, 1984, for information about H-flumes). Its temporal resolution for the period used in this chapter was 15 min.

The flume at the catchment outlet is situated in a dam perpendicular to the brook with a higher level than the rim of the flume (Fig. 3.7). In post-event field surveys no evidence was found that water had flowed over the dam. Hence all water must have passed through the flume.

It is not likely that water levels in the flume rose higher than the measuring range of the stilling well. The maximum water height measured in the flume was 1.504 m, only 4 mm higher than the rim not yet reaching the bar, leading to a computed peak discharge of $4.98 \, \mathrm{m^3 \, s^{-1}}$.

Because the flume is slightly narrower than a standard H-flume, the flume was calibrated in the Wageningen University hydraulics laboratory in 1969 and 1983 (Fig. 3.1). For low discharges a prototype was used and for high discharges a scale model. The flume was calibrated up to a water level of 1.22 m and corresponding discharge of $3.02 \, \mathrm{m^3 \, s^{-1}}$. The obtained stage-discharge relationship was extrapolated to the maximum water level of 1.5 m, resulting in a discharge of $4.94 \, \mathrm{m^3 \, s^{-1}}$.

To examine if such an extrapolation is valid, we compared laboratory experiments from our flume to those of standard H- and HL-flumes, which have been calibrated to the rim (Kilpatrick and Schneider, 1983). For each flume, water levels and discharges are normalized with respect to their maximum values and plotted against each other (Fig. 3.1). The deviations between the stage-discharge relationships of the different types of H-flumes were very small, from which we conclude that the employed extrapolation does not introduce significant errors.

During the second post-event field survey (see Sect. 3.2.4), the flume was found to be partially submerged (i.e., the water level downstream of the flume was higher than the crest of the flume). When flumes are submerged, water downstream of the flume introduces an additional resistance, leading to higher stage heights in the flume at a given dis-
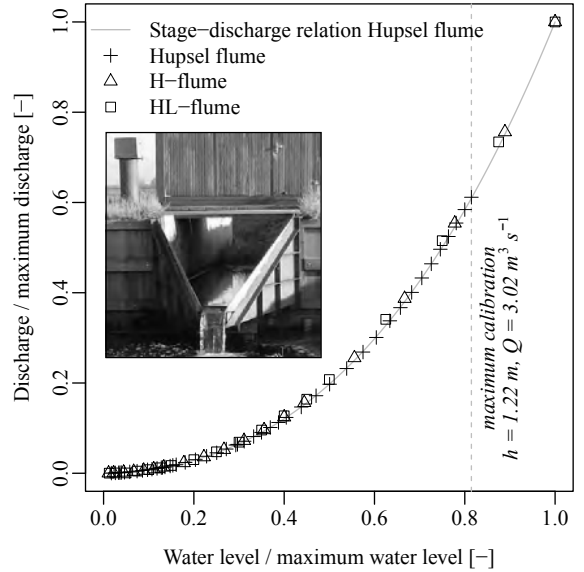
Figure 3.1: Stage-discharge relationships for different types of H-flumes. Points: Calibration data of stage-discharge relationships of standard H- and HL-flumes and the flume at the outlet of the Hupsel Brook catchment. Line: The employed stage-discharge relationship for the Hupsel flume, extrapolated from $h = 1.22 \, \mathrm{m}$. Water levels and discharges have been normalized with respect to their maximum values (Hupsel flume: $h_{\mathrm{max}} = 1.50 \, \mathrm{m}$, $Q_{\mathrm{max}} = 4.94 \, \mathrm{m^3 \, s^{-1}}$; H-flume: $h_{\mathrm{max}} = 1.37 \, \mathrm{m}$, $Q_{\mathrm{max}} = 2.39 \, \mathrm{m^3 \, s^{-1}}$; HL-flume: $h_{\mathrm{max}} = 1.22 \, \mathrm{m}$, $Q_{\mathrm{max}} = 3.31 \, \mathrm{m^3 \, s^{-1}}$). Calibration data of the H- and HL-flumes are taken from Kilpatrick and Schneider (1983). The inset shows the Hupsel flume.

charge. When measured stage heights are used to compute discharges without accounting for (partial) submergence, the discharge will be overestimated.

Fortunately, H-flumes are not sensitive to submergence. When the submergence ratio (water level downstream of the flume divided by stage height, both with respect to the crest) of a standard H-flume is 50%, the stage height is overestimated by only 3 % (Brakensiek et al., 1979). A submergence ratio of 60 % leads to a stage height over-estimation of 5 %. These values may differ slightly for the Hupsel flume. During post-event field survey II, the submergence ratio was estimated to be 56 % ($h_{\mathrm{upstream}} = 1.23 \, \mathrm{m}$ and $h_{\mathrm{downstream}} = 0.7 \, \mathrm{m}$). This leads to an overestimation of the stage height by 4 % (based on data for H-flumes) and a possible overestimation of the discharge by 10 % ($3.07 \, \mathrm{m^3 \, s^{-1}}$ as an initial estimate and $2.80 \, \mathrm{m^3 \, s^{-1}}$ after correction). During the peak, this effect might even have been smaller. Since detailed information on downstream water levels were not available, possible errors due to submergence are assumed to be small

Table 3.1: Overview of the post-event field surveys (photos in Fig. 3.7).

	Date	Activities
I	27 Aug, 06:00 UTC	Photographing
II	27 Aug, 13:00 UTC	General catchment inspection, instrument inspection, search for flood marks, interviews with inhabitants, photographing
III	29 Aug, 17:00 UTC	Photographing
IV	3 Sep, 10:00 UTC	General catchment inspection, instrument inspection, search for flood marks, groundwater data collection, photographing
V	13 Sep, 14:00 UTC	Photographing

enough to be neglected.

3.2.4 Post-event field surveys

Post-event field surveys can provide valuable information on water levels and flow processes in ungauged parts of the catchment (Gaume and Borga, 2008; Marchi et al., 2009). Such surveys were performed directly after the event on 27 August, as well as during several phases of the recession following the flash flood. During these surveys, photographs were taken on several locations in the catchment and all instrumentation was inspected. Additional information was provided by local inhabitants. A summary of the surveys is provided in Table 3.1.

3.3 Rainfall event

3.3.1 Synoptic situation and rainfall pattern

The synoptic chart at 26 August, 18:00 UTC shows an elongated region with multiple shallow low pressure centres stretching from the Bay of Biscay to Poland (Fig. 3.3, left panel). The low pressure centres were sandwiched between bands of high pressure over the north Atlantic and southern Europe, which allowed the system to remain stationary during most of the day. Because pressure gradients were small, wind speeds were low and storm cells moved slowly.

Along these low pressure centres a warm front was present, which divided warm, humid air in the south from cooler air in the north. The temperature gradients over The Netherlands were large. For ex-

ample, a difference of 8 °C in maximum daily surface temperature was found over 150 km.

The frontal transition zone of warm air in the south and cooler air in the north of The Netherlands caused several active disturbances during 26 August. In the course of the afternoon the atmosphere south of the warm front became unstable, giving rise to some very heavy, mostly convective rain showers in the middle and eastern part of the country. These disturbances were part of a mesoscale convective system and passed The Netherlands with a west-southwesterly flow, locally resulting in extraordinary accumulations of rainfall (see Schumacher and Johnson, 2005, for a description of a mesoscale convective system). Similar accumulations were recorded in parts of Northwestern Germany (Fig. 3.3).

Because storm cells moved along a stationary line, it rained continuously for long periods of time in several places. More than 18 h of near-continuous rainfall was recorded in De Bilt (the location of one of the employed KNMI weather radars).

The rainfall pattern which lead to these heavy intensities was highly variable, containing both convective and stratiform rainfall. Figure 3.4 presents a clear example of the spatial variability in the rainfall field as observed by the weather radar in De Bilt at 19:15 UTC. This weather radar scans at different elevation angles, which makes it possible to obtain a vertical profile of radar reflectivity (Hazenberg et al., 2011). In Fig. 3.4 both the horizontal and vertical extent of the convective area (reflectivity exceeding 40 dBZ) can be clearly identified.

The convective cells were part of a larger southwest-northeast oriented squall line that became apparent in the Hupsel Brook catchment at 15:30 UTC (see also Fig. 3.5). In this squall line new convective cells with heavy precipitation were generated upstream of the Hupsel Brook catchment until 22:15 UTC. This happens often in mesoscale convective systems and can lead to extreme rainfall accumulations (Schumacher and Johnson, 2008). The convective areas were highly variable in space, but many passed over the Hupsel Brook catchment. After 22:15 UTC rainfall became more stratiform.

3.3.2 Estimation using rain gauges and weather radar

Figure 3.2 shows daily rainfall depths for 26 August, 08:00 UTC to 27 August, 08:00 UTC for the gauge-adjusted radar composite and the interpolated manual rain gauge data. Locations of the manual rain gauges and their observed daily sums are also shown.

The highest manual rain gauge rainfall depth for this day (138 mm) was observed in Lievelde, 4 km southwest of the catchment. This, for Dutch con-
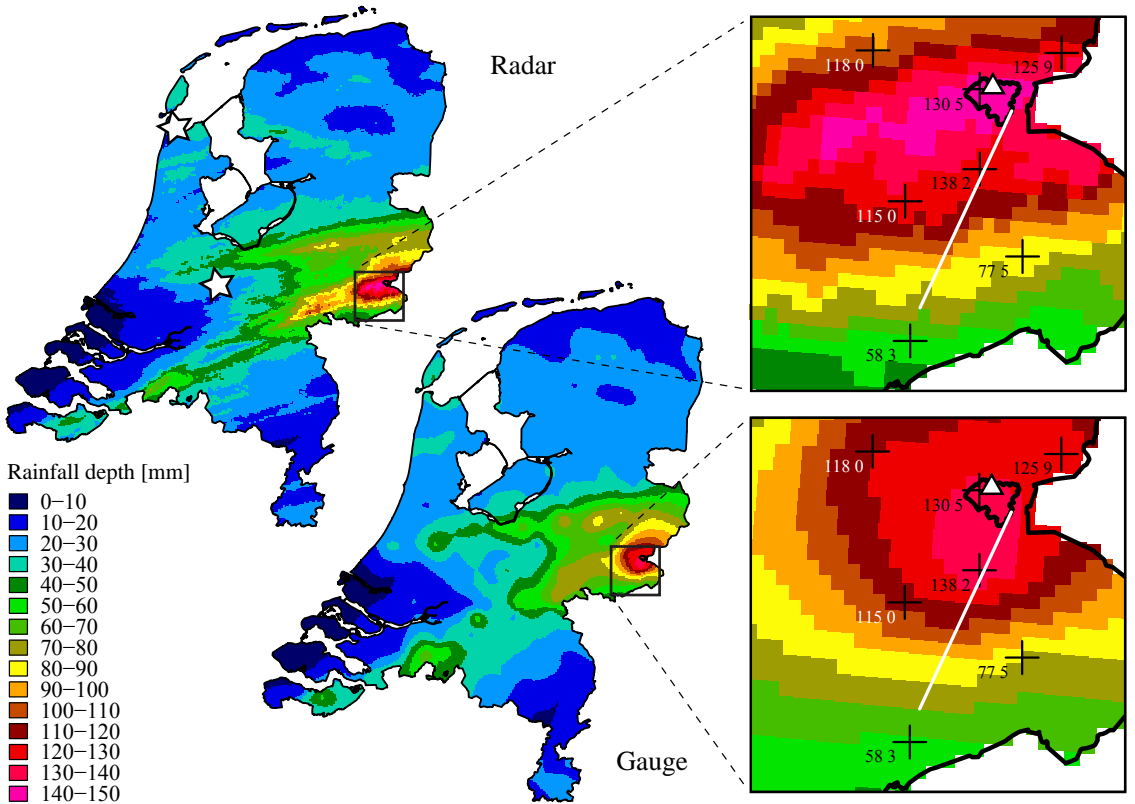
Figure 3.2: Daily rainfall depths for 26 August, 08:00 UTC to 27 August, 08:00 UTC for The Netherlands and the region around the Hupsel Brook catchment. Upper panels: depths for the gauge-adjusted radar composite. Lower panels: depths for the interpolated manual rain gauge data. Also plotted are: weather radars (stars), manual rain gauges and their daily rainfall depths (plusses), automatic rain gauge (triangle), and microwave link path (line). Because the automatic rain gauge at Hupsel stopped recording at 21:00 UTC no daily rainfall depth was plotted for this gauge.
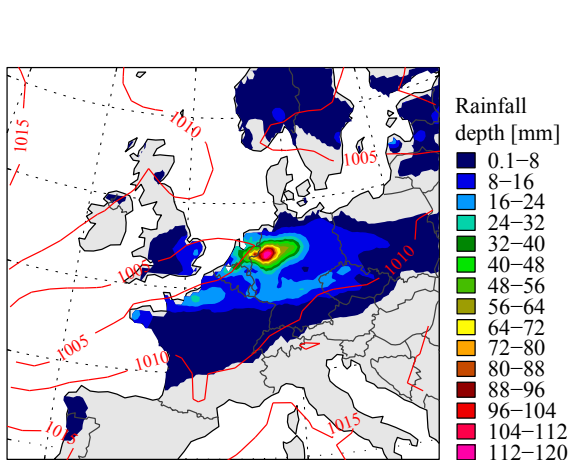
Figure 3.3: Large-scale patterns of mean sea level pressure (hPa) and precipitation accumulation for 26 August 2010 (00:00–24:00 UTC). Pressure data come from the ERA Interim reanalysis (18:00 UTC). Precipitation is taken from the daily gridded observational dataset provided by the ECA & D (Haylock et al., 2008)
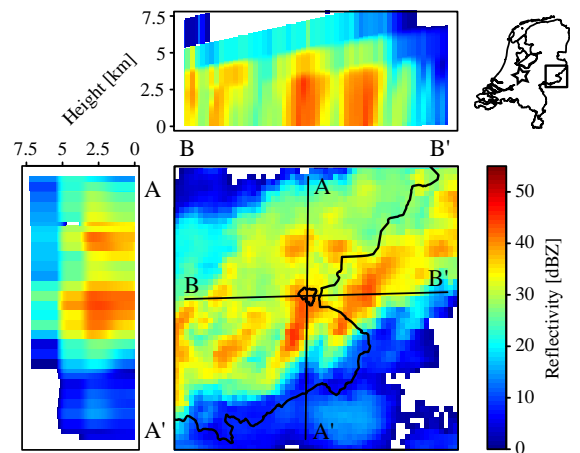
Figure 3.4: Spatial variation in radar reflectivity for 26 August, 19:15 UTC. Reflectivity is derived from the 14-elevation volume scan of the KNMI weather radar in De Bilt (star). Side panels show the vertical distribution of the reflectivity for two transects over the Hupsel Brook catchment.
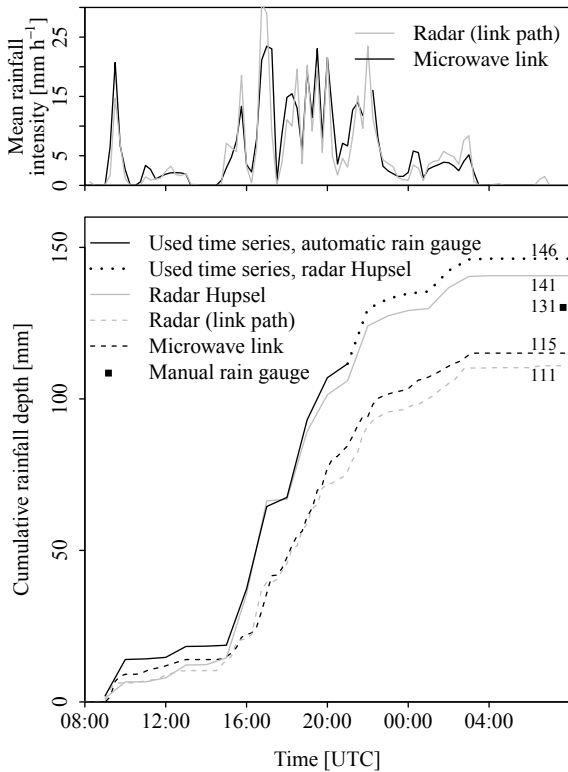
Figure 3.5: Top: temporal dynamics of rainfall intensity. Black: microwave link. Grey: path-averaged gauge-adjusted radar data. The temporal resolution is 15 min. Rainfall intensities from radar data are shifted 15 min forward in time, because it takes some time for the droplets measured aloft by the radar to reach the level of the microwave link. Bottom: cumulative rainfall depths from 26 August, 08:00 UTC to 27 August, 08:00 UTC. Solid black: automatic rain gauge. Dotted black: gauge-adjusted radar data at the location of the automatic rain gauge, which were used to fill gaps of the automatic rain gauge data. Solid grey: gauge-adjusted radar data at the location of the automatic rain gauge. Dashed grey: gauge-adjusted radar data averaged over the microwave link path. Dashed black: microwave link. One black point: manual rain gauge.

ditions, extraordinary accumulation is among the highest ever recorded in The Netherlands since official registration of the national rain gauge network started in 1951. The highest daily rainfall depth measured (with manual rain gauges) since 1951 was 148 mm, the second highest 146 mm (source: KNMI). The 3rd, 5th and 7th places are occupied by Lievelde (138 mm), Hupsel (131 mm) and Rekken (126 mm) respectively, all from 26 August, 08:00 UTC to 27 August, 08:00 UTC (all plotted in Fig. 3.2). On 3 August 1948, 208 mm of rainfall was

measured elsewhere in the Netherlands, but this event is not included in the official records because not all protocols were standardized in that period.

At the location of the automatic rain gauge in the catchment a gauge-adjusted radar rainfall depth of 141 mm was measured (08:00–08:00 UTC). Based on the data series from the automatic rain gauge (gaps filled with radar data), the maximum daily (08:00–08:00 UTC) rainfall depth is 146 mm and the maximum 24-h rainfall depth is 160 mm (04:00–04:00 UTC). This is larger than the largest 24-h rainfall depth observed in the 11-year climatological radar data set for the entire land surface of The Netherlands (142 mm for a radar pixel of 6 km^2).

Figure 3.5 shows that the cumulative rainfall depths from 26 August, 08:00 UTC to 26 August, 21:00 UTC from the automatic rain gauge and the gauge-adjusted radar hardly differ. Daily accumulations from radar and manual rain gauge are comparable, which is partly induced by the gauge-adjustment of the radar data. Temporal rainfall variations from radar and rain gauge (not induced by daily gauge-adjustment) are quite similar as well.

The rainfall event can be divided into roughly four parts according to rainfall intensity (see also Figs. 3.5 and 3.7). From 04:00 to 10:00 UTC rainfall was moderately intense (27 mm; mean rainfall intensity 5 mm h^{-1}), from 10:00 to 15:00 UTC rainfall was light (5 mm; mean rainfall intensity 1 mm h^{-1}), from 15:00 to 22:00 UTC rainfall was intense (111 mm; mean rainfall intensity 16 mm h^{-1}) and from 22 to 03:00 UTC rainfall was moderately intense (16 mm; mean rainfall intensity 3 mm h^{-1}).

The spatial extent (including a part of Germany) of the extreme event is derived for the largest 24-h rainfall depths (04:00–04:00 UTC) from the gauge-adjusted radar composite. The 24-h rainfall depth exceeds 100 mm for a 2100 km^2 area, 120 mm for a 740 km^2 area, and 140 mm for a 170 km^2 area. The scale of this event is considerably larger than the largest scale of the 24-h rainfall depth exceeding 100 mm, ~450 km^2, as found in the 11-year climatological radar dataset for The Netherlands (Overeem et al., 2010).

3.3.3 Estimation using microwave link

During the event of 26 August, the microwave link connection remained stable 93 % of the time – high rainfall intensities did not cause instrumentation problems. The obtained depths correspond well to the radar depths measured over the same path (Fig. 3.5). The top panel in Fig. 3.5 shows that the dynamics of the link-based rainfall intensities are similar to those obtained from path-averaged gauge-adjusted radar rainfall intensities. This confirms that microwave links are a useful addition to the ex-

isting gauge networks and that they can be used to estimate rainfall in areas where no gauges are available.

This is a simple, first-order attempt to estimate rainfall intensities from this commercial microwave link. Some important sources of error were not taken into account: (1) there may be attenuation due to wet antennas, (2) mean rainfall intensities are simply calculated as the average of the minimum and maximum rainfall intensities, and (3) the large spatial rainfall variability, as indicated by Figs. 2 and 5, can cause overestimation for a link of this frequency (15.3 GHz) (Overeem et al., 2011).

3.3.4   Estimation of return period

While the rainfall event can easily be characterized as extraordinary based on the analysis in Sect. 3.3.2, the question remains what the occurrence probability of such an event is. Figure 3.6 shows a probability plot of 24-h rainfall depths, based on Overeem et al. (2008), who performed an extreme value analysis of rainfall depths from time series of 12 automatic rain gauges in The Netherlands (altogether 514 years of data). The concatenation of time series from the 12 stations to a single record of 514 years is justified according to Overeem et al. (2008). A rough estimate of the average return period of the 24-h rainfall depth for this event (based on automatic rain gauge and radar data), 160 mm (black square), is in the order of 6000 years for a given location.

When the extreme value analysis is repeated including the 160 mm rainfall depth, the average return period decreases to the order of 3000 years. Note that this hardly influences the quantiles of rainfall depths for average return periods up to about 100 years. Of course, these return periods are significantly larger than the return period of 160 mm being exceeded in 24 h at an arbitrary location in The Netherlands.

The uncertainties due to sampling variability have been shown to be large (Overeem et al., 2008). Using the bootstrap method the 95 % confidence interval was obtained. For the 24-h accumulation for a return period of 6000 years this interval ranges from 129 to 199 mm. Despite this large uncertainty, it is clear from Fig. 8 that the return period is well above 1000 years. The probability of such an event occurring at our experimental catchment between the start of the measurements in the 1960s and now is estimated to be about 0.8 %.
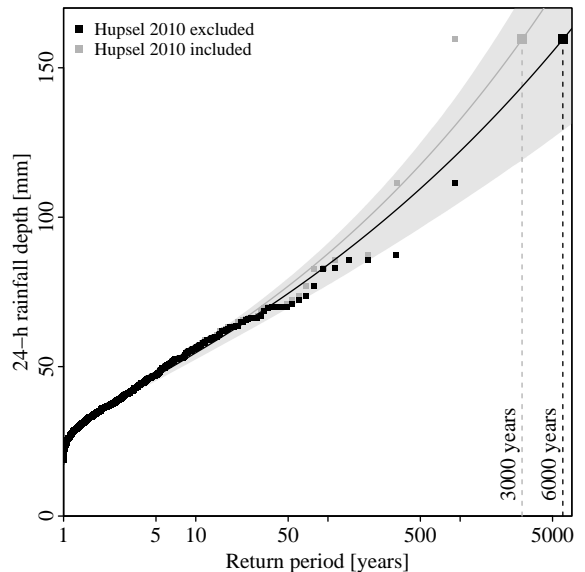
Figure 3.6: Probability plot with the GEV distribution fitted to annual 24-h rainfall maxima. The method of L-moments was used (Hosking and Wallis, 1997). Black points: the 514 ordered annual maxima from Overeem et al. (2008) plotted with the Gringorten plotting position. Grey points: same data including the recent Hupsel maximum. Lines: GEV fits. Larger black and grey squares: the 24-h accumulation of 160 mm and corresponding return periods. Grey-shaded area: the 95 % confidence interval based on the bootstrap method.

3.4   Hydrologic response

3.4.1   Soil moisture response

When rainfall infiltrates into the unsaturated zone, soil moisture can be expected to react before groundwater and runoff. Figure 3.7 shows the observed local response of soil moisture content. Before the rainfall event, the soil was relatively dry. The soil moisture content measured by the available sensor at 40 cm depth was initially 23 % and started to rise at 27 August, 07:00 UTC, 3 h after the start of the rainfall event. As a result of the first part of the rainfall event with moderate intensities (04:00–09:00 UTC) the soil moisture content rose slowly to 32 % at 10:00 UTC. Between 09:00 and 10:00 UTC 12 mm of rainfall was recorded, leading to a steep increase in soil moisture content up to 41 % at 11:00 UTC. Between 10:00 and 12:00 UTC there was hardly any rainfall and the soil moisture content remained constant, but between 12:00 and 13:00 UTC another 3.6 mm of rainfall occurred and the soil moisture content reached saturation (45 %) at 14:30 UTC. After that, the soil moisture content

slowly decreased, but remained above 40 % until 27 August, 19:30 UTC. The high soil moisture contents contributed to the strong groundwater table response. It should be noted that soil moisture contents returned to pre-event levels within 3 days.

3.4.2 Groundwater response

The depth and dynamics of the groundwater levels depend on the distance to ditches and drainpipes and on the microtopography (Van der Velde et al., 2010). In Fig. 3.7 groundwater depths are shown for 2 piezometers; one located in a local depression and one on a local elevation.

Initially, groundwater depths measured by two piezometers shown in Fig. 3.7 were 90 (depression) and 115 cm (elevation) below surface. Groundwater levels started to rise slowly at 11:30 UTC, more than 4.5 h after the initial increase in soil moisture content was observed. In the groundwater time series, the influence of single peaks in rainfall intensity is not visible. At 17:30 UTC, when groundwater levels were 48 and 88 cm below surface, groundwater rise accelerated. This was 7.5 h after the soil moisture content increase accelerated. Groundwater rise accelerated when soil moisture content increased, because less water could be stored in the unsaturated zone. In addition, rainfall intensity increased after 15:00 UTC and therefore more water was available to fill the pore spaces.

Around 20:15 UTC, the soil at the local depression became completely saturated and ponding occurred. Due to the larger available storage, it took until 22:45 UTC for the soil at the local elevation to become completely saturated. Ponding was less pronounced here likely due to water flowing into the local depressions. Because ponding did not occur, the groundwater level at the local elevations showed strong dynamics during and after rainfall events, while the groundwater level in the local depression remained above land surface for 6 days, with a maximum ponding depth of 11 cm. Similar ponding depths were also observed in the field during post-event field survey II, with many of the local depressions still filled.

During post-event field survey II, water was still flowing overland from the ponds in the fields to the ditches at several places. Overland flow is usually assumed to be of little importance in relatively flat areas, but can occur in lowland areas such as The Netherlands in case of high groundwater tables and/or high rainfall intensities (Appels et al., 2011). During post-event field survey II some farmers were seen digging small channels in the field to reduce ponding and transport the water to the ditches more quickly.

Uncertainty in interpreting these measurements arises mostly from sampling variability. Both soil moisture content and groundwater depth are highly variable in space. Therefore, these measurements do not provide the catchment representative soil moisture content or groundwater depth, but provide a mere indication of their local dynamics.

3.4.3 Spatial variation in saturation excess

The groundwater depth was on average 1559 mm before the rainfall event; a depth which is exceeded 96 % of the time. Because groundwater depths are not distributed uniformly in the Hupsel Brook catchment, we used the model by Van der Velde et al. (2009) to create a map of potential saturation excess as a proxy for surface runoff generation (Fig. 3.8).

With spatially variable initial groundwater depths, 59 % of the catchment area is saturated at the end of the rain storm (after 160 mm). This has consequences for the mean saturation excess after 160 mm (4 mm for uniform or 11 mm for variable initial groundwater depths) and therefore for ponding and surface runoff.

In the southeastern part of the catchment, the aquifer is less thick and the permeability of the soil is lower, leading to shallower initial groundwater levels and therefore to higher potential saturation excess values (see Fig. 3.8). During post-event field survey II, we observed a high outflow at the sub-catchment outlet (circle in Fig. 3.8) which drains this part of the catchment. Because no measurement devices were installed at that weir, unfortunately no quantitative information is available.

3.4.4 Discharge response

Discharge showed little to no response to the first 35 mm of rainfall which were absorbed in the soil. Discharge started to rise slowly 7 h after the start of the rainfall event. Within 23 h, from 26 August 04:15 UTC to 27 August 02:45 UTC, discharge increased from 4.4×10^{-3} $m^3 s^{-1}$ to the maximum observed value of $4.98 \, m^3 s^{-1}$, i.e., by more than three orders of magnitude. The discharge increased from 5.0×10^{-2} to $4.5 \, m^3 s^{-1}$ in 7 h. The most spectacular rise took place on 26 August between 17:30 and 22:30 UTC, when discharge increased from $0.42 \, m^3 s^{-1}$ to $4.0 \, m^3 s^{-1}$.

Discharge remained above $1 \, m^3 s^{-1}$ for 28 h and exceeded the 99th percentile ($0.46 \, m^3 s^{-1}$) for 4 days (Sect. 3.4.5). In Fig. 3.7e it seems that discharge has dropped to its pre-event level within days, but on a logarithmic scale (Fig. 3.7d) it can be seen that this would have taken weeks. On 3 September (at the end of the period shown in
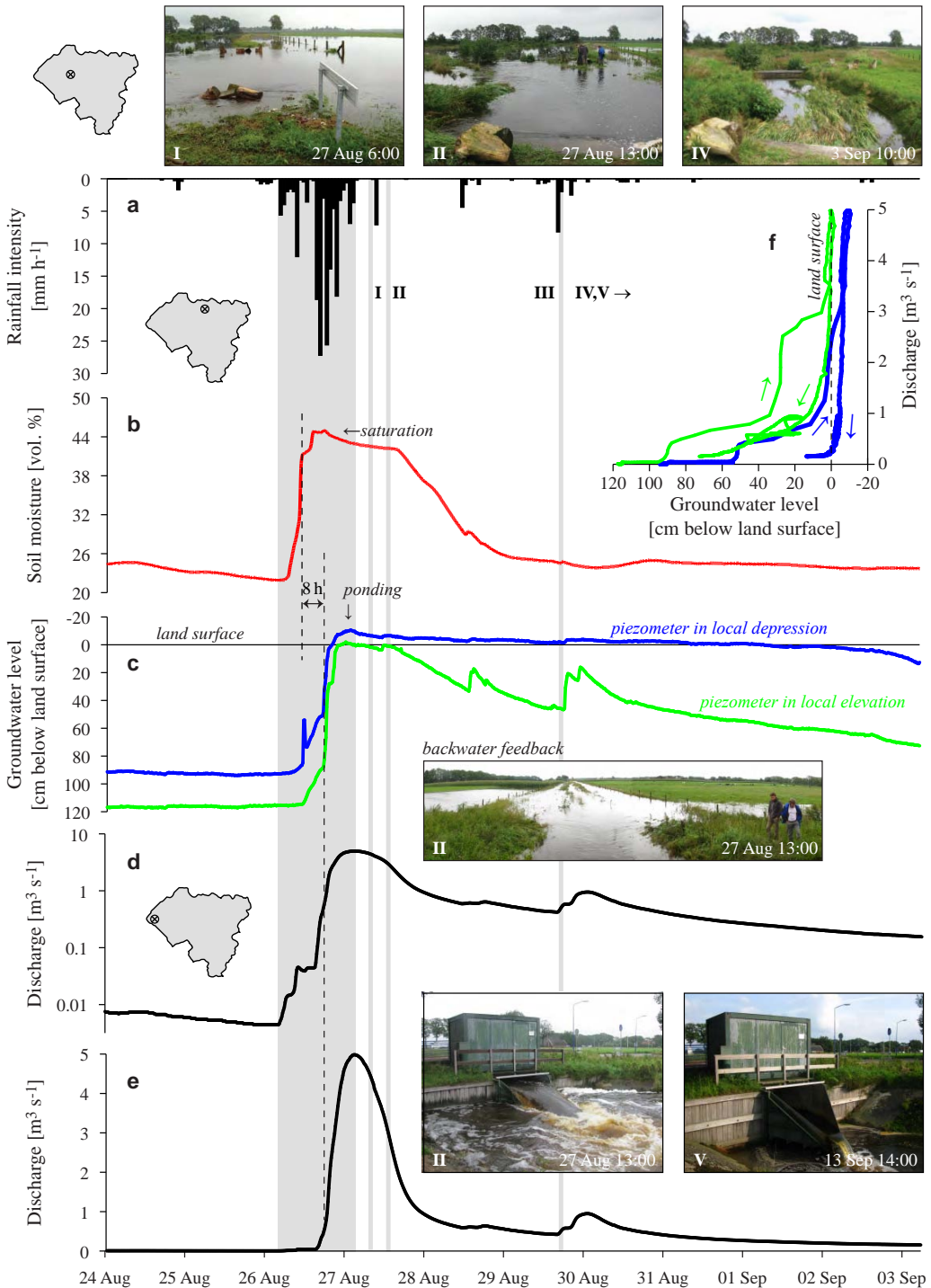
Figure 3.7: Hydrological response of the Hupsel Brook catchment to the 26 August 2010 rainfall. **(a)** hourly rainfall depths measured with the automatic rain gauge (gaps filled with radar estimates), **(b)** soil moisture content at 40 cm depth, **(c)** groundwater level in two piezometers, **(d)–(e)** discharge at the catchment outlet on logarithmic and linear axes, and **(f)** relation between discharge and groundwater depth. The grey band indicates the rainfall period. The roman numbers and grey lines indicate the post-event field surveys (Table 3.1). The small catchment maps show (1) the location of the three upper photos, (2) the location of the rainfall, soil moisture and groundwater measurements and (3) the location of the catchment outlet and the three lower photos.

Fig. 3.7) discharge was still $0.15\,\mathrm{m^3\,s^{-1}}$; a value which is exceeded only 10 % of the time.

Between 26 August and 7 September, 184 mm of rainfall were recorded (by the automatic rain gauge, with data gaps filled with gauge-adjusted radar data). In the same period 92 mm were discharged, yielding a runoff ratio of 50 %. The other 50 % has been stored in the soil ($\sim$70 mm) or has evaporated (20–25 mm).

There are some constructions in or around the brook which become obstacles in case of high discharges. The most important structures influencing the flow regime are the culverts. When discharge exceeds the design discharge of the culverts, a much larger head difference is needed between both sides of culvert, leading to floods upstream of the culvert in the brook or on the floodplain. Just 100 m upstream of the catchment outlet a culvert with a design discharge of about $5\,\mathrm{m^3\,s^{-1}}$ is located, which likely limited the discharge peak at the flume to about $5\,\mathrm{m^3\,s^{-1}}$.

When catchment storage increases, the dense network of drainpipes and ditches becomes more important. Before the rainfall event, groundwater levels were below the level of drainpipes, tertiary ditches and most of the secondary ditches. The drainage network was therefore not fully used and water was mostly transported through the subsurface and therefore relatively slowly. When groundwater levels rose, drainpipes and ditches started to transport water, leading to an increase in discharge capacity and in discharge itself. Without this drainage network, ponding depths and the resulting damage would have been larger in the Hupsel Brook catchment.

The peak of $4.98\,\mathrm{m^3\,s^{-1}}$ corresponds to a specific discharge of $0.77\,\mathrm{m^3\,s^{-1}\,km^{-2}}$, or $2.8\,\mathrm{mm\,h^{-1}}$, which is exceptional for a small catchment with an average slope of only 0.8 %. We applied the extreme value analysis of Sect. 3.3.4 to the discharge peak, using a Gumbel distribution. The 95 %-confidence interval of the highest discharge in the period 1969–2009, $21\,\mathrm{mm\,d^{-1}}$ (return period of 98 years) is already large: 18–$25\,\mathrm{mm\,d^{-1}}$. Because of this, the relatively limited number of years for which discharge data are available prevent an accurate estimation of the return period of the peak discharge of $42\,\mathrm{mm\,d^{-1}}$, which is almost twice as large.

3.4.5 Discharge regime and previous extreme discharges

It is relevant to put the 27 August discharge peak, as well as the conditions prior to 26 August, into historical perspective. Based on a time series of mean daily discharge from 1969 to 2010 some statistics have been computed. Mean discharge at the out-

let of the Hupsel Brook catchment is $0.06\,\mathrm{m^3\,s^{-1}}$ ($0.8\,\mathrm{mm\,d^{-1}}$). During 1 % of the time $0.17\,\mathrm{m^3\,s^{-1}}$ is exceeded and during 0.1 % of the time $0.92\,\mathrm{m^3\,s^{-1}}$ is exceeded. In the last decade of August (20–31 August), mean discharge is $0.016\,\mathrm{m^3\,s^{-1}}$ and during 10 % of the time $0.043\,\mathrm{m^3\,s^{-1}}$ is exceeded.

Sometimes there is no or hardly any discharge. During 10 % of the days in the last decade of August $1.1 \times 10^{-3}\,\mathrm{m^3\,s^{-1}}$ is not reached. Before the start of this rainfall event, discharge was $4.4 \times 10^{-3}\,\mathrm{m^3\,s^{-1}}$, a value which is exceeded 81 % of the days overall and on 45 % of the days in the last decade of August. A discharge of $4.4 \times 10^{-3}\,\mathrm{m^3\,s^{-1}}$ is therefore low in terms of the mean for the end of August, but it is not exceptional.

Since 1969, a daily mean discharge of $1\,\mathrm{m^3\,s^{-1}}$ was exceeded six times (including this event). In Fig. 3.10 time series of cumulative precipitation and discharge are shown for these events. Compared to these previous events, the initial discharge on 26 August 2010 was about 50 times smaller. The low initial discharge and storage made it possible that a 4 times larger precipitation event led to "just" a 2 times larger discharge peak. The difference in initial discharge is clearly visible in the hydrograph on logarithmic y-axis (bottom). This graph also shows that on 26 August 2010 the first 78 mm of rainfall were used to increase the discharge to the initial discharge level of the previous events.

3.5 Synthesis of the hydrologic response

In many catchments, a close relation exists between the discharge at the outlet and the total amount of mobile water stored in the catchment (e.g., Kirchner, 2009; Teuling et al., 2010). While storage cannot be measured directly at the catchment scale, storage changes can be calculated by using the water balance over periods during which all fluxes are known. In case of the Hupsel flash flood, the contribution of evapotranspiration to the water balance is negligible around the discharge peak. Rainfall measured at the meteorological station may be considered representative for the whole $6.5\,\mathrm{km^2}$ catchment. Hence, storage S can be calculated with respect to an arbitrary reference level S_0 by integrating the difference between rainfall P and discharge Q over time t:

$$S \;=\; S_0 \;+\; \int_{t=t_0}^{t} (P - Q)\,\mathrm{d}t. \qquad (3.1)$$

In Fig. 3.9 both discharge and groundwater levels are plotted against total catchment storage as calculated by Eq. (3.1) for the period between 25 August 18:00 UTC and 27 August 18:00 UTC.
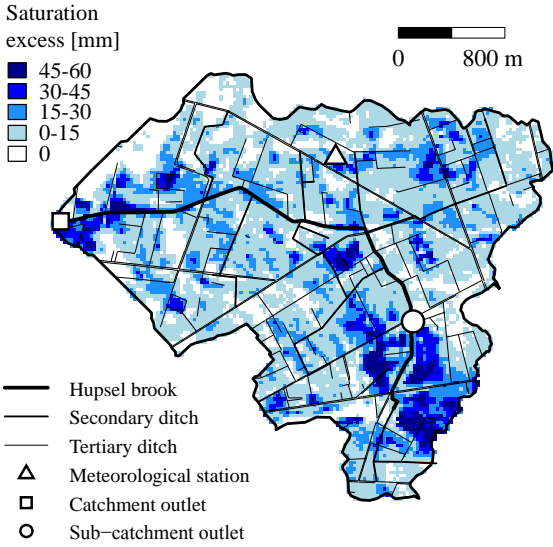
Figure 3.8: Potential saturation excess, computed from the initial groundwater level, a specific storage of 10 % and the total amount of rainfall of 160 mm.
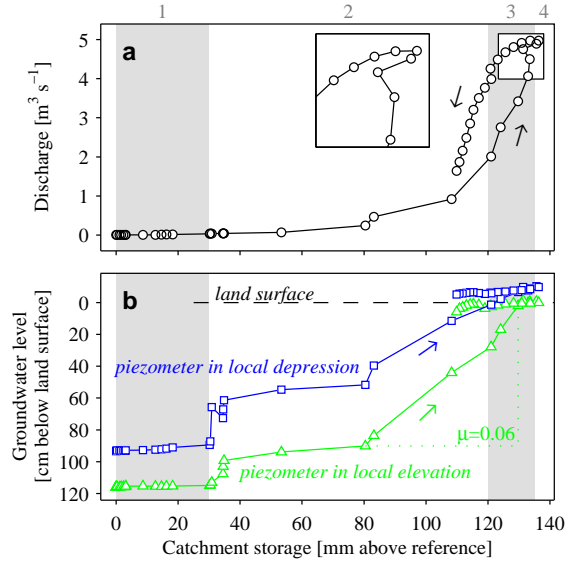
Figure 3.9: Discharge at the outlet (upper panel) and local groundwater level (lower panel) as a function of estimated catchment storage for the period 25 August, 18:15 UTC to 27 August, 18:00 UTC. Points are drawn for each hour. The grey and white bands denote the four stages.
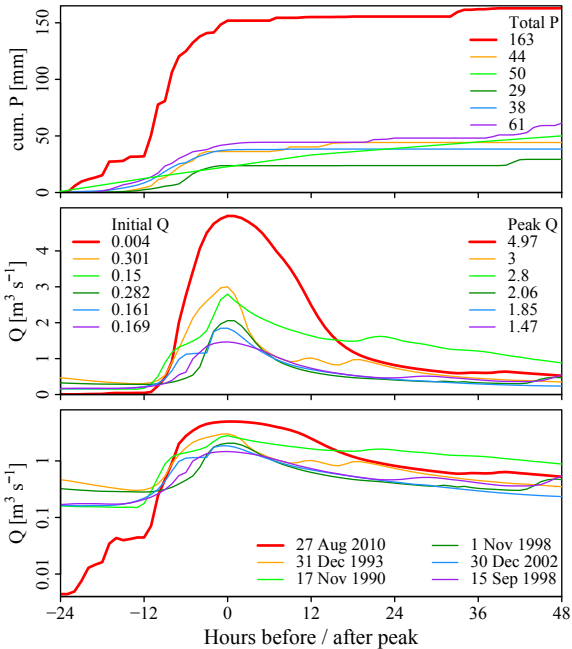
Figure 3.10: Cumulative precipitation (top) and discharge on linear (middle) and logarithmic axis (bottom) of the six highest discharges since 1969.

Figure 3.11: The role of culverts during the 27 August 2010 flash flood. The roman numbers indicate the post-event field surveys (Table 3.1). Upper panels: Situation directly after the flood. Upwelling water reveals the exit of the submerged culvert. The resulting backwater feedback allows water to bypass the obstacle on the right by flowing over the road and the adjacent field back into the brook (arrows). Lower left panel: upstream entry of the culvert. Logs (black arrows) deposited by flood and flow marks in grass (upper left panel) indicate that water flowed over the culvert at flood peak. Lower right panel: situation two weeks after flood with flood marks indicated. The photos in the top panels of Fig. 3.7 are taken from the same location as the photos in this figure, but in upstream rather than downstream direction.

When interpreting the lines in Fig. 3.9 it should be noted that water can be stored in the catchment in different ways: (1) as soil moisture in the unsaturated zone, (2) as groundwater in the saturated zone, (3) as ponds in local depressions on the fields or (4) as surface water in the brook or on banks and land surface in the floodplain. The subsequent filling of these storages, along with the interaction between them, ultimately determines the catchment response during the onset and peak of the flood. We hypothesize that the discharge dynamics at the catchment outlet reflects the following stages, each of which has a different sensitivity of discharge to storage changes:

1. *Soil moisture reservoir filling* – initially the upper part of the soil is dry, and rainfall is readily absorbed in the unsaturated zone. This leads to an increase in soil moisture content, but a lack of conductivity prevents groundwater levels from rising in conjunction with soil moisture. As a result, the discharge during this phase is hardly sensitive to storage changes up to a storage increase of ∼30 mm.

2. *Groundwater response* – the unsaturated zone is near saturation and additional rainfall readily leads to saturation of the soil matrix. Under these conditions the specific yield μ is very small (0.06 over a large part of the storage increase in Fig. 3.9) and groundwater levels can rise rapidly. Since groundwater levels strongly control the field-scale subsurface flow to the network of secondary and tertiary ditches, the discharge is moderately sensitive to changes in total catchment storage. The rapid rise of groundwater levels continues up to a storage increase of ∼120–130 mm, when groundwater levels reach the surface and ponding occurs.

3. *Surface depression filling and surface runoff* – when ponding occurs, two mechanisms come into play with contrasting effects on the discharge increase. First, the specific yield strongly increases (since for ponded areas $\mu = 1$), effectively reducing the increase in hydraulic heads in response to rainfall. Secondly, however, when ponds start to connect to the network of ditches, overland flow becomes an important runoff mechanism and discharge increases rapidly. This is a typical mechanism during flash floods, and the moment at which overland flow is initiated determines for a large part the timing of flash flood response (Marchi et al., 2010). This is also the case in the Hupsel Brook catchment. The slope of the line in Fig. 3.9a is very steep between total catchment storage of 120 mm and 135 mm. Measured groundwater levels indicate phreatic surfaces extending

to above the local height of the land surface (which was confirmed by observations during post-event field surveys).

4. *Backwater feedback* – in the fourth phase discharge increases to above the design discharge of the culverts, leading to backwater feedbacks and extensive flooding of fields upstream of the culverts (Fig. 3.11). Such flooding was observed during post-event field surveys I and II (Fig. 3.7), especially in the area with elevations below 26 m (Fig. 2.1). The backwater effects strongly reduce the local pressure gradients that drive the flow of water through the subsurface. At the same time, they flatten the discharge peak. Figure 3.9 shows that high discharge levels persist during the decrease of the initial 20 mm of storage – consistent with the role of backwater.

Because initial groundwater levels, initial soil moisture contents, hydrogeology and land use vary spatially over the catchment, the timing of the different phases also varies spatially. During post-event field survey II more flooding was visible in the southeastern part of the catchment, where the aquifer is thinner and groundwater levels shallower than in the western part. Therefore these phases cannot be separated exactly in Fig. 3.9. Nevertheless, these four stages appear to describe the observed hydrological response of the Hupsel Brook catchment to the extraordinary rainfall of 26 August 2010 well.

The stages resemble the stages identified by Maréchal et al. (2009), who described a flash flood response in a karstic area. Here, a first rainfall event only caused soil saturation but a second caused a flash flood due to overland flow. In addition, Maréchal et al. (2009) reported on backwater feedbacks at locations with limited discharge capacity.

We believe that because of the rapid increase in runoff during stage 3, in combination with the extremity of the rainfall, the magnitude of the specific discharge peak, the local flooding and widespread surface runoff, this runoff event is best characterized as a lowland flash flood.

3.6 Conclusion

On 26 August 2010 the eastern part of The Netherlands was struck by a series of very heavy rainfall events leading to unprecedented peak discharges.

Rainfall was measured in the Hupsel Brook catchment with rain gauges (one automatic and one manual), a weather radar and a microwave link. The maximum 24-h rainfall depth was 160 mm. This rainfall depth corresponds to an estimated return period of more than 1000 years. The temporal dynamics of rainfall intensities measured by the microwave link

compare well to those of radar rainfall intensities averaged over the path of the microwave link, which proves that this alternative source of rainfall data can be used in extreme situations. This may provide opportunities for poorly equipped catchments.

This rainfall event lead to a catchment response that is best described as a lowland flash flood, because of the extremity of the rainfall and the widespread surface runoff. Discharge at the catchment outlet increased from $4.4 \times 10^{-3}\,\mathrm{m}^3\,\mathrm{s}^{-1}$ to nearly $5\,\mathrm{m}^3\,\mathrm{s}^{-1}$ (i.e. a specific discharge of $0.77\,\mathrm{m}^3\,\mathrm{s}^{-1}\,\mathrm{km}^{-2}$, or $2.8\,\mathrm{mm}\,\mathrm{h}^{-1}$). Although this event was extreme, a detailed analysis has revealed that discharge has been measured relatively accurately.

We found that the catchment response can be divided in four stages:

1. *Soil moisture reservoir filling* – water is used to replenish soil moisture and discharge hardly rises.

2. *Groundwater response* – groundwater levels rise and discharge rises slowly.

3. *Surface depression filling and surface runoff* – ponds form in local depressions on the land surface, leading to surface runoff and rapid rise of discharge.

4. *Backwater feedback* – brook discharges exceed maximum discharge capacity of culverts in the brook. Water is stored behind the culverts, discharge hardly increases and local gradients that drive subsurface flow are reduced.

During this extreme event some thresholds became apparent that do not play a role during average conditions. Culverts hardly influence the rainfall-runoff characteristics in average situations, but become an important factor in case of high discharges, when discharges reach a ceiling and groundwater gradients are reduced. Often rainfall-runoff models are designed and calibrated with less extreme discharge data and then used to forecast peak flows. In these models, thresholds are not taken into account and as a consequence peak discharges are overestimated. Incorporation of such thresholds in hydrological models is currently being performed and shall be reported in future work.

Low initial catchment storage acted as a soil buffer and reduced the magnitude of the hydrologic response. The first 35 mm of rainfall were stored in the soil without a significant increase in discharge. Compared to the 5 highest discharge peaks since the 1960s, the initial discharge was 50 times smaller, which resulted in "just" a 2 times larger discharge peak after a 4 times larger rainfall event. These results show that for flood prediction, information on the initial hydrological state of the catchment can be as important as rainfall forecasts.

4 | Storage-discharge relations

elations between storage and discharge are essential characteristics of many rainfall-runoff models. The simple dynamical systems approach, in which a rainfall-runoff model is constructed from a single storage-discharge relation, has been successfully applied to humid catchments. Here, we investigate (1) if and when the less humid lowland Hupsel Brook catchment also behaves like a simple dynamical system by hydrograph fitting, and (2) if system parameters can be inferred from streamflow recession rates or more directly from soil moisture storage observations. Only 39 % of the fitted hydrographs yielded Nash-Sutcliffe efficiencies above 0.5, from which we can conclude that the Hupsel Brook catchment does not always behave like a simple dynamical system. Model results were especially poor in summer, when evapotranspiration is high and the thick unsaturated zone attenuates the rainfall input. Using soil moisture data to obtain system parameters is not trivial, mainly because there is a discrepancy between local and catchment storage. Parameters obtained with direct storage-discharge fitting led to a strong underestimation of the response of runoff to rainfall, while recession analysis lead to an overestimation.

4.1 Introduction

In most catchments, discharge depends strongly on the total amount of water stored. Head differences cause groundwater to flow towards channels and quick runoff processes such as overland flow, subsurface stormflow or drainpipe flow occur only when the catchment is sufficiently wet. Because the relation between storage and discharge is essential to describe runoff generating processes, it is a major component of most rainfall-runoff models: in physically-based models groundwater flow is computed from differences in groundwater levels between cells, conceptual models contain one or more reservoir components, and in the simplest models the whole catchment is represented as one (non)linear reservoir.

It would be advantageous if the storage-discharge relation could be easily derived from a limited amount of observations or catchment characteristics, which would allow application in the desired model without calibration. This has been a hydrological research topic for many decades. Brutsaert and Nieber (1977) investigated discharge recession curves, Kirchner (2009) used system parameters obtained with recession analysis in a simple hydrological model and Teuling et al. (2010) used this model to obtain system parameters by means of calibration. There are many other studies in which storage-discharge relations have been found by means of discharge (recession) analysis, but a more obvious approach, namely using storage data directly, is not known to the authors. However, local storage computed with a groundwater model has been used in direct storage-discharge fitting (Rupp et al., 2009). Examples of studies in which solutions to the Boussinesq equation for sloping aquifers have been em-

ployed in order to investigate storage-discharge relations are Troch et al. (1993), Brutsaert (1994) and Rupp and Selker (2006b). We refer to the review article by Troch et al. (2013) and references therein for a more complete overview.

While storage-discharge relationships have been investigated in detail for mountainous catchments and in humid climates, it is unclear whether the approach can be extended to lowland catchments or less humid climates. Lowland catchments cover an extensive part of the world's most densely populated areas and therefore adequate discharge forecasts in these catchments are of large societal and economic value. Kirchner (2009) used the Plynlimon catchment (runoff ratio = 0.79) to illustrate his simple dynamical systems approach, in which a nonlinear reservoir model is based on the storage-discharge relation. Teuling et al. (2010) applied this approach to the slightly less humid Rietholzbach catchment (runoff ratio = 0.73), where the approach worked well during wet conditions, but failed during dry summers.

Here, we investigate (1) if and when the less humid lowland Hupsel Brook catchment (runoff ratio = 0.39) also behaves like a simple dynamical system by hydrograph fitting, and (2) if system parameters can be inferred from discharge recession rates or, more directly, from biweekly profile soil moisture observations. We compare system parameters estimated using different methods and seasons, and their associated uncertainties and we evaluate the applicability of storage data for direct storage-discharge fitting.

For this Chapter, data from the Hupsel Brook catchment have been used: all hourly data of precipitation P, potential evapotranspiration ET_{pot} and discharge Q, and soil moisture contents and groundwater levels measured biweekly at 6 sites from 1976

through 1984 (for locations, see Fig. 2.1). The catchment and measurement techniques are described in detail in Sect. 2.1. The Hupsel Brook catchment is less humid than the catchments to which the simple dynamical systems approach has been applied before. Evapotranspiration dynamics have a large impact on catchment storage and consequently on runoff processes and the discharge response to rainfall (see Sect. 2.3). We used this difference to evaluate the relation between wetness and model performance, which might be extrapolated to drier catchments.

4.2 Methodology

4.2.1 Combining storage-discharge relationship and water budget into a simple hydrological model

Recently, Kirchner (2009) analyzed the relation between catchment storage and discharge of two small, humid, and hilly catchments and proposed a method to use this relation in a simple hydrological model. Because his method plays a central role our study, the principles are explained in this section. For the relationship between discharge (Q) and storage (S),

$$Q = f(S) , \qquad (4.1)$$

it is assumed that f is a strictly monotonically increasing function (i.e. no hysteresis), that all Q originates from storage and that flow routes (e.g., macropore flow, overland flow) are only related to catchment storage and not to rainfall intensity.

Under these assumptions the sensitivity of Q to changes in S, $f'(S)$, is expressed solely as a function of Q through the so-called discharge sensitivity function $g(Q)$:

$$g(Q) = \frac{\mathrm{d}Q}{\mathrm{d}S} . \qquad (4.2)$$

When the numerator and denominator of the right-hand side are both divided by $\mathrm{d}t$, and $\mathrm{d}S/\mathrm{d}t$ is replaced with the other terms of the water budget equation ($P - ET_{\mathrm{act}} - Q$), the change of discharge over time can be computed as

$$\frac{\mathrm{d}Q}{\mathrm{d}t} = g(Q) \, (P - ET_{\mathrm{act}} - Q) . \qquad (4.3)$$

This implies that at a given initial storage, a certain change in storage (caused by P, ET or Q) should always lead to the same discharge response, both in timing and magnitude.

When $P = 0$ and $ET_{\mathrm{act}} = 0$, the sensitivity function $g(Q)$ can be obtained from data by plotting the recession rate $-\mathrm{d}Q/\mathrm{d}t$ against Q. In several studies power law relations between Q and $-\mathrm{d}Q/\mathrm{d}t$ have

been found (e.g. Brutsaert and Nieber, 1977):

$$-\frac{\mathrm{d}Q}{\mathrm{d}t} = g(Q) \cdot Q = a \cdot Q^b , \qquad (4.4)$$

where $b = 1$ corresponds to a linear reservoir. To obtain recession coefficients a and b, we used three techniques: hydrograph fitting (sec. 4.2.2), recession analysis (sec. 4.2.3) and direct estimation using soil moisture data (sec. 4.2.4).

To simulate the streamflow hydrograph, we substitute $g(Q)$ from eq. (4.4) (aQ^{b-1}) in eq. (4.3):

$$\frac{\mathrm{d}Q}{\mathrm{d}t} = a \cdot Q^{b-1} \cdot (P - ET_{\mathrm{act}} - Q) . \qquad (4.5)$$

Because this equation can lead to numerical instabilities when integrated, eq.(4.5) is solved in terms of the logarithm of Q. In addition, a parameter f is used to account for the difference between ET_{pot} and ET_{act}:

$$\frac{\mathrm{d}(\ln Q)}{\mathrm{d}t} = a \cdot Q^{b-1} \cdot \left(\frac{P - f \cdot ET_{\mathrm{pot}}}{Q} - 1 \right) . \qquad (4.6)$$

Eq. (4.6) was solved numerically with a 4th order Runge-Kutta integration scheme. Observed Q at $t = 0$ was taken as starting value for modeled Q. To avoid numerical instability when ET becomes several orders of magnitude larger than S, we introduced a fixed lower limit for Q ($10^{-5}\,\mathrm{mm\,h^{-1}}$).

4.2.2 Method 1: hydrograph fitting

This method is largely similar to standard rainfall-runoff model calibration and explores the potential of the simple hydrological model for this catchment. For this method, we fitted the discharge modeled with eq. (4.6) to the observations by optimizing a, b and f for each month without data gaps (consistent with Teuling et al. (2010)). We also removed months with snow events from the analysis. We used the quasi-Newtonian optimization method of Byrd et al. (1995) and the sum of squares of Q as objective function. When the Nash-Sutcliffe efficiency of the fit was above 0.5, we plotted a line segment with slope b and intercept $\ln a$ in a ($Q, -\mathrm{d}Q/\mathrm{d}t$)-plot with logarithmic x- and y-axes, along the range of Q values measured during that month, following the method of Teuling et al. (2010). The line segments were converted into points which are equally spaced on the logarithmic x-axis. A line was fitted through these points by minimizing the sum of squares (with linear regression between $\ln Q$ and $\ln(-\mathrm{d}Q/\mathrm{d}t)$) to obtain the overall values for a and b. To investigate the effect of choice of fitting method, we also used the sum of squares of $\ln Q$ as objective criterion for the hydrograph fitting and nonlinear regression between Q and $-\mathrm{d}Q/\mathrm{d}t$.

4.2.3 Method 2: recession analysis

In this method, the parameters are not optimized globally, but obtained from discharge data from selected periods, following the approach of Kirchner (2009). From the total data set, periods without P and ET were selected. In practice this implied that a measurement Q_t was selected if $P = 0$ between hours $t-3$ and t and if global radiation was zero at $t-1$ and t. Intervals with precipitation in the preceding three hours were excluded because we wanted to avoid cases of overland flow. It is assumed that $ET = 0$ when there is no global radiation. Because discharge measurements are discrete, the change of discharge over one hour is often zero ($\sim 60\%$ of the selected points). Therefore, we increased the interval length n whenever $-(Q_{t+n\Delta t} - Q_t)/(n\Delta t) = 0$ until a change in discharge was observed (and all other conditions still hold), following Rupp and Selker (2006a).

Recession rates $-(Q_{t+n\Delta t} - Q_t)/(n\Delta t)$ are plotted against discharges $(Q_{t+n\Delta t} + Q_t)/2$ in a double logarithmic graph. Following the procedure of Kirchner (2009), data points (including negative values) have been collected in bins and within the bins means and standard errors of $-\mathrm{d}Q/\mathrm{d}t$ were computed. In these bins, points with values of $-\mathrm{d}Q/\mathrm{d}t \leq 0$ were included because they probably result from random measurement errors. If only measurement errors resulting in $-\mathrm{d}Q/\mathrm{d}t \leq 0$ would be removed, a bias would be introduced. The size of the bins was first set at 1% of the logarithmic range of Q, but was gradually increased when the logarithm of the standard error of $-\mathrm{d}Q/\mathrm{d}t$ within the bin was larger than 0.5. A linear regression line was fitted through logarithms of the means of Q and $-\mathrm{d}Q/\mathrm{d}t$ within the bins to estimate a and b (taking Q as independent variable). In addition, a nonlinear regression line was fitted through the original values to investigate the effect of the choice of fitting in log space.

4.2.4 Method 3: direct storage-discharge fitting

Through this method, we investigate if profile soil moisture measurements can be used to derive system parameters directly by fitting a relation between storage and discharge. For each soil moisture measurement location and time, total storage in the top 360 cm of soil was computed. The value of 360 cm was chosen because groundwater never dropped below this depth at any of the sites and therefore all variation in both saturated and unsaturated storage was taken into account. To obtain a vertical profile of volumetric water content, we used the top measurement as representative for the upper 5 cm of soil and interpolated between the measurements in

the range from 5 to 210 cm. For each location, the temporal maximum soil moisture content measured at 210 cm depth was assumed to be the soil moisture content at saturation (θ_{sat}). When groundwater levels were less than 210 cm deep, we used θ_{sat} for the remaining 210 cm to 360 cm depth. When groundwater levels were below 210 cm, we interpolated linearly between the soil moisture measurement at 210 cm depth and θ_{sat} at the groundwater table and used θ_{sat} below the groundwater table.

If a power law between Q and $-\mathrm{d}Q/\mathrm{d}t$ is assumed (eq. (4.4)), eq. (4.1) can be solved explicitly (Kirchner, 2009):

$$Q = [(2-b)a(S-S_0)]^{1/(2-b)} , \qquad (4.7)$$

where S_0 is the limit representing the residual storage when discharge becomes zero (if $b < 2$) or the upper limit of storage when discharge goes to infinity (if $b > 2$). In an $(S, \ln Q)$-plot, a determines the slope, b the curvature and S_0 moves the curve horizontally across the (arbitrarily chosen) S-axis. When $b = 2$, the relation between storage and discharge reduces to

$$Q = Q_{\mathrm{ref}}\, e^{a(S-S_0)} , \qquad (4.8)$$

where S_0 is the storage when discharge equals the arbitrary reference discharge Q_{ref}.

For each location, total storage was plotted versus the discharge measured at the catchment outlet at noon on the same day (as the exact timing of the soil moisture measurements was unknown). To find the best values of a, b and S_0, the quasi-Newtonian optimization function by Byrd et al. (1995) has been used again, both for $b = 2$ and $b \neq 2$ and as objective function both the sum of squares of Q and $\ln Q$ (leading to 4 results per data set). Note that the period for which soil moisture data were available is much shorter than the period used for hydrograph fitting and recession analysis.

4.2.5 Seasonal variability and sampling uncertainty

To examine the effect of seasonality regarding water budget terms and hydrological processes on the obtained recession coefficients, the data set has been split into four seasonal data sets: winter (Dec–Feb), spring (Mar–May), summer (Jun–Aug) and autumn (Sep–Nov). All analyses described in the previous sections have been repeated for each of these seasonal data sets.

To examine the sampling uncertainty of parameters a and b, the bootstrap technique has been employed (Efron and Tibshirani, 1993). From an original data set of length N, being (1) months for which hydrographs were fitted, (2) selected discharges ($(Q_{t+n\Delta t} + Q_t)/2$) with corresponding reces-
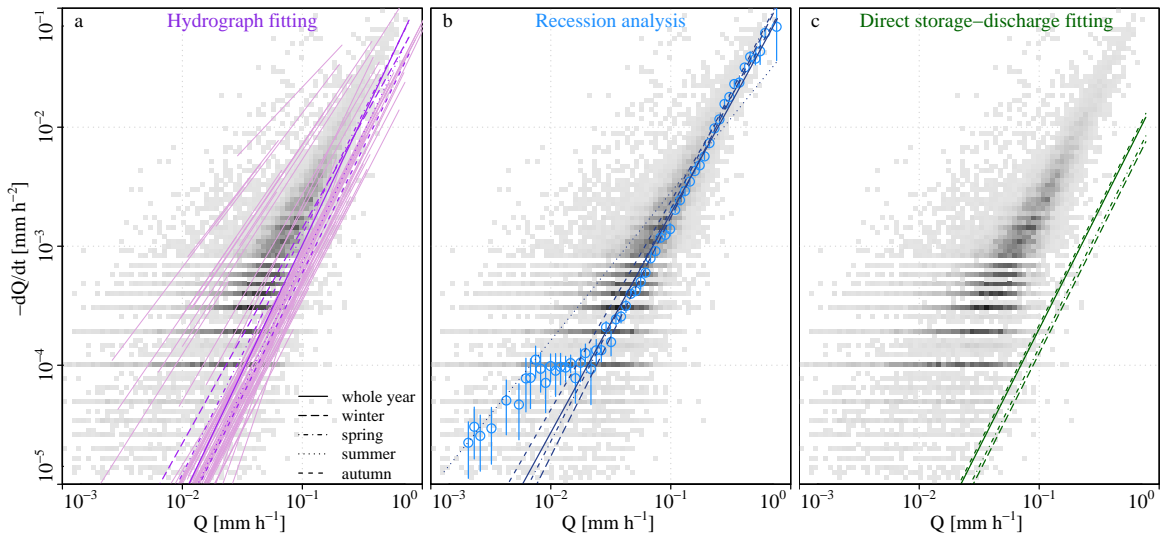
Figure 4.1: Dependency of recession rate on discharge for the three methods to obtain the storage-discharge relation. **(a)** Line segments of all fitted hydrographs and their regression lines. **(b)** Means and standard errors of bins and regression lines found in the recession analysis. **(c)** Regression lines found from a direct fit of total storage at the meteorological station and discharge. Grey shades indicate recession analysis data points (horizontal stripes are caused by discrete measurements).
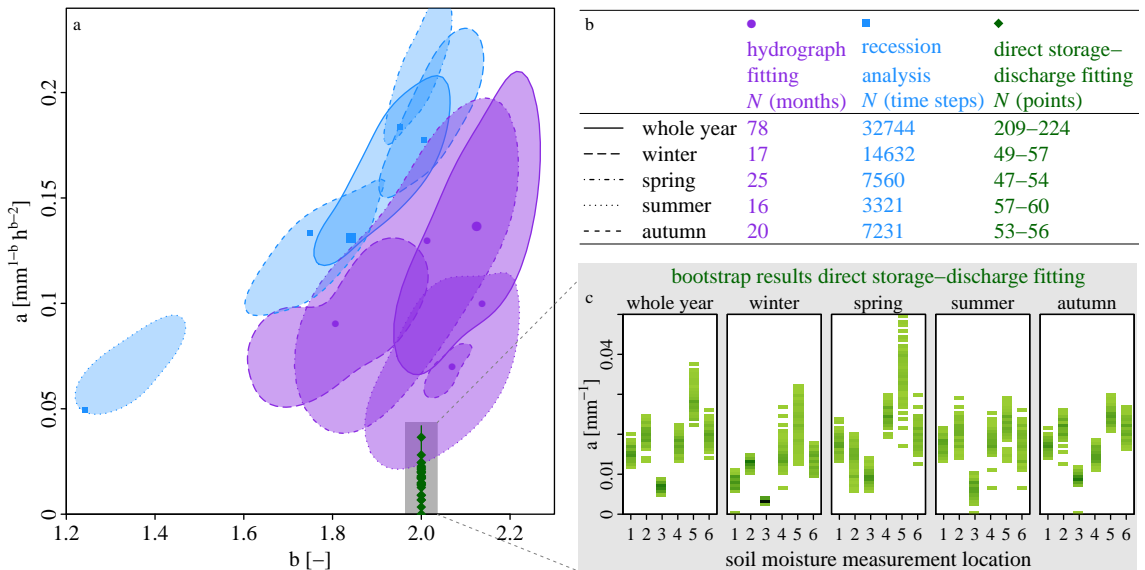
Figure 4.2: The effect of seasonality and sampling uncertainty on the parameters of the power-law storage-discharge relation for the three methods presented in Figure 4.1. **(a)** Values of a and b found for each method and seasonal data set (points). The clouds of a and b values are represented by the contour lines encompassing 40 % of the probability mass estimated using kernel densities (Wand and Jones, 1995). **(b)** Size of each data set (number of months used for hydrograph fitting, time steps in recession analysis and points in (S,Q)-fit). **(c)** Results from storage-discharge fitting are further specified in the bottom right plots: the values of a found in the bootstrap analysis (with $b = 2$) for each season and each soil moisture measurement location (ordered from high (1) to low (6) transmissivity).

sion rates ($-(Q_{t+n\Delta t} - Q_t)/(n\Delta t)$) or (3) soil moisture measurements with corresponding discharge measurements, N points were randomly sampled with replacement and used to obtain a and b. This exercise has been repeated 100 times, leading to 100 combinations of a and b. To make the comparison between the different (seasonal) data sets for a given method more objective, the length of the smallest data set for each method was taken as N for all data sets.

4.3 Results and discussion

4.3.1 Results of hydrograph fitting and performance of the simple dynamical systems approach

The results of the three methods are combined in Figs. 4.1 and 4.2 to allow easy comparison. In Fig. 4.2, we show the statistical dependency between fitted a and b. All line segments and the resulting regression lines for each seasonal data set are plotted in Fig. 4.1a. The parameter b (the slopes of the lines in Fig. 4.1) ranges from 1.8 (winter data set) to 2.1 (summer data set). The cloud of parameter values a and b are not uniformly distributed in the parameter space (Fig. 4.2): a line with large a and b will be steeper in Fig. 4.1 than a line with small a and b, but both go through the center of the cloud of data points. Note that the value of a depends on the units of Q employed: when units of Q are multiplied with a factor c, the values of a are multiplied with a factor c^{1-b}.

We can conclude that in the Hupsel Brook catchment discharge depends on storage (as $b \neq 0$) and that it is not well represented by a linear reservoir (as $b \neq 1$). It is not surprising that storage and discharge are closely linked, even though in the Hupsel Brook catchment, as in most densely populated lowland areas around the world, runoff generation is strongly influenced by an intensive artificial drainage network. Discharge, which is the combined effect of different flowpaths, is in the same manner storage-dependent in artificial as in natural drainage networks: when catchment storage increases, certain flowpaths will be activated, be it macropores or drainpipes.

The degree of nonlinearity varies seasonally. One of the assumptions of the simple dynamical systems approach is that it does not matter whether water leaves the system via drainage or evapotranspiration, while in different environments or climates these two processes might have a different effect on the composition of total storage (distribution over saturated and unsaturated zone), leading to a different reaction to rainfall events. For example, when the topsoil is dry due to high ET rates, infiltrating water will not affect Q directly due to a limited connectivity in the unsaturated zone.

Table 4.1: Results of hydrograph fitting (global and per season): number of fits (N) and percentage of fits with Nash-Sutcliffe efficiencies (NS) above 0.5, 0.75 and 0.9.

	N	NS> 0.5	NS> 0.75	NS> 0.9
whole year	173	39 %	19 %	1 %
winter	28	43 %	21 %	0 %
spring	38	61 %	29 %	5 %
summer	47	32 %	15 %	0 %
autumn	36	47 %	25 %	0 %

In general, the performance of the rainfall-runoff model (eq. (4.6)) was rather poor: of all fitted monthly hydrographs, 39 % had a Nash-Sutcliffe efficiency above 0.5 and 19 % above 0.75 (Table 4.1). From this we can conclude that the Hupsel Brook catchment does not often behave like a simple dynamical system. Model results were especially poor in summer, when evapotranspiration is high and the unsaturated zone plays an important role in attenuating the rainfall input. The fixed lower limit on Q we introduced to avoid negative discharges prevents the model from collapsing in summer, but does not lead to satisfactory results.

For each fit with Nash-Sutcliffe efficiency above 0.5, we plotted a line segment in a ($Q, -dQ/dt$)-plot with double logarithmic axes to obtain the overall a and b. The line segments seem to overlap relatively well, but the sampling variability as obtained with the bootstrap analysis is quite large, indicated by the 40 % contour line of the kernel density in Fig. 4.2 (note that sample sizes differ between methods). Fitting hydrographs using the minimum sum of squares of the deviations of $\ln Q$ as objective criterion (23 % of the fits were good enough) lead to higher values of a (0.29) and b (2.2) than the original (0.14 and 2.1) and nonlinear regression between Q and $-\mathrm{d}Q/\mathrm{d}t$ to lower values (0.08 and 1.7).

4.3.2 Results of recession analysis

All points selected for recession analysis, means and standard errors of the bins and resulting regression lines are plotted in Figure 4.1b. Values of a are comparable to those obtained with hydrograph fitting, but values of b are smaller (Fig. 4.2), resulting in higher recession rates for the discharge domain of the Hupsel Brook: the lines in Fig. 4.1b are higher than in Fig. 4.1a. This means that, based on recession analysis, discharge decreases more slowly than based on hydrograph fitting. Nonlinear fits be-

tween Q and $-\mathrm{d}Q/\mathrm{d}t$ (not shown) yield similar results ($a = 0.15$, $b = 1.78$) as the linear fits between $\ln Q$ and $\ln(-\mathrm{d}Q/\mathrm{d}t)$ ($a = 0.13$, $b = 1.84$).

The bins with $Q < 0.03$ mm h^{-1} are not described well by the regression line: the line through these bins is flatter (smaller b) and recession rates are higher than for the regression line through all points. This means that during dry conditions, the discharge decreases more quickly than the regression line indicates. An explanation could be that during the selected night-time hours, water is extracted from the groundwater by capillary rise to replenish the soil moisture deficit created during the day, causing an additional decrease in discharge. One should note, however, that the uncertainty in the logarithm of the discharge becomes very large when discharge drops below 10 l s^{-1}, which corresponds to 5.5×10^{-3} mm h^{-1}.

Sampling uncertainty is quite large (as was the case for the hydrograph fitting method): the contour lines in Figure 4.2 span a few tenths of b and are larger than the range between the seasonal data sets, which implies that the differences found between seasons are probably not significant (except for summer).

4.3.3 Results of direct storage-discharge fitting

Although soil moisture storage in the Hupsel Brook catchment shows a significant correlation with discharge (see, e.g. Fig. 4.3a for Site 2), there is considerable scatter in the relations obtained with $b \neq 2$ (Q can vary over two orders of magnitude with the same S). The fitted curves are very sensitive to b: the optimal relations often exhibit a strong curvature on either side of the fitting interval. This illustrates that, in this case, fitting a curve with three parameters (a, b and S_0 in eq. (4.7)) caused too much parameter uncertainty. Therefore, b is assumed to be 2 and eq. (4.8) was used to obtain a. All results from storage-discharge fitting (with $b = 2$) are shown in Figure 4.2.

A value of $b = 2$ is not much different from the values obtained with hydrograph fitting and recession analysis, but the corresponding a-values found with storage-discharge fitting are much lower. Therefore the lines appear below the cloud of points in Figure 4.1c, leading to a 10 times lower recession rate for a given discharge than for the hydrograph fitting and recession analysis methods. These results are in correspondence with Rupp et al. (2009), who found that their recession analysis and the storage-discharge fitting analysis returned inconsistent parameters and speculated that the causes were related to vadose attenuation of rainfall recharge and spatial inhomogeneity in subsurface properties.

The sampling variability is, in accordance with the hydrograph fitting and recession analysis techniques, larger than the seasonal variability, but smaller than the variability between stations (Fig. 4.2). This means that spatial variability is larger than temporal variability and sampling uncertainty.

When (for each site) the change in storage between two soil moisture measurements (local storage change) is compared to the change in storage computed from the water budget over the same period (catchment storage change, $\Sigma P - \Sigma Q - \Sigma ET_{\mathrm{act}}$), a consistent difference is observed, as illustrated, for example, for Site 2 in Fig. 4.3b. The local storage change is 2–6 times (depending on the station) larger than the catchment storage change. Deviations between estimated and field averaged system parameters of the same order have been reported by Rupp et al. (2004). This difference may be caused by the location of the soil moisture measurement sites, which are all relatively far from draining channels and therefore show a larger than average temporal variation in groundwater level. When we correct for this difference, the range of the x-axis in Figure 4.3a becomes 2–6 times smaller and the slope (and thus a) 2–6 times larger. But even with this correction, the values of a remain small (0.05–0.09).

The differences in inferred parameters between stations can to some extent be explained by variations in local soil hydrological conditions. At station 2, the aquifer is thicker and permeability higher than at station 5. Consequently, the groundwater table is less variable at station 2, leading to a smaller range of the x-axis and steeper slope (larger a) in the (S,Q)-plot. In addition, the difference between local and catchment storage change is larger.

4.3.4 Discussion of parameter uncertainty: effect on rainfall-runoff model performance

To show what the effect of different values of a and b is on the simulated hydrographs, we ran the model (eq. (4.6)) for all months with available data using the parameter values obtained with the three methods, for the total and seasonal data sets and for all parameter sets obtained in the bootstrap analyses. As an example, some of the model runs for one month (which is long enough to show the trends and short enough to show detail) are shown in Figure 4.4.

The parameters obtained with hydrograph fitting lead to the best results of the three methods, but recessions are too flat and peaks are overestimated because water from previous events has not been
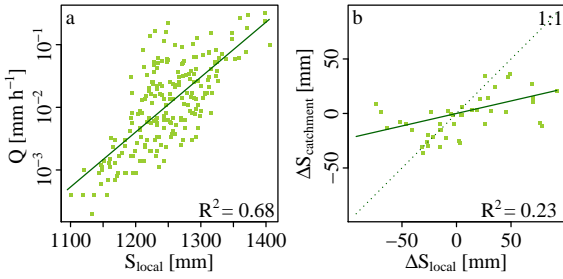
Figure 4.3: Relations between local and catchment scale observations **(a)** Relation between total storage in the upper 360 cm of soil at Site 2 (at the meteorological station) and discharge at catchment outlet. **(b)** Relation between local storage computed from soil moisture measurements at Site 2 and catchment storage computed from the water budget.

4.4 Conclusion and perspectives

The lowland Hupsel Brook catchment does not always behave like a simple dynamical system — only 39 % of the fitted monthly hydrographs yielded Nash-Sutcliffe efficiencies above 0.5. Model results were especially poor in summer, when evapotranspiration is high and the unsaturated zone plays an important role in attenuating the rainfall input.

The three methods we used to obtain the parameters of the power-law storage-discharge relation yielded the following values: 0.14 (a) and 2.12 (b) for hydrograph fitting, 0.13 (a) and 1.84 (b) for recession analysis and 0.02 (a) and 2 (b) for storage-discharge fitting. Using soil moisture data to obtain a and b is not trivial because there is a discrepancy between local and catchment storage and because an additional parameter needs to be fitted on a limited

discharged yet (initial conditions were too wet) and because the high value of b results in a stronger reaction of discharge to changes in storage when discharge is high.

The parameters obtained with recession analysis cause discharge to respond too quickly to rainfall: peaks are overestimated and recessions too steep. The effect of the large b in combination with a small a obtained with storage-discharge fitting is clearly visible: the discharge responds too slowly to changes in catchment storage (which was already concluded from Fig. 4.1). The storage change computed from soil moisture measurements shows large temporal and spatial variation and does not resemble modeled storage change. These results indicate that there is a significant difference between catchment storage and local groundwater and soil moisture storage.

The simulations for the month shown in Fig. 4.4 are quite poor: the Nash-Sutcliffe efficiencies are 0.37 for parameters obtained with hydrograph fitting and less for recession analysis and storage-discharge fitting. Nevertheless, they are representative for the entire dataset (the Nash-Sutcliffe efficiencies obtained with hydrograph fitting given in Table 4.1 are higher than for the results shown in Fig. 4.4, but these values cannot be compared directly since Table 4.1 shows calibration results and Fig. 4.4 validation results). The bands indicating the effect of sampling uncertainty are quite large. For example, the simulations of the first peak, on 9 December, range from 0.14 to 1.82 mm h^{-1} (hydrograph fitting) and from 0.41 to 0.72 mm h^{-1} (recession analysis). The simulations with parameters obtained with hydrograph fitting on ln Q and from seasonal data sets are not shown in Fig. 4.4 but yielded comparable results.

Figure 4.4: Illustration of simulated discharge **(a,b)** and storage **(c)** for a case in December 1983. Parameters from the whole (not seasonal) dataset and all three methods are used. The bands indicate the range between the 10th and 90th percentiles of the modeled discharge and storage obtained with all parameters from the bootstrap analysis for the hydrograph fitting and recession analysis methods. The six lines for the storage-discharge fitting method indicate the results for different soil moisture sites. The observed storage change was computed for each site, using the measurements on 1 or 2 December as reference.

amount of data. This suggests that it is not straight-forward to use soil moisture data directly to obtain system parameters. In addition, the uncertainty in parameter estimates caused by seasonal variability, spatial variability and sampling uncertainty is quite large.

Different parameter values result in different model performance: the reaction of discharge to rainfall events is much too strong (recession analysis), much too weak (storage-discharge fitting) or too weak when discharge is low and too strong when discharge is high (hydrograph fitting).

Finally, our results suggest that the performance of the simple dynamical systems approach decreases when humidity decreases: for Plynlimon (Kirchner, 2009) results were quite good, for the Rietholzbach (Teuling et al., 2010) results were mostly good, but less in summer, and for the Hupsel Brook catchment results are only good in certain periods. Previous studies show that hydrographs in the Hupsel Brook catchment can be simulated well with more complex models: Stricker and Warmerdam (1982) developed a conceptual model (Wageningen Model) which takes into account processes such as evapotranspiration reduction caused by soil moisture stress and capillary rise, and Van der Velde (2011) developed the Lowland Groundwater-Surface Water Interaction Model, in which different flow routes are simulated separately. This suggests that for such climatic conditions and catchment characteristics, application of the simple dynamical systems approach is not warranted given the multitude and complexity of hydrological processes affecting catchment behaviour.

5 | The Wageningen Lowland Runoff Simulator (WALRUS)

We present the Wageningen Lowland Runoff Simulator (WALRUS), a novel rainfall-runoff model to fill the gap between complex, spatially distributed models which are often used in lowland catchments and simple, parametric models which have mostly been developed for mountainous catchments. WALRUS explicitly accounts for processes that are important in lowland areas, notably (1) groundwater-unsaturated zone coupling, (2) wetness-dependent flow routes, (3) groundwater-surface water feedbacks and (4) seepage and surface water supply. WALRUS consists of a coupled groundwater-vadose zone reservoir, a quickflow reservoir and a surface water reservoir. WALRUS is suitable for operational use because it is computationally efficient and numerically stable (achieved with a flexible time step approach). In the open source model code default relations have been implemented, leaving only four parameters which require calibration. For research purposes, these defaults can easily be changed. Numerical experiments show that the implemented feedbacks have the desired effect on the system variables.

5.1 Introduction

Many types of hydrological models exist and they vary widely in their degree of complexity. The appropriate degree of complexity depends on the objectives of the model study and the catchment it is applied to (Wagener et al., 2001). Here, we focus on models to forecast catchment runoff, or, more accurately, the changes in river discharge resulting from hydrological processes within the catchment (the terms runoff and discharge are used interchangeably in this paper). Between detailed, spatially distributed models and black box models lies the class of parametric rainfall-runoff models, which simplify hydrological systems into a collection of reservoirs and flowroutes, capturing the essence of the hydrological processes, while restricting the number of parameters (Wagener and Wheater, 2004).

For realistic simulations of runoff, the model structure should represent the main catchment processes and therefore several models have been developed for specific catchment and climate types: (Dynamic) TOPMODEL (Beven and Kirkby, 1979; Beven and Freer, 2001a) for mountainous catchments, VIC (Liang et al., 1996) for areas prone to saturation excess overland flow and LGSI (Van der Velde et al., 2009) for data-rich lowland catchments. In addition, flexible model frameworks, e.g. (SUPER)FLEX (Fenicia et al., 2006, 2011) and FUSE (Clark et al., 2008) have been developed to allow for adaptation of the model structure to individual catchments.

A parametric rainfall-runoff model for lowland catchments, the Wageningen Model, was developed at the Hydrology and Quantitative Water Management Group of Wageningen University in the 1970s (Stricker and Warmerdam, 1982). This parametric model accounts for certain lowland-specific processes: capillary rise and a dynamic division between fast and slow flow routes as a function of catchment wetness. However, other lowland-specific processes are not included in the Wageningen Model: the saturated and unsaturated zone are disconnected and no feedbacks are possible between groundwater and surface water. The Wageningen Model has been applied with success in many catchments inside and outside The Netherlands, but users have indicated the need for a successor with more robust seasonal simulation capabilities.

In response to this demand, we have developed the Wageningen Lowland Runoff Simulator (WALRUS). We aimed for a model to simulate runoff in lowland catchments, which can be used for both multi-year water balance studies and for single rainfall-runoff events. The model was designed to have an understandable model structure that incorporates the most important processes and feedbacks, with fewer than 6 parameters of which the values do not change with the temporal resolution at which the model is run.

In this Chapter we present WALRUS. In Sect. 1.3, I described several lowland-specific hydrological phonomena and in Sect. 5.2 we describe their representation in WALRUS. In Sect. 5.3 we explain the model structure in detail. Sect. 5.4 contains the implementation of the model in code and Sect. 5.5 the conclusions.

5.2 Representation of lowland catchments

WALRUS accounts for several characteristics of lowland catchments which are often not accounted for in parametric rainfall-runoff models (Sect. 1.3):

1. *Groundwater-unsaturated zone coupling* – WALRUS contains one soil reservoir, which can be divided effectively by the (dynamic) groundwater table into a groundwater zone and a vadose zone. The condition of this soil reservoir is described by two strongly dependent variables: the groundwater depth and the storage deficit (the effective thickness of empty pores). The water balance in the whole soil reservoir is maintained through the storage deficit, while the groundwater depth is only used as pressure head to compute the groundwater drainage flux. The groundwater table reacts to changes in storage deficit (after rain or evapotranspiration) by moving towards an equilibrium between storage deficit and groundwater depth. Although the soil moisture profile is not simulated explicitly, this implementation enables upward movement of groundwater when the top soil has dried through evapotranspiration.

2. *Shallow groundwater and plant water stress* – We assume that in lowlands the whole unsaturated zone can be used by plant roots. Spatial variation in vegetation cover is not modelled explicitly to reduce the risk of overparameterisation (data on the detailed functioning of the system are scarce) and because the entire system of feedbacks between plants and water is complex on small scales, but likely less complex on larger scales. The effect of vegetation diversity on potential evapotranspiration can be accounted for by preprocessing.

3. *Wetness-dependent flowroutes* – The storage deficit determines the division of rain between a soil reservoir (slow routes: infiltration, percolation and groundwater flow) and a quickflow reservoir (quick routes: drainpipe, macropore and overland flow).

4. *Groundwater-surface water feedbacks* – Surface water forms an integral part of the model structure. Drainage depends on the difference in water level between the surface water and groundwater reservoirs (rather than groundwater levels alone), allowing for feedbacks and infiltration of surface water into the soil.

5. *Seepage and surface water supply* – Seepage and surface water supply or extraction are added to or subtracted from the soil or surface water reservoir. These external fluxes affect the whole system through the groundwater-surface water feedbacks and saturated-unsaturated zone coupling described above.

5.3 Model description

In this section we provide a detailed description of all model components: reservoirs, states, fluxes and feedback mechanisms. The model contains several relations between model variables which can be specified by the user. We implemented defaults for these relations, such that WALRUS can be used directly by practitioners, while retaining the option to change them for research purposes.

5.3.1 General overview

WALRUS is a water balance model with three reservoirs and fluxes between the reservoirs. The model can be split into several compartments (Fig. 5.1; for abbreviations of variables, see Tab. 5.1):

1. *Land surface* – At the land surface, water is added to the different reservoirs by precipitation P. A fixed fraction is led to the surface water reservoir P_S. The soil wetness index W determines which fraction of the remaining precipitation percolates slowly through the soil matrix (P_V) and which fraction flows towards the surface water via quick flow routes (P_Q). Water is removed by evapotranspiration from the vadose zone ET_V and surface water reservoir ET_S.

2. *Vadose zone within the soil reservoir* – The vadose zone is the upper part of the soil reservoir and extends from the soil surface to the dynamic groundwater table d_G, including the capillary fringe. The dryness of the vadose zone is characterised by a single state: the storage deficit d_V, which represents the effective volume of empty pores per unit area. It controls the evapotranspiration reduction β and the wetness index W.

3. *Groundwater zone within the soil reservoir* – The phreatic groundwater extends from the groundwater depth d_G downwards, thereby assuming that there is no shallow impermeable soil layer and allowing groundwater to drop below the depth of the drainage channels c_D in dry periods. The groundwater table responds to changes in the unsaturated zone storage and determines together with the surface water level groundwater drainage or infiltration of surface water f_{GS}.

4. *Quickflow reservoir* – All water that does not flow through the soil matrix, passes through the quickflow reservoir to the surface water (f_{QS}).
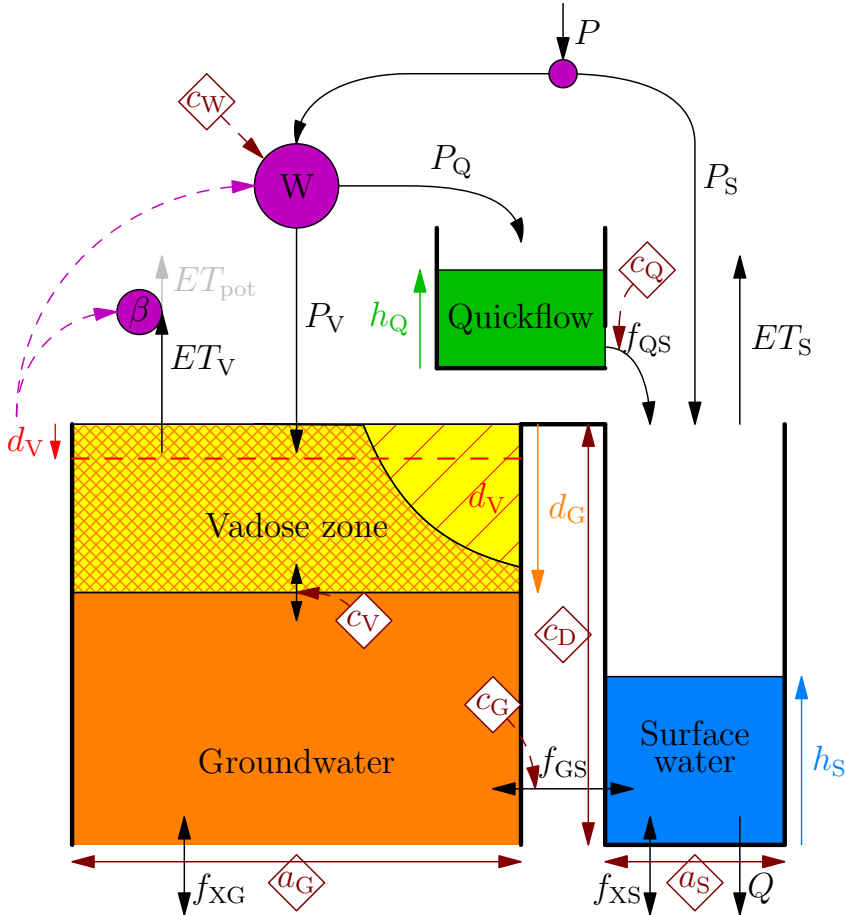
Figure 5.1: Overview of the model structure with the five compartments: land surface (purple), vadose zone within the soil reservoir (yellow/red hatched), groundwater zone within the soil reservoir (orange), quickflow reservoir (green) and surface water reservoir (blue). Fluxes are black arrows, model parameters brown diamonds and states in the colour of the reservoir they belong to. For a complete description of all variables, see Table 5.1 and Sec. 5.3.1. The names of the fluxes are derived from the reservoirs (for example f_{XS}: f stands for flow, the X for external and the S for surface water – water flowing from outside the catchment into the surface water network).

This represents macropore flow through drainpipes, animal burrows and soil cracks, but also local ponding and overland flow.

5. *Surface water reservoir* – The surface water reservoir has a lower boundary (the channel bottom c_D), but no upper boundary. Discharge Q is computed from the surface water level h_S.

6. *External fluxes* – Water can be added to or removed from the soil reservoir by seepage f_{XG} and to/from the surface water reservoir by surface water supply or extraction f_{XS}.

The area of the surface water reservoir a_S is the fraction of the catchment covered by ditches and channels, which is supplied by the user and can generally be derived from maps. The area of the soil reservoir a_G is the remainder ($1 - a_S$). The area

of the quickflow reservoir is taken equal to a_G, but this is arbitrary since the outflow depends on the volume of water in the reservoir and a parameter (see Sect. 5.3.8). In the following sections the processes occurring within and between each compartment are discussed.

Because the soil reservoir has no lower boundary and the surface water reservoir no upper boundary, the groundwater depth d_G is measured with respect to the soil surface and the surface water level h_S with respect to the channel bottom. The channel bottom c_D, with respect to the soil surface, is used to compute the difference in level, which is necessary for the computation of groundwater drainage. The quickflow reservoir level h_Q is measured with respect to the bottom of that reservoir. The storage

deficit d_V is an effective thickness, instead of a level or depth.

5.3.2 Precipitation and wetness index

Precipitation P is divided between the 3 reservoirs: a fixed fraction a_S falls directly onto the surface water (P_S) and the remainder is divided between the vadose zone (P_V) and the quickflow reservoir (P_Q). The wetness index W gives the fraction of the rainfall that is led to the quickflow reservoir and ranges from 0 (dry – all water is led to the soil reservoir) to 1 (wet – all water is led to the quickflow reservoir). The wetness index is a function of storage deficit d_V (Sect. 5.3.4). This relation can be supplied by the user, but as default a cosine function has been implemented, which starts at 1 when the soil is completely saturated ($d_V = 0$) and drops to zero when d_V is equal to the wetness parameter c_W [mm], which has to be calibrated:

$$W = \cos\left(\frac{\max(\min(d_V, c_W), 0) \cdot \pi}{c_W}\right) \cdot \frac{1}{2} + \frac{1}{2} . \quad (5.1)$$

A negative value of d_V can occur in rare cases of large-scale ponding (Sect. 5.3.11).

The effect of this variable division between quick and slow flow paths is investigated by running WALRUS twice for an artificial example: with and without the variable W. Six rainfall events with a duration of one day and an intensity of $2\,\mathrm{mm\,h^{-1}}$, separated by four dry days yield the same quickflow f_{QS} and discharge Q response when the divider is not depending on soil moisture storage, but f_{QS} and Q increase in case of a wetness-dependent divider (Fig. 5.3). The storage deficit d_V decreases quickly during rainfall events and increases slowly in dry intervals. The variable wetness index W follows d_V without delay and the groundwater depth d_G responds with a delay caused by the unsaturated zone (represented by its relaxation time parameter c_V, see Sect. 5.3.6). With a variable W, the groundwater level rises quickly at first, but more slowly at the end, because less water is led to the soil reservoir when it is already wet. This numerical experiment shows that the variable wetness index ensures that WALRUS can simulate feedbacks between groundwater, vadose zone and quickflow and that variables at the soil surface do not only influence variables in the ground (as in most models), but also the other way around.

5.3.3 Evapotranspiration

Evapotranspiration (ET) takes place from the surface water reservoir (ET_S) and the vadose zone (ET_V). The actual evapotranspiration from the vadose zone depends on the potential evapotranspiration rate and the storage deficit (Fig. 5.2). The
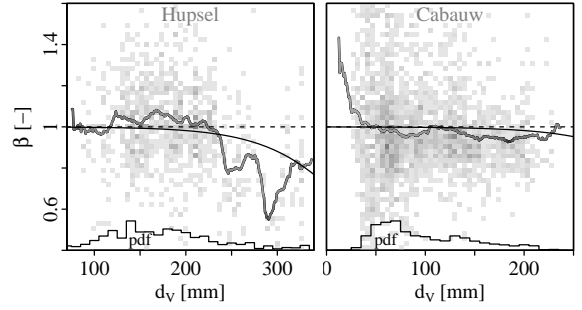

Figure 5.2: Determining the evapotranspiration reduction function. Soil moisture data are from the meteorological station in the Hupsel Brook catchment and the mean of 4 sites in the Cabauw polder. The thick greyscale lines connect the bin means, with the colour ranging from low (light) to high (dark) inverse variance. The black lines, with coefficients $\zeta_1 = 0.02$ and $\zeta_2 = 400$, are implemented as default in WALRUS. The histograms represent the probability density functions of storage deficit.

relation between the evapotranspiration reduction factor β and the storage deficit can be supplied by the user. As a default, a two-parameter function has been implemented:

$$\beta = \frac{ET_{\mathrm{act}}}{ET_{\mathrm{pot}}} = \frac{1 - \exp[\zeta_1(d_V - \zeta_2)]}{1 + \exp[\zeta_1(d_V - \zeta_2)]} \cdot \frac{1}{2} + \frac{1}{2} \quad (5.2)$$

The evapotranspiration reduction factor approaches one (no reduction) when the soil is saturated and decreases with storage deficit: first slowly, then more quickly and then more slowly again (although this end of the curve is never reached in practice). Eq. (5.2) has two parameters: ζ_1 determines the curvature and ζ_2 determines at which value of d_V the reduction factor is 0.5 (the inflection point). Note that Eq. (5.2) does not account for the effects of waterlogging on transpiration, although the net effect on ET is likely limited because of the compensating effect of soil evaporation. In addition, under extremely dry conditions Eq. (5.2) will overestimate the soil moisture stress, but such conditions approach the limits of the range for which the assumptions behind WALRUS are valid.

Data from the two catchments (Sect. 2) are used to estimate ζ_1 and ζ_2 (Fig. 5.2). The scatter in the observed evapotranspiration data is very large, but when data points are collected in 25 mm wide sliding bins and averaged, a decrease in β with d_V can be observed (think line). In the Cabauw polder, the storage deficit is never large and therefore hardly any evapotranspiration reduction occurs. In the Hupsel Brook catchment, reduction is around 10 % when d_V exceeds 300 mm, which corresponds to a rare groundwater depth of about 2 m (about 14 % of the

Table 5.1: Overview of variables, parameters and functions. All fluxes are catchment averages, both external ones (including Q and f_{XS}) and internal fluxes (which are multiplied with the relative surface area of the reservoir in question). Note that d_V, h_Q and h_S result from the mass balances in the three reservoirs, while d_G is only used as pressure head to compute the groundwater drainage flux.

	States		
d_V	storage deficit	$\rightarrow \frac{\mathrm{d}d_V}{\mathrm{d}t} = -\frac{f_{XG}+P_V-ET_V-f_{GS}}{a_G}$	[mm]
d_G	groundwater depth	$\rightarrow \frac{\mathrm{d}d_G}{\mathrm{d}t} = \frac{d_V-d_{V,eq}}{c_V}$	[mm]
h_Q	level quickflow reservoir	$\rightarrow \frac{\mathrm{d}h_Q}{\mathrm{d}t} = \frac{P_Q-f_{QS}}{a_G}$	[mm]
h_S	surface water level	$\rightarrow \frac{\mathrm{d}h_S}{\mathrm{d}t} = \frac{f_{XS}+P_S-ET_S+f_{GS}+f_{QS}-Q}{a_S}$	[mm]
	Dependent variables		
W	wetness index	$= \mathrm{func}(d_V)$	[-]
β	evapotranspiration reduction factor	$= \mathrm{func}(d_V)$	[-]
$d_{V,eq}$	equilibrium storage deficit	$= \mathrm{func}(d_G)$	[mm]
	External fluxes: input		
P	precipitation		[mm h^{-1}]
ET_{pot}	potential evapotranspiration		[mm h^{-1}]
Q_{obs}	discharge (for calibration and Q_0)		[mm h^{-1}]
f_{XG}	seepage (up/down) / extraction		[mm h^{-1}]
f_{XS}	surface water supply / extraction		[mm h^{-1}]
	External fluxes: output		
ET_{act}	actual evapotranspiration	$= ET_V + ET_S$	[mm h^{-1}]
Q	discharge	$= \mathrm{func}(h_S)$	[mm h^{-1}]
	Internal fluxes		
P_S	precip. into surface water reservoir	$= P \cdot a_S$	[mm h^{-1}]
P_V	precipitation into vadose zone	$= P \cdot (1-W) \cdot a_G$	[mm h^{-1}]
P_Q	precipitation into quickflow reservoir	$= P \cdot W \cdot a_G$	[mm h^{-1}]
ET_V	actual evapotranspiration vadose zone	$= ET_{pot} \cdot \beta \cdot a_G$	[mm h^{-1}]
ET_S	actual ET surface water	$= ET_{pot} \cdot a_S$	[mm h^{-1}]
f_{GS}	groundw. drainage / surface w. infiltration	$= \frac{(c_D-d_G-h_S)\cdot\max((c_D-d_G),h_S)}{c_G} \cdot a_G$	[mm h^{-1}]
f_{QS}	quickflow	$= \frac{h_Q}{c_Q} \cdot a_G$	[mm h^{-1}]
	Model parameters		
c_W	wetness index parameter		[mm]
c_V	vadose zone relaxation time		[h]
c_G	groundwater reservoir constant		[mm h]
c_Q	quickflow reservoir constant		[h]
	Supplied parameters		
a_S	surface water area fraction		[-]
a_G	groundwater reservoir area fraction	$= 1 - a_S$	[-]
c_D	channel depth		[mm]
	User-defined functions with defaults		
$W(d_V)$	wetness index	$= \cos\left(\frac{\max(\min(d_V,c_W),0)\cdot\pi}{c_W}\right) \cdot \frac{1}{2} + \frac{1}{2}$	[-]
$\beta(d_V)$	evapotranspiration reduction factor	$= \frac{1-\exp[\zeta_1(d_V-\zeta_2)]}{1+\exp[\zeta_1(d_V-\zeta_2)]} \cdot \frac{1}{2} + \frac{1}{2}$	[-]
$d_{V,eq}(d_G)$	equilibrium storage deficit	$= \theta_s\left(d_G - \frac{d_G^{1-1/b}}{(1-\frac{1}{b})\psi_{ae}^{-1/b}} - \frac{\psi_{ae}}{1-b}\right)$	[mm]
$Q(h_S)$	stage-discharge relation	$= c_S\left(\frac{h_S-h_{S,min}}{c_D-h_{S,min}}\right)^{x_S}$	[mm h^{-1}]
	Parameters for default functions		
ζ_1	curvature ET reduction function		[-]
ζ_2	translation ET reduction function		[mm]
b	pore size distribution parameter		[-]
ψ_{ae}	air entry pressure		[mm]
θ_s	soil moisture content at saturation		[-]
c_S	surface water parameter: bankfull Q		[mm h^{-1}]
x_S	stage-discharge relation exponent		[-]
$h_{S,min}$	surface water level when $Q = 0$		[mm]

Table 5.2: Parameters of the Brooks-Corey equilibrium soil moisture profile. The first 11 rows are taken from Clapp and Hornberger (1978). The last two lines are obtained from combined soil moisture and groundwater observations in the two catchments (see also Fig. 5.5).

Soil type	b [-]	ψ_{ae} [mm]	θ_s [-]
Sand	4.05	121	0.395
Loamy sand	4.38	90	0.410
Sandy loam	4.90	218	0.435
Silt loam	5.30	786	0.485
Loam	5.39	478	0.451
Sandy clay loam	7.12	299	0.420
Silt clay loam	7.75	356	0.477
Clay loam	8.52	630	0.476
Sandy clay	10.40	153	0.426
Silty clay	10.40	490	0.492
Clay	11.40	405	0.482
Hupsel	2.63	90	0.418
Cabauw	16.77	9	0.639

data in Fig. 5.2 was obtained during the extremely dry summer of 1976).

The open water evaporation is assumed to be equal to the potential evapotranspiration ET_{pot} of a well-watered soil. A Penman approximation would be more appropriate, but for most catchments only one estimate for evapotranspiration is available. In addition, the area fraction of open water and consequently the error is small. No evapotranspiration from the surface water occurs when the surface water reservoir is empty. Because the groundwater and surface water reservoirs together cover the entire catchment area, no evapotranspiration occurs from the quickflow reservoir.

5.3.4 Storage deficit

The dryness of the vadose zone is expressed by the storage deficit d_V, representing the volume of empty soil pores per unit area, or in other words, the depth of water necessary to reach saturation. The vertical profile of soil moisture is not simulated explicitly and, as WALRUS is a lumped model, neither is its horizontal variability. The storage deficit controls the precipitation division between groundwater and quickflow (W), evapotranspiration reduction (β) and the change in groundwater depth (d_G) and is itself the result of all fluxes into or out of the soil reservoir, both the vadose zone and the groundwater zone.

In the field, time series of storage deficit d_V can be estimated from soil moisture (θ [-]) profile data. For each depth the soil moisture content at saturation θ_s [-] has to be determined, which can often be done by taking the highest measured soil moisture

content at that depth. The difference between the profiles of θ and θ_s gives the profile of the fraction of soil filled with air (and the remainder, $1-\theta_s$, gives the soil particle fraction). The storage deficit is obtained by integrating this air profile over depth d from the groundwater table d_G to the soil surface:

$$d_V = \int_0^{d_G} (\theta_s - \theta) \ dd \ . \qquad (5.3)$$

5.3.5 Equilibrium storage deficit

For every groundwater depth d_G, an equilibrium soil moisture profile exists where at all depths gravity is balanced by capillary forces, and no flow occurs. From this profile the equilibrium storage deficit $d_{V,eq}$ can be derived in the same way as d_V, namely by integrating the volume of empty soil pores over depth. The relation between $d_{V,eq}$ and d_G can be estimated from combined observations of groundwater and soil moisture. By assuming that on average $d_{V,eq}$ equals d_V, the relation can be read from a (d_G,d_V)-plot and supplied to WALRUS.

Alternatively, one can assume a relation based on parametrisations of steady-state (i.e. no-flow) profiles reported by e.g. Brooks and Corey (1964) and Van Genuchten (1980). WALRUS uses the power law of Brooks and Corey as default because it requires only two parameters. The profile of soil moisture content θ [-] as a function of height above the groundwater table h [mm] according to Clapp and Hornberger (1978) is

$$\theta = \theta_s \left(\frac{h}{\psi_{ae}} \right)^{-1/b} \ . \qquad (5.4)$$

with b the pore size distribution parameter [-] and ψ_{ae} the air entry pressure [mm]. The air entry pressure raises the power law distribution above the groundwater table to allow for the capillary fringe (the saturated area above the groundwater table). The parameters b, ψ_{ae} and θ_s differ per soil type and selected results from laboratory experiments by Clapp and Hornberger (1978) are given in Table 5.2 (see Cosby et al., 1984, for interpolations between soil types). When the part of the profile between the capillary fringe and the soil surface from Eq. (5.4) is substituted in Eq. (5.3), the relation between equilibrium storage deficit and groundwater depth becomes

$$d_{V,eq} = \int_{\psi_{ae}}^{d_G} \left[\theta_s - \theta_s \left(\frac{h}{\psi_{ae}} \right)^{-1/b} \right] \ dh$$

$$= \theta_s \left(d_G - \frac{d_G^{1-1/b}}{(1-\frac{1}{b})\psi_{ae}^{-1/b}} - \frac{\psi_{ae}}{1-b} \right) \ . \qquad (5.5)$$
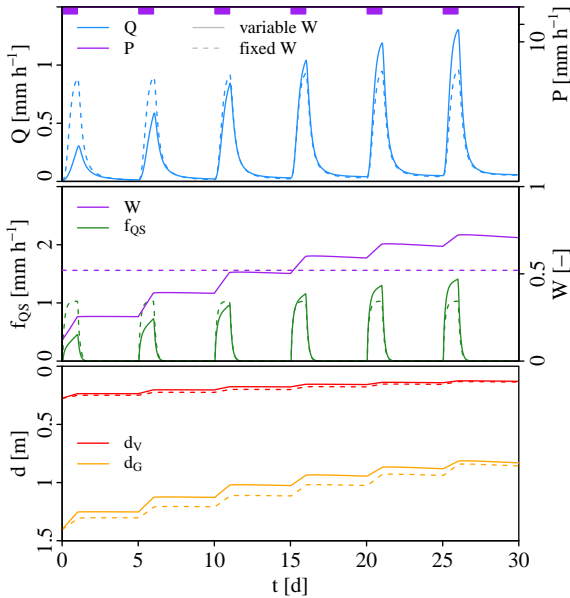
Figure 5.3: Effect of a wetness-dependent divider between slow and quick flowroutes. Results of two cases with (solid) and without (dashed) a variable divider. A change in W propagates through the model and alters nearly all model variables. We used parameter values obtained for the Hupsel Brook catchment (Brauer et al., 2014b, i.e. $c_W = 365$ mm, $c_V = 0.2$ h, $c_G = 5 \times 10^6$ mm h, $c_Q = 3.3$ h, $c_D = 1500$ mm, $a_S = 0.01$ and the local Q-h-relation and soil parameters).
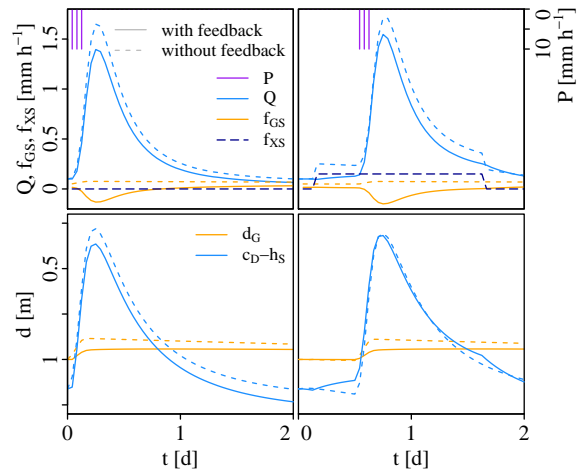
Figure 5.4: The effect of the groundwater-surface water feedback. Results of a numerical experiment with (solid) and without (dashed) using h_S in the groundwater drainage flux f_{GS} computation. Right panels also include the effect of surface water supply f_{XS}. For the dashed lines in the left panels, h_S was computed without f_{XS} and f_{XS} was added to Q afterwards. The same parameter values as in Fig. 5.3 were used.
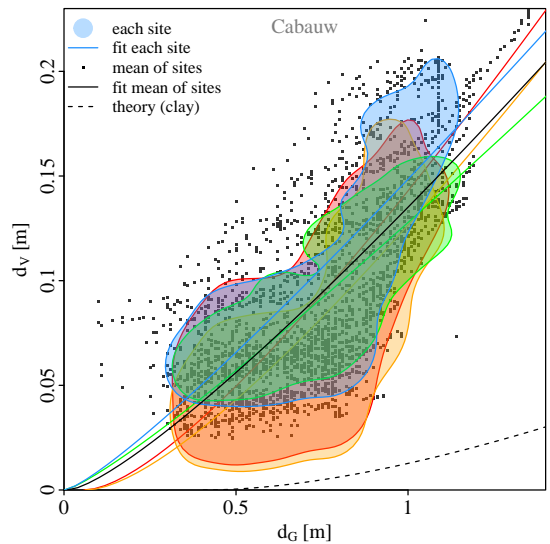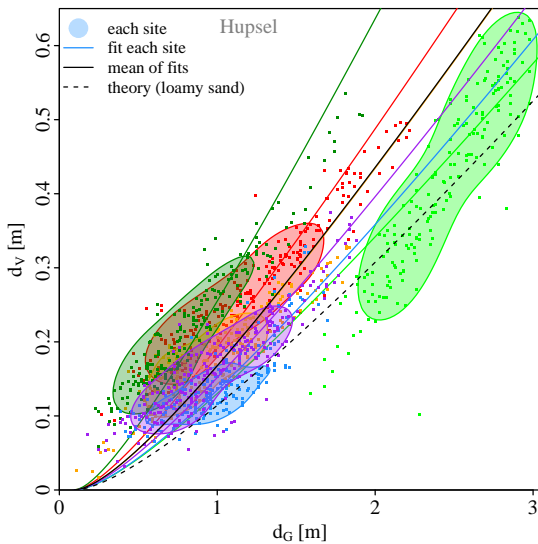
Figure 5.5: Relation between groundwater depth d_G and storage deficit d_V. Coloured lines: data from six and four sites in the two catchments. Dashed black line: relation derived from the Brooks-Corey curve belonging to loamy sand (left) and clay (right). Coloured lines: relation with b fitted on data. Solid black line: relation with the average b of the stations. The clouds are represented by the contour lines encompassing 70 % of the probability mass estimated using kernel densities (Wand and Jones, 1995).

Heterogeneities, such as soil layering or disruption by plant roots, macrofauna and human activity, cause differences between laboratory and field observations. In Fig. 5.5 d_G is plotted as a function of d_V for several sites in the Hupsel Brook catchment and Cabauw polder area with corresponding theoretical curves. We computed the temporal maximum θ per depth (at the meteorological station in Hupsel and the average of four profiles in Cabauw) and averaged over the entire measured depth (205 cm in Hupsel and 72 cm in Cabauw) to obtain a single value of θ_s. For Hupsel, we fitted b while retaining ψ_{ae}, but for Cabauw it was necessary to fit both b and ψ_{ae} to obtain curves which describe the data points relatively well. The values obtained with these fits are listed in Table 5.2. Note that the data are actual storage deficits, which may not be in equilibrium with the groundwater depth measured at the same time. In addition, sites differ considerably and will deviate from the catchment average.

5.3.6 Percolation and capillary rise

In practice, the soil moisture profile and storage deficit are never perfectly in equilibrium with the groundwater depth. Addition (e.g. through precipitation) and removal (e.g. by drainage or evapotranspiration) of water cause an imbalance between gravity and capillary forces, leading to downward (percolation) or upward (capillary rise) flow towards a new equilibrium situation. Because the flow decreases with proximity to the equilibrium, this equilibrium will only be reached asymptotically. The exact profile of relative saturation is not simulated explicitly in WALRUS, but the temporal dynamics of d_V and d_G caused by the interactions between groundwater and vadose zone are taken into account. The groundwater depth responds to changes in storage deficit. The change in groundwater depth is parameterised as a function of the difference between the actual storage deficit (computed from the water budget in the soil reservoir) and the equilibrium storage deficit corresponding to the current groundwater level:

$$\frac{\mathrm{d}d_G}{\mathrm{d}t} = \frac{d_V - d_{V,eq}}{c_V} \ , \tag{5.6}$$

with c_V the vadose zone relaxation time constant, which determines how quickly the system advances towards a new equilibrium. Four situations may occur (illustrated in Fig. 5.6). (1) Water is added to the vadose zone through percolation. The actual storage deficit is smaller than the equilibrium for the current groundwater depth. Water will flow downward and the groundwater level will rise gradually to the depth corresponding to the actual storage deficit. (2) Water is removed from the vadose zone through evapotranspiration. The actual storage deficit exceeds the equilibrium for the current groundwater depth. Water will flow upward to replenish the shortage in the top soil and the groundwater level will drop gradually. (3) Water is removed from the soil reservoir though drainage, downward seepage or groundwater extraction. Air is sucked into the soil and the actual storage deficit increases. This happens instantaneously, because water is incompressible. Water will percolate to reach an equilibrium profile again and the groundwater level will drop gradually. (4) Water is added to the soil reservoir through infiltration from surface water or upward seepage. The storage deficit decreases directly and the groundwater table rises gradually.

5.3.7 Groundwater

Drainage of groundwater towards the surface water reservoir or infiltration of surface water f_{GS} is computed as

$$f_{GS} = \frac{(c_D - d_G - h_S) \cdot \max((c_D - d_G), h_S)}{c_G} \cdot a_G \ , \tag{5.7}$$

with d_G the depth of the groundwater table below the soil surface, c_G a reservoir constant [mm h] and c_D the average channel depth [mm] (see also Table 5.1 and Fig. 5.1). The parameter c_G represents the combined effect of all resistance and variability therein and depends on soil type (hydraulic conductivity) and drainage density. The first term of Eq. (5.7), $c_D - d_G - h_S$, expresses the pressure difference driving the flow. The second term, $\max((c_D - d_G), h_S)$, expresses the contact surface (parameterised as a depth) through which the flow takes place. These terms can be compared to the pressure head difference and layer thickness commonly used in groundwater models. The contact surface-term accounts for decreasing drainage efficiency when groundwater and surface water levels drop and headwaters run dry. With this term, the variable source area concept (Beven and Kirkby, 1979) is implemented effectively and without additional parameters.

When groundwater drops below the surface water level, infiltration will be computed with the same relation, decreasing to zero when the surface water reservoir is empty (the second term $\max((c_D - d_G), h_S)$ becomes zero). The same parameter c_G is used for both groundwater drainage and surface water infiltration to limit the number of parameters, even though the resistance may be different in practice.

The groundwater-surface water feedback is illustrated by a numerical experiment. We ran the model for an artificial 3-hour rainfall event with an intensity of 10 mm h^{-1} with and without using h_S in the drainage flux computation. Including h_S leads
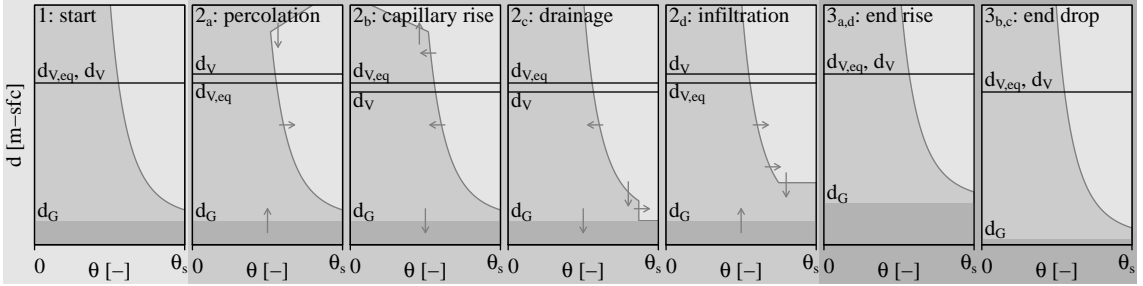
Figure 5.6: Illustration of the four scenarios for change in groundwater levels: **(a)** percolation after rainfall, **(b)** capillary rise after evapotranspiration, **(c)** percolation after drainage and **(d)** capillary rise after infiltration. WALRUS only simulates the solid lines of d_G, d_V and $d_{V,eq}$ and not the profiles of relative saturation (dashed). The areas right of the curves (the integral of $(\theta_s - \theta)$ over d) is equal to the values of d_V.

to a decrease in drainage f_{GS} and even infiltration (negative f_{GS}) during the peak (Fig. 5.4, left panels). This causes an attenuation of the discharge peak and higher groundwater levels after the peak. This feedback is an important characteristic of WALRUS: in most parametric models, surface water levels are not modelled explicitly and this feedback cannot take place.

5.3.8 Quickflow

The quickflow reservoir simulates the combined effect of all water flowing through quick flow paths towards the surface water: overland, macropore and drainpipe flow. This reservoir can therefore be seen as a collection of ponds, small drainage trenches or gulleys, soil cracks, animal burrows and drainpipes. Quickflow f_{QS} depends linearly on the elevation of the water level in the quickflow reservoir h_Q, with a time constant (reservoir constant) c_Q:

$$f_{QS} = \frac{h_Q}{c_Q} \cdot a_G \quad . \tag{5.8}$$

Water cannot flow from the surface water into the quickflow reservoir. Therefore, a sudden surface water level rise caused by an increase in surface water supply or weir elevation does not affect the quickflow reservoir directly.

The water level in the quickflow reservoir cannot be coupled to measurable variables directly – groundwater level measurements show the combined effect of the seasonal variation of the groundwater depth and the high resolution dynamics of the quickflow reservoir. Even though quickflow is parameterised as a single linear reservoir, it is essential to include this reservoir to mimic the large and variable contribution of these flowroutes (see Sect. 1.3.3).

5.3.9 Surface water

The surface water level h_S represents the water level in the average channel with respect to the channel bottom. The distance between channel bottom and soil surface c_D is calibrated or estimated from field observations. The stage-discharge relation $Q = \mathrm{func}(h_S)$ specifies the relation between surface water level and discharge at the catchment outlet (in $\mathrm{mm\,h^{-1}}$). It is provided by the user as a function, e.g. the relation belonging to the weir at the catchment outlet, or as a lookup table. A threshold level $h_{S,min}$ can be included in the stage-discharge relation to account for a weir or other water management structures. If applicable, a value or time series of $h_{S,min}$ should be provided. When the surface water level drops below the crest of a weir, discharge will be zero, but because there may still be drainage, infiltration and evaporation, it is important to include standing water. A default stage-discharge relation with the shape of a power law with a default exponent x_S of 1.5 has been implemented:

$$Q = c_S \left(\frac{h_S - h_{S,min}}{c_D - h_{S,min}} \right)^{x_S} \tag{5.9}$$

for $h_S \leq c_D$. The default exponent value 1.5 for x_S is inspired by equilibrium flow in open channels (Manning, 1889). The parameter c_S corresponds to the discharge at the catchment outlet (in $\mathrm{mm\,h^{-1}}$) when the surface water level reaches the soil surface, comparable to the bankfull discharge. It can be calibrated or provided based on field observations.

5.3.10 Seepage and surface water supply

All fluxes across the catchment boundary, except for the discharge at the catchment outlet, are combined in the external groundwater flow term f_{XG} (downward or upward seepage and lateral groundwater inflow or outflow) and the external surface water flow

term f_{XS} (supply or extraction). Positive values denote flow into the catchment. If applicable, time series of f_{XG} or f_{XS} should be provided by the user.

Because these fluxes are added to the soil reservoir or surface water reservoir, they influence other variables through the different feedbacks implemented in the model. Most parametric rainfall-runoff models do not contain a surface water reservoir and therefore surface water supply can only be added to discharge afterwards and the impact of surface water increase on groundwater level and the groundwater drainage flux is not considered.

To investigate the effect of WALRUS' set-up considering surface water supply, we modelled an artificial event with two model set-ups: (1) f_{XS} is added to the surface water reservoir and groundwater-surface water feedbacks are considered (as implemented in WALRUS) and (2) f_{XS} is added to Q afterwards and h_S is not used in the groundwater drainage computation. Adding f_{XS} to the surface water reservoir causes a gradual increase in h_S and gradually rising Q (Fig. 5.4, right panels). When f_{XS} is added to Q afterwards, h_S is not affected by f_{XS} and only increases after rainfall, and Q rises and falls instantly after changes in f_{XS}. When a larger fraction of the catchment is covered by surface water (a_S), the increase in h_S and Q becomes more gradual, because the supplied surface water volume is spread out over a larger surface. Including the groundwater-surface water feedback leads to an attenuated discharge peak, caused by a decrease in drainage as a result of a decreasing difference between d_G and h_S. In dry periods, f_{XS} may cause h_S to rise above d_G, leading to infiltration of surface water, which indicates that seepage and groundwater-surface water feedback should be implemented together.

5.3.11 Large-scale ponding and flooding

The quickflow reservoir simulates the effect of local ponding and overland flow, but large-scale ponding may also occur. When the storage deficit becomes zero (i.e. all soil pores are filled with water), the groundwater level will rise directly to the surface (as observed by Gillham, 1984; Brauer et al., 2011). Storage deficit and groundwater depth continue to drop (i.e. become more negative) together as there are no capillary forces any more and water level and pressure head coincide – negative d_V and d_G express ponding depths. Note that the levels rise less quickly above ground as the storativity becomes 1.

Unfortunately, few quantitative, catchment-scale observations exist of different fluxes during floods. Because WALRUS has no spatial dimensions, the complex process of overland flow must be simplified. It is assumed that when the groundwater or surface water level rises above the soil surface, the groundwater drainage/surface water infiltration flux f_{GS} will include overland flow and is instantaneous, because overland flow is much faster than groundwater flow. When the surface water level exceeds the soil surface, discharge becomes less sensitive to changes in surface water level, represented by an abrupt change in the stage-discharge relation. However, as soon as the surface water level exceeds the soil surface, the excess water is led to the soil reservoir directly and therefore h_S hardly rises above the soil surface. Therefore, we keep the same stage-discharge relation when $h_S > c_D$ as a default. When the modelled groundwater table reaches the soil surface, an abrupt change in catchment discharge occurs. This is in contrast to the gradual activation of different flowpaths when the catchment effective groundwater table is below surface (as represented by the wetness index).

We investigated the option of making the surface water area fraction a_S a function of h_S, representing gradual widening of brooks and inundation of areas close to the surface water network, thereby smoothing the effect of flooding on discharge at the catchment outlet. Unfortunately, this approach made the model structure less intuitive and introduced more degrees of freedom to define the shape of this function. Because flooding of the surface water reservoir only occurs during extremely wet situations, we chose to keep the model structure simple and leave a_S fixed.

5.3.12 Outlook: possible model extensions

Some processes are not taken into account in the core model yet, but a user could easily add preprocessing and postprocessing steps to adapt WALRUS to catchment-specific situations. (1) The potential evapotranspiration estimated at a meteorological station may not be representative for the collection of vegetation types in the catchment. Therefore, one could use land cover distributions and crop factors to determine the catchment average potential evapotranspiration. (2) Currently, WALRUS is set-up to receive liquid precipitation, but preprocessing steps to account for snow and/or interception can be added. For example, the delay in precipitation input caused by snow accumulation and melt can be simulated with methods based on the land surface energy balance (Kustas et al., 1994) or a degree-day method (Seibert, 1997). (3) Interception can be parameterised with a threshold. Only the rainfall which exceeds the threshold is used as input for the model. The intercepted water evaporates directly and is not subtracted from ET_{pot} (Teuling and Troch, 2005). (4) Paved surfaces have a low infiltration

capacity, which limits groundwater recharge. This can be parametrized by decreasing the groundwater reservoir area a_G, introducing a paved surface area and leading the fraction of the rainfall belonging to this area directly to the surface water. (5) For large catchments, the discharge pulse from the model can be delayed and attenuated in the channels. It is possible to add a routing function to account for the delay and attenuation.

Another possibility is to couple WALRUS to other models. The outflow Q of one catchment can be used as surface water supply f_{XS} for another WALRUS-unit downstream. With this technique, one could make a chain of WALRUS units to model subcatchments (with possibly different catchment characteristics and therefore parameter values) separately. Groundwater flow from one unit to the next can be computed from groundwater levels in adjacent cells and equation 5.7. This groundwater flow is added to or subtracted from the seepage flux f_{XG} for both units. Regional groundwater flow from a distributed groundwater model can be added to or subtracted from the soil reservoir through the seepage flux f_{XG}. This can be specified with a time series or an external groundwater level. The outflow of the model can be used as input for a hydraulic model. Discharge from an upstream catchment as computed from a hydraulic model can also be used as input f_{XS}.

5.4 Model implementation

In this section we describe some key parts of the model implementation, which affect the model application and performance.

5.4.1 Code set-up

The model code is written in R, but can be easily translated into any vector-oriented interpreted language. The code consists of several scripts. Two functions form the core of the model code: *WALRUS_loop* and *WALRUS_step*. In *WALRUS_loop* the initial conditions are set, a for-loop over each time step is run and output data are organized. For every time step, the function *WALRUS_step* is called, which contains the actual model computations. Some additional scripts (not included in the supplementary material, but available upon request) provide help by preprocessing forcing data, setting default parameters, and postprocessing of the model output: figures, water balance computations and analysis of residuals. Another script provides a template in which functions are called for preprocessing, calibrating, running the model and postprocessing.
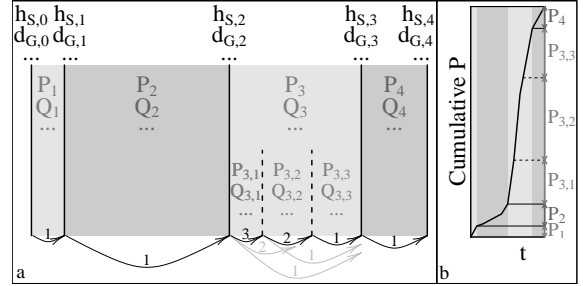

Figure 5.7: Illustration of the variable time step procedure. **(a)** The non-equidistant output time steps (black lines) are used as first attempts for computations of fluxes (light and dark grey) and states (black), but during time step number 3, the precipitation sum is too large (panel **b**) and the step is divided into substeps: it is halved and then halved again until the criterion was reached. Note that even though the size of output time step 2 is larger, it is not divided into substeps, because all criteria are met.

5.4.2 Initial conditions

The model can (as default) compute initial conditions for all states automatically, based on a stationary situation (thereby avoiding long burn-in periods). The quickflow reservoir is initially empty. The initial surface water level is derived from the first discharge observation and the stage-discharge relation. The initial groundwater depth is computed with the assumption that initial groundwater drainage (f_{GS}) is equal to the initial discharge. It is also possible to supply the fraction of the initial discharge originating from drainage G_{frac} and the model will solve

$$Q_0 \cdot G_{frac} = \frac{(c_D - d_{G,0} - h_{S,0}) \cdot (c_D - d_{G,0})}{c_G} \quad (5.10)$$

for $d_{G,0}$ with the quadratic formula and then use the remainder of the discharge to compute the initial quickflow reservoir level:

$$h_{Q,0} = Q_0 \cdot (1 - G_{frac}) \cdot c_Q . \quad (5.11)$$

Alternatively, the initial groundwater depth can be supplied (or calibrated) by the user and $h_{Q,0}$ is computed such that $Q_0 = f_{GS,0} + f_{QS,0}$ again. The initial storage deficit is assumed to be the equilibrium value belonging to the initial groundwater depth.

5.4.3 Parameters

WALRUS has four parameters which require calibration: c_W, c_V, c_G and c_Q. These parameters have a physical meaning and can be explained qualitatively with catchment characteristics. The channel depth c_D and surface water area fraction a_S can

be estimated from field observations. When the default stage-discharge relation is used, the bankfull discharge c_S and (if applicable) the weir elevation $h_{S,min}$ need to be supplied (or calibrated) as well. Parameters are catchment-specific, but time-independent, to allow a calibrated model to be run for both long periods and events. We did not implement a specific calibration routine in the model, but used the HydroPSO package, which is a particle swarm optimization technique (Zambrano-Bigarini and Rojas, 2013). The user can define the (multi-) objective function.

5.4.4 Forcing

Forcing data can be supplied as a time series or as a function (e.g. a sine function for ET_{pot} or a Poisson rainfall generator). Observation times do not need to be equidistant, which is especially useful for tipping-bucket rain gauges. Forcing time series are converted to functions (e.g. cumulative P as function of time), which allows other time steps than used for the original forcing.

5.4.5 If-statements

If-statements associated with thresholds cause non-linearities in a model and their abrupt changes hamper calibration, in particular when using gradient-based methods. It is therefore important to know that there are four causes for abrupt changes in the model: (1) The stage-discharge relation (supplied by a user) may show abrupt changes at the elevation of the crest of the weir or at the soil surface; (2) No evaporation occurs from empty channel beds; (3) If the storage deficit becomes negative or exceeds the groundwater depth, the groundwater depth becomes equal to the storage deficit; (4) If either groundwater or surface water level exceeds the soil surface, overland flow is instantaneous.

5.4.6 Integration scheme

The model is implemented as an explicit scheme, because nonlinearities caused by feedbacks and if-statements do not allow for the use of an implicit scheme. The states at the end of the previous time step are used to compute the fluxes during the current time step, which are then used to compute the states at the end of the current time step (Fig. 5.7). The output data file lists the sums of the fluxes during and the states at the end of each time step.

5.4.7 Time step

The user can specify at which moments output should be generated, for example with a fixed in-
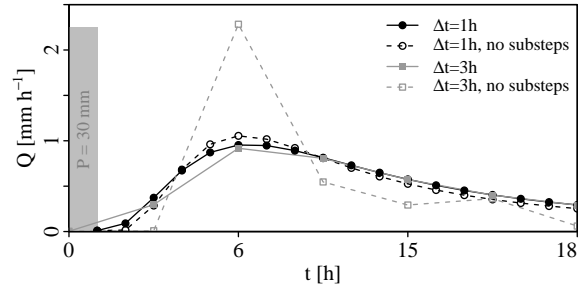

Figure 5.8: The effect of variable time steps on the model output. An artificial case with a rainfall event of 30 mm in the first hour and no evapotranspiration. The lines connect the discharge modelled at the end of a time step (instantaneous value), and do not represent the sum over the time step (which is given in the output file). The same parameter values as in Fig. 5.3 were used.

terval (i.e. each hour or day), with increased frequency during certain events or after each millimeter of rainfall. The output time steps can be both larger and smaller than those of the forcing.

An important feature of the model code is the flexible computation time step. The model first attempts to run a whole output time step at once, but the time step is decreased when (1) the rainfall sum, discharge sum or change in discharge, surface water level or groundwater depth during the time step exceeds a certain threshold, or when (2) the surface water level is negative at the end of the time step. The first criterion prevents numerical instability caused by the explicit integration scheme and a delayed the response to rainfall as a result of the explicit model code (it takes one step to update the surface water level and another for the discharge). The second criterion is necessary because the total surface water outflow, computed from water levels at the start of the time step and the time step size, can exceed the available water. Because this means that non-existing water flowed out, there is a physical reason to avoid this.

The procedure of decreasing time steps is illustrated in Fig. 5.7 (3rd step). First the original time step is halved and the model is run for this substep (of course with the forcing corresponding to this substep). When the criteria are still not met, the step size will be halved again and again until the criteria are met. When one substep is completed, the fluxes are stored and the states at the end of the time step are used as initial values for the next substep. Then the model is run for the remainder of the original time step and, if necessary, the substep is halved until the criteria are met. This will continue until the end of the intended output time step is reached. The sum of the fluxes of the substeps and the states of the

last substep are stored in the output file.

The effect of the variable time step is illustrated in Figure 5.8, in which the output of the model ran with a fixed time step and with variable time steps is shown. Note the erroneous time delay and magnitude of the discharge peak when no substeps are used, in particular for the three hourly time step.

5.4.8 Water balance

WALRUS is a mass conserving model, and therefore the model water budget, computed as

$$
\begin{aligned}
\Sigma P - \Sigma ET_{\text{act}} - \Sigma Q + \Sigma f_{\text{XG}} + \Sigma f_{\text{XS}} = \\
-\Delta d_{\text{V}} \cdot a_{\text{G}} + \Delta h_{\text{Q}} \cdot a_{\text{G}} + \Delta h_{\text{S}} \cdot a_{\text{S}} ,
\end{aligned}
\tag{5.12}
$$

always closes, although rounding errors may cause small deviations. The minus sign before Δd_{V} appears because d_{V} expresses a deficit and a decrease in storage deficit implies an increase in water in the reservoir. The groundwater level does not appear explicitly in the water balance, because it only plays a role as a pressure level driving groundwater drainage and surface water infiltration fluxes, while the storage deficit accounts for volume changes in the whole soil reservoir.

5.5 Conclusion

The Wageningen Lowland Runoff Simulator (WALRUS) is a new rainfall-runoff model, which is suitable for lowlands where shallow groundwater and surface water influence runoff generation. The model includes:

1. *Groundwater-unsaturated zone coupling* – WALRUS contains one soil reservoir, which is divided effectively by the (dynamic) groundwater table into a groundwater zone and a vadose zone. The condition of this soil reservoir is described by two strongly dependent variables: the groundwater depth and the storage deficit (the effective thickness of empty pores). This implementation enables capillary rise when the top soil has dried through evapotranspiration.

2. *Wetness-dependent flowroutes* – The storage deficit determines the division of rain water between the soil reservoir (slow routes: infiltration, percolation and groundwater flow) and a quickflow reservoir (quick routes: drainpipe, macropore and overland flow).

3. *Groundwater-surface water feedbacks* – Surface water forms an explicit part of the model structure. Drainage depends on the difference between surface water level and groundwater level (rather than groundwater level alone), allowing for feedbacks and infiltration of surface water into the soil.

4. *Seepage and surface water supply* – Groundwater seepage and surface water supply or extraction (pumping) are added to or subtracted from the soil or surface water reservoir. These external fluxes affect the whole system through the groundwater-surface water feedbacks and saturated-unsaturated zone coupling.

The open source model code is implemented in R and the model is set-up such that it can be used by both practitioners and researchers. For direct use by practitioners, defaults are implemented for relations between model variables and to compute initial conditions, leaving only four parameters which require calibration. For research purposes, the defaults can easily be changed. WALRUS is computationally efficient, which allows operational forecasting and uncertainty estimation by creating ensembles. An approach for flexible time steps increases numerical stability and makes model parameter values independent of time step size, which facilitates use of the model with the same parameter set for multi-year water balance studies as well as detailed analyses of individual flood peaks.

Numerical experiments shows that the implemented feedbacks have the desired effect on the system variables: (1) the wetness-dependent division between slow and quick flowroutes results in more quickflow, less recharge and higher discharge peaks during wet periods; (2) the surface water level attenuates drainage during discharge peaks or when surface water is supplied upstream.

6 | Application of WALRUS

he Wageningen Lowland Runoff Simulator (WALRUS) is a new rainfall-runoff model which accounts explicitly for processes that are important in lowland areas, such as groundwater-unsaturated zone coupling, wetness-dependent flowroutes, groundwater-surface water feedbacks, and seepage and surface water supply (Brauer et al., 2014a). Lowland catchments can be divided into slightly sloping, freely draining catchments and flat polders with controlled water levels. Here, we apply WALRUS to two contrasting Dutch catchments: the Hupsel Brook catchment and Cabauw polder. In both catchments, WALRUS performs well: Nash-Sutcliffe efficiencies obtained after calibration on one year of discharge observations are 0.87 for the Hupsel Brook catchment and 0.83 for the Cabauw polder, with values of 0.74 and 0.76 for validation. The model also performs well during floods and droughts and can forecast the effect of control operations. Through the dynamic division between quick and slow flowroutes controlled by a wetness index, temporal and spatial variability in groundwater depths can be accounted for, which results in adequate simulation of discharge peaks as well as low flows. WALRUS performance is most sensitive to parameters controlling the wetness index and the groundwater reservoir constant, and to a lesser extent to the quickflow reservoir constant. The effects of these three parameters can be identified in the discharge time series, which indicates that the model is not overparameterised (parsimonious). Forcing uncertainty was found to have a larger effect on modelled discharge than parameter uncertainty and uncertainty in initial conditions.

6.1 Introduction

There is growing awareness that for simulation and prediction of water and energy fluxes in lowland areas, models need to explicitly account for the dynamic groundwater table (Alley et al., 2002; Maxwell and Miller, 2005; Kollet and Maxwell, 2006; Bierkens and van den Hurk, 2007; Maxwell and Kollet, 2008). In many modelling approaches, existing models of vertical water movement in the unsaturated zone are coupled to groundwater models which simulate the horizontal flow (e.g. Gilfedder et al., 2012; Zampieri et al., 2012). This approach, however, has clear limitations in flat lowland areas where the shallow groundwater table (<2 m below surface) often rises to within the unsaturated model domain, or even to the land surface (Appels et al., 2011; Brauer et al., 2011). In addition, surface water networks are generally dense and surface water levels influence drainage fluxes and groundwater levels. These groundwater-surface water interactions are important in both freely draining catchments and polders. Not surprisingly, hydrological models with a more traditional structure (i.e. without coupling and feedbacks) often fail to reproduce discharge dynamics in lowland catchments (Bormann and Elfert, 2010; Koch et al., 2013). Thus, instead of coupling existing models, hydrological models for application in lowland areas should be derived from a conceptually sound and strong coupling between groundwater and the unsaturated zone as well as between groundwater and surface water.

We developed a rainfall-runoff model for application in lowland areas. This model, the Wageningen Lowland Runoff Simulator (WALRUS) is described in detail in Ch. 5. The structure of WALRUS (see Fig.5.1) is different from that of traditional lumped rainfall-runoff models. Firstly, the unsaturated and saturated zones are tightly coupled, so that any increase in groundwater level automatically leads to a decrease in unsaturated zone thickness and vice versa. Secondly, the model conceptualises the varying contribution of fast flowroutes through a wetness-dependent divider (inspired by Stricker and Warmerdam, 1982). Finally, the model explicitly accounts for groundwater-surface water interaction through the inclusion of a surface water reservoir, which represents the channel network. This allows for negative feedbacks on subsurface flow during peak discharges or as a result of surface water supply.

WALRUS consists of three reservoirs: a soil reservoir (including vadose zone and groundwater), a quickflow reservoir and a surface water reservoir (Fig. 5.1). At the land surface, water is added to the different reservoirs by precipitation (P). A fixed fraction is led to the surface water reservoir (P_S). The soil wetness index (W) determines which fraction of the remaining precipitation percolates slowly through the soil matrix (P_V) and which fraction flows towards the surface water via quick flow routes (P_Q). Water is removed by evapotranspiration from the vadose zone (ET_V) and surface water reservoir (ET_S). The vadose zone is the upper part of the soil reservoir and extends from the soil surface to the dynamic groundwater table (d_G), including the capillary fringe. The dryness of the vadose zone is characterised by a single state: the storage deficit (d_V),
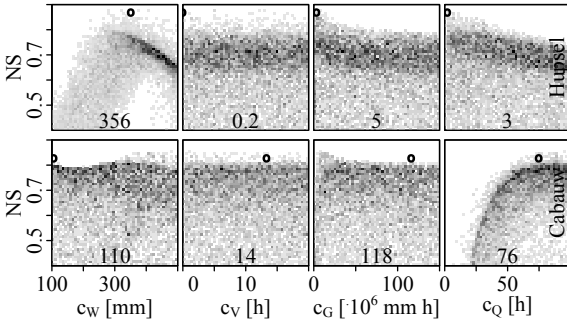
Figure 6.1: Relation between Nash-Sutcliffe efficiency and parameter values for The Hupsel Brook catchment (top row) and the Cabauw polder (bottom row). The 10,000 grey dots are obtained with Monte Carlo analyses. The black circles and numbers indicate the parameter values and resulting Nash-Sutcliffe efficiencies obtained with HydroPSO.

which represents the effective thickness of empty pores (or the amount of water necessary to saturate the profile). It controls the evapotranspiration reduction (β) and the wetness index (W). The phreatic groundwater extends from the groundwater depth (d_G) downwards, thereby assuming that there is no shallow impermeable soil layer and allowing groundwater to drop below the bottom of the drainage channels (c_D) in dry periods. The groundwater table responds to changes in the storage deficit and determines, together with the surface water level, groundwater drainage or infiltration of surface water (f_{GS}). All water that does not flow through the soil matrix, passes through the quickflow reservoir to the surface water (f_{QS}). This represents macropore flow through drainpipes, animal burrows and soil cracks, but also local ponding and overland flow. The surface water reservoir has a lower boundary (the channel bottom c_D), but no upper boundary. Discharge (Q) is computed from the surface water level (h_S). Water can be added to or removed from the soil reservoir by seepage (f_{XG}) and to/from the surface water reservoir by surface water supply or pumping (f_{XS}). Model equations and abbreviations of variables used in this chapter are listed in Tab. 5.1. For a more detailed model description, see Ch. 5.

Whenever models are developed from a certain conceptualization of reality, they should be thoroughly tested under different circumstances to find out whether the model yields the intended outcome and to thoroughly understand the feedbacks between states, fluxes and parameters (e.g. Klemeš, 1986; Oreskes et al., 1994; Refsgaard and Knudsen, 1996; Beven, 2007; Kavetski and Fenicia, 2011). Evaluation of rainfall-runoff models can focus on (1) performance, often measured with objective functions such as the Nash-Sutcliffe efficiency, (2) uncertainty in parameter values and model structure or (3) realism of the simulated processes, by comparing to the modeller's understanding of the hydrological system and the intended function of model components (Wagener, 2003). Here we focus our evaluation on these different aspects.

In this Chapter we will use almost all hydrological measurements described in Ch. 2 from the freely draining Hupsel Brook catchment and the Cabauw polder with controlled water levels to evaluate the performance of WALRUS during calibration (Sec. 6.2) and several validation runs (Sec. 6.3). In Section 6.4, we examine sensitivity of WALRUS to parameters, objective functions used for calibration and default functions. In Section 6.5 we investigate the effect of uncertainty in forcing, initial conditions and parameters on modelled discharge.

6.2 Calibration

Because geology, slope and drainage densities differ between catchments, the model parameters expressing the effects of these characteristics differ as well. Although the parameters have physical connotations, they are effective values representing the entire catchment (including the effect of heterogeneity). Therefore, they cannot be estimated from field measurements directly, but have to be calibrated. Fitting simulations to observations yields catchment-specific parameter values, which (as they are assumed to be time-invariant) can be used to simulate discharge during other periods.

For both the Hupsel Brook catchment and the Cabauw polder, we optimized four model parameters: the wetness index parameter c_W, vadose zone relaxation time c_V, groundwater reservoir constant c_G and the quickflow reservoir constant c_Q (see Fig. 5.1 and Tab. 5.1 for a complete overview of all model variables, parameters and relations). We used the stage-discharge relations of the outlet weirs (which were calibrated in the laboratory) and channel depths c_D of 1500 mm (estimated from observations). The weir level $h_{S,min}$ in the Cabauw polder was set to 500 (winter) and 600 (summer) mm from the channel bottom (based on field estimates). We used default functions for $W(d_V)$, $d_{V,eq}(d_G)$ and $\beta(d_V)$ and soil physical parameters b, ψ_{ae} and θ_s based on observations in the Hupsel Brook catchment and the Cabauw polder (see Brauer et al., 2014a).

For the calibration, we used hourly data of the periods November 2011–October 2012 (Hupsel) and October 2007–September 2008 (Cabauw). Unfortunately, it was not possible to use the same period for both catchments, since time series were not contin-
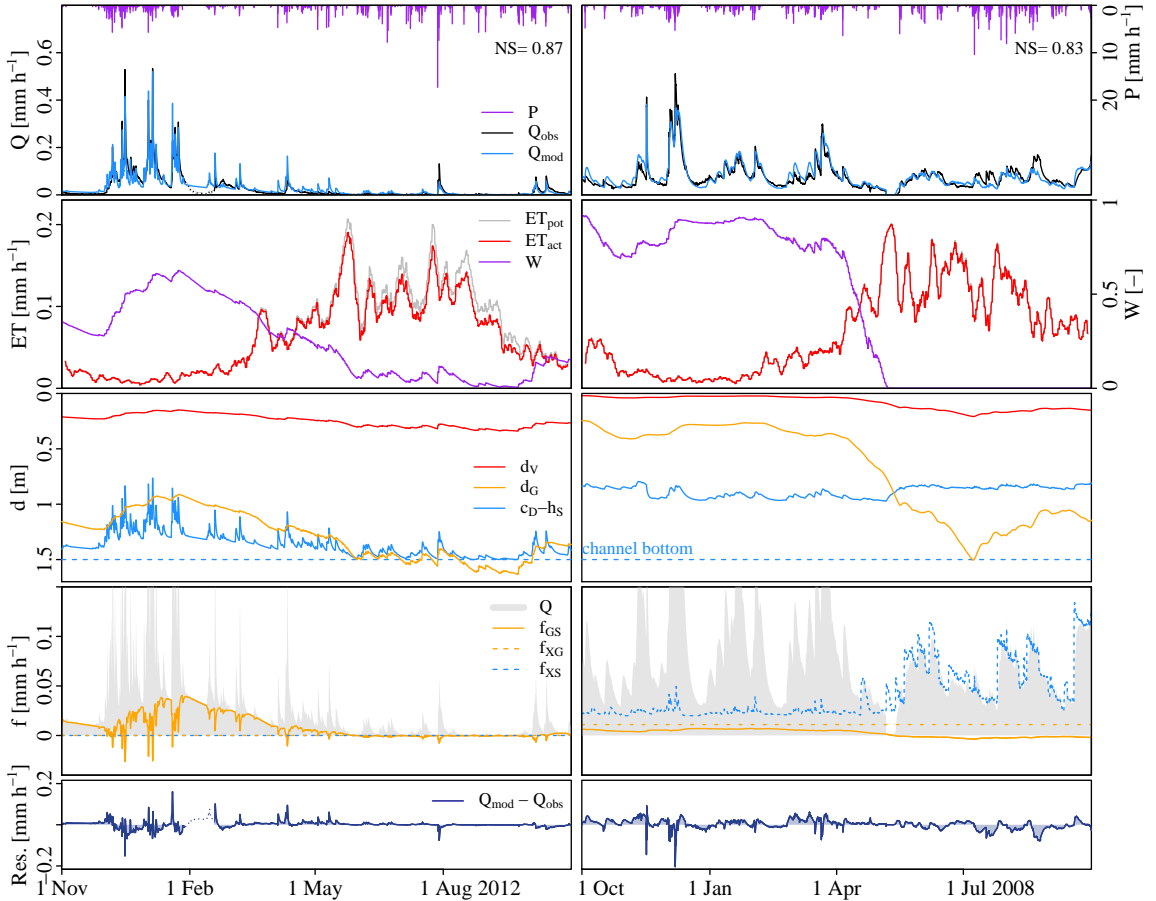
Figure 6.2: Model output after calibration. Evapotranspiration data are 5-day moving averages to eliminate daily cycles and focus on long-term differences between ET_{pot} and ET_{act}. The dotted part of Q_{obs} in Feb. 2012 denotes a period with sub-zero temperatures. The surface water level h_S is measured with respect to the channel bottom, while the groundwater depth is measured with respect to the soil surface. The channel depth c_D relates the two to each other. The storage deficit d_V is not a measurable depth, but rather an effective thickness.

uous. Both periods are not exceptionally dry or wet and do not contain long periods of sub-zero temperatures (except Feb. 2012). Several choices of objective functions are compared in Sect. 6.4.5, but a classical Nash-Sutcliffe efficiency of the discharge was used as main objective function (Nash and Sutcliffe, 1970).

We used a particle swarm optimization technique by Zambrano-Bigarini and Rojas (2013), called HydroPSO, which is less sensitive to discontinuities in the response surface (i.e. due to thresholds in the model) and more likely to find a global optimum than other gradient-based methods. The parameter values obtained with this HydroPSO calibration are used throughout the chapter. A comparison of optimization algorithms is outside the scope of our study. In addition to the calibration with HydroPSO, a Monte Carlo analysis was used to explore uncer-

tainty in and dependency between parameters (in Fig. 6.1, Sect. 6.4.4 and Sect. 6.5.1). For the Monte Carlo analysis, we generated 10,000 random parameter sets with ranges 100–500 mm (c_W), 0.1–20 h (c_V), 0.1–150 mm h (c_G) and 1–100 h (c_Q).

6.2.1 Calibrated parameter values

The optimal parameter values found with HydroPSO and the relations between parameter values and Nash-Sutcliffe efficiencies obtained with the Monte Carlo analysis are shown in Fig. 6.1. Finding optimal parameter values is not trivial (e.g. Beven and Freer, 2001b; Melsen et al., 2013). We used HydroPSO to obtain one optimal parameters set, but the dotty plots show that equally good results (in terms of Nash-Sutcliffe efficiency) could have been obtained with different combinations.

Table 6.1: Water balance terms [mm] for the calibration and validation periods. ΔS denotes a change in soil moisture storage – a negative change in soil moisture storage denotes a depletion of the soil reservoir. It is possible for ET_{act} to exceed ET_{pot} in the Hupsel Brook catchment in 1979–1980 because measurements were independent.

| | Hupsel | | | | Cabauw | | | |
| | cal | | val | | cal | | val | |
	obs	mod	obs	mod	obs	mod	obs	mod
ΣP	725	-	682	-	723	-	594	-
ΣET_{pot}	587	-	480	-	607	-	635	-
ΣET_{act}	-	531	496	454	574	604	606	629
ΣQ	230	249	286	239	668	688	969	1012
Σf_{XG}	0	-	0	-	97	-	96	-
Σf_{XS}	0	-	0	-	359	-	803	-
Σf_{GS}	-	74	-	57	-	22	-	13
Σf_{QS}	-	174	-	189	-	303	-	203
ΔS	-	-54	-15	-11	-62	-110	-92	-143
residual	-	0	-78	0	0	0	10	0

When comparing the Cabauw polder to the Hupsel Brook catchment, differences in parameter values can be observed and explained. Parameters c_V, c_G and c_Q are higher, indicating that all flow is slower. Parameter c_W is smaller, causing earlier activation of quick flowroutes (at higher storage deficits). Compared to the Hupsel Brook catchment, the clayey soil in the Cabauw polder is less permeable, leading to slower groundwater flow (c_G) and a slower response of groundwater to changes in the unsaturated zone (c_V). There are more cracks, gullies and drainpipes per unit area (c_W), but quickflow is slower because slopes of land surface (overland flow) and drainpipes are lower (c_Q). It is not a coincidence that the drainage density increases when permeability decreases. Farmers install drainpipes and dig gullies when ponding hampers agricultural activities, animals (moles, mice and muskrats) dig more burrows to drain their dens and cracks occur more quickly in clayey soils.

6.2.2 Calibrated results

Discharge is reproduced well during the calibration period, both for peaks in winter and for low flows and small peaks in summer (Fig. 6.2). Nash-Sutcliffe efficiencies of 0.87 for the Hupsel Brook catchment and 0.83 for the Cabauw polder are reached. This shows that the model with the optimal parameters is able to capture the hydrological response of lowland catchments.

In February 2011 the headwaters of the Hupsel Brook were frozen, which caused a decrease in observed discharge. Because WALRUS in the present form does not take freezing conditions and snow into account, the simulated discharge does not decrease as quickly.

WALRUS simulates the discharge in summer relatively well. Although the groundwater level dropped below the channel bottom (in agreement with reality), the channel did not run dry, because both discharge and infiltration of surface water decrease rapidly at low water levels. Only evapotranspiration can empty the channel completely. During summer field visits, we frequently observed that, while a large part of the surface water network is dry, some storm water is still discharged at the outlet after rain events. Even when the soil is dry, some quickflow will occur close to the ditches or over paved areas.

The modelled groundwater depth d_G shows seasonal variation, but does not respond quickly to rainfall events. In the model, percolating water is significantly delayed in the vadose zone and the dynamic response to rainfall is modelled by the quickflow reservoir. The groundwater depth does influence the catchment's quick response to rainfall events, because when groundwater is shallow, percolation is slow and storage deficits are small, resulting in a high wetness index and a large portion of the rain being led through the quickflow reservoir.

Groundwater drainage (f_{GS}) shows both long-term and short-term dynamics. The seasonality in f_{GS} is caused by seasonality in groundwater levels, which are higher in winter due to the precipitation surplus. The quick decreases are caused by fluctuations in surface water level, which rise and fall rapidly after rainfall events. This shows that the groundwater-surface water feedback is implemented appropriately: during discharge peaks, drainage is limited by high surface water levels.

The surface water levels are much more constant in the Cabauw polder than in the Hupsel Brook catchment. Surface water supply prevents headwa-
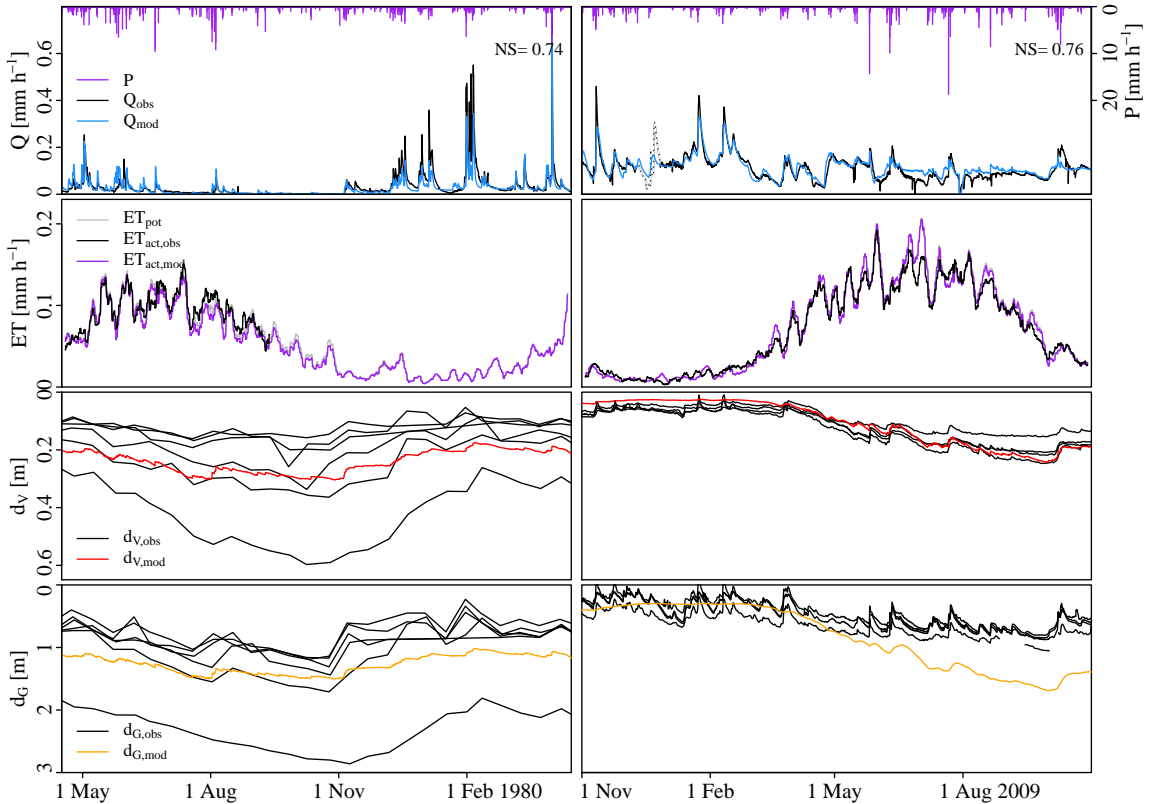
Figure 6.3: Validation of model results with discharge, actual evapotranspiration, soil moisture and ground-water data. Note that the temporal resolution of the soil moisture and groundwater data in the Hupsel Brook catchment is 14 days and evapotranspiration data are 5-day moving averages (to eliminate daily cycles and focus on long-term changes). The different lines for observed d_V and d_G represent different locations. A culvert was blocked and opened in the Cabauw polder in Dec. 2008 (dotted part in Q_{obs}).

ters from running dry in summer. In addition, the Cabauw polder has a five times larger fraction of surface water, which acts as a buffer and absorbs inflow peaks caused by rainfall events.

6.2.3 Water budget

In the Hupsel Brook catchment, quickflow (f_{QS}) accounts for 70 % of total drainage ($f_{GS} + f_{QS}$; Table 6.1). This is consistent with the important role of quickflow found in previous studies. Van der Velde et al. (2011) measured drainpipe flow in one field in the Hupsel Brook catchment and found that the contribution of drainpipe flow (one of the components of quickflow) to the total drainage was 80 % for that field and estimated it to be 25–50 % for the entire catchment.

In the Cabauw polder, the contribution of groundwater drainage is limited. However, the groundwater depth plays an important role in dividing the water between the soil reservoir and the quickflow reservoir.

In both catchments the change in storage in the soil reservoir is considerable: -54 mm in the Hupsel Brook catchment and -110 mm in the Cabauw polder. Observations of discharge in the Hupsel Brook catchment (as a proxy for storage) and soil moisture in the Cabauw polder show that both years chosen for calibration ended drier than they started. However, the decrease in storage in the Cabauw polder was overestimated.

Evapotranspiration reduction is negligible in the Cabauw polder ($604/607 = 0.5$ %), but significant in the Hupsel Brook catchment ($531/587 = 10$ %).

6.3 Validation

The parameter values obtained during the calibration runs described in the previous section were used in validation studies for whole years, a short period to focus on groundwater dynamics, major flood and drought events, and a case with management operations. We altered the initial groundwater depth for every validation run to match the real catchment

wetness at the start of each validation period (because in contrast to parameters, initial conditions are not time-invariant).

6.3.1 Validation on yearly timescale

For both catchments, we selected one year for which actual evapotranspiration, soil moisture and groundwater data were available: the period 15 April 1979–15 April 1980 for the Hupsel Brook catchment and 1 Nov. 2008–1 Nov. 2009 for the Cabauw polder. These additional data are used to test whether the model only reproduces the observed discharge or also the hydrological processes involved. The requirement of these additional data and allowing no gaps limited the choice of years for validation studies to one or two (different) years for each catchment and we chose years that are not exceptionally dry or wet and do not contain long periods of freezing conditions (except Jan. 2009).

Model results and measurements are shown in Figure 6.3 and some annual sums of water balance terms are shown in Table 6.1. For both catchments, Nash-Sutcliffe efficiencies are lower for the validation runs than for the calibration runs, but still acceptable: they decrease from 0.87 to 0.74 for the Hupsel Brook catchment and from 0.83 to 0.76 for the Cabauw polder. This relatively small decrease in performance indicates that the model is parsimonious. In both catchments the highest discharge peaks are underestimated.

During a field visit in the Cabauw polder in December 2008, a culvert was found clogged with loose vegetation, reducing discharge capacity and raising water levels upstream. When the blockage was removed, the water stored upstream was released, leading to a sharp discharge peak.

In the Hupsel Brook catchment, modelled storage deficits and groundwater depths fall within the range of observations of the different stations, but in the Cabauw polder, the groundwater depth is overestimated at the end of the year. Including groundwater levels in the calibration procedure (multiobjective calibration) may lead to better estimates.

6.3.2 Groundwater dynamics

To evaluate the modelled response of groundwater to rainfall events, we selected two periods for which groundwater data with high temporal resolution were available (for locations, see Fig. 2.1). In the Hupsel Brook catchment, the piezometers were well distributed over the catchment, leading to a large variability in observed groundwater depths and dynamics (Fig. 6.4). The piezometer with the shallowest and most dynamic groundwater table is located close to the surface water network, in the part of the catchment where the aquifer is thin. As a consequence, ponding and overland flow occur relatively quickly and the drainage density is large. The two piezometers with the deepest and least dynamic groundwater tables are located where the aquifer is thick and permeable. The relatively thick unsaturated zone attenuates infiltrating water and ponding and overland flow hardly ever occur.

The modelled groundwater depth falls within the range of observations in the Hupsel Brook catchment, but hardly varies in time. This is caused by the function of the groundwater reservoir in WAL-RUS. The groundwater reservoir only simulates the seasonal groundwater dynamics for groundwater drainage, while the quickflow reservoir accounts for the dynamic response to individual rainfall events. Observed groundwater levels measured at different locations are the results of different contributions of quickflow and groundwater flow. The most dynamic groundwater tables in Fig. 6.4 can be compared to a combination of the quickflow and groundwater reservoirs, while the least dynamic groundwater tables mainly represent the groundwater reservoir alone. In the Cabauw polder, observed groundwater depths are much more variable than simulated ones (Fig. 6.4). This indicates that the contribution of quickflow is large in all measured locations.

By using two reservoirs to simulate the characteristic "coupled dynamics" of groundwater tables, the discharge can be reproduced well. Using groundwater time series for calibration or validation is possible, but not trivial (as is the case for all lumped rainfall-runoff models). In addition, piezometers are often situated in locations with large seasonal dynamics. The 6 piezometers used in the Hupsel Brook catchment in the 1970s and 1980s overestimate the variation in total catchment storage (reflecting the seasonal variation), which may be caused by the installation of piezometers in the centre of fields rather than near the channels (Brauer et al., 2013).

6.3.3 Extreme rainfall and flash flood

On 26 August 2010, an extreme rainfall event occurred in the Hupsel Brook catchment (Brauer et al., 2011). In 24 hours, about 160 mm rainfall was observed, corresponding to a return period of more than 1000 years. This resulted in soil saturation, overland flow and inundation. Some of the lessons learnt from the analysis of this flash flood event, such as the importance of the groundwater-surface water feedback and wetness-dependent flowroutes, were taken into account during the development of WALRUS (Brauer et al., 2014a). The flood in August 2010 has triggered a model intercomparison study (without WALRUS) initiated by the Dutch Hydrolog-
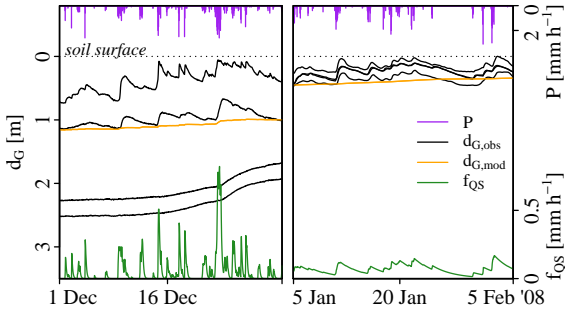
Figure 6.4: Comparison of modelled and observed groundwater depths. The different black lines are observations at different locations in the catchments (denoted as diamonds in the map in Fig. 2.1).
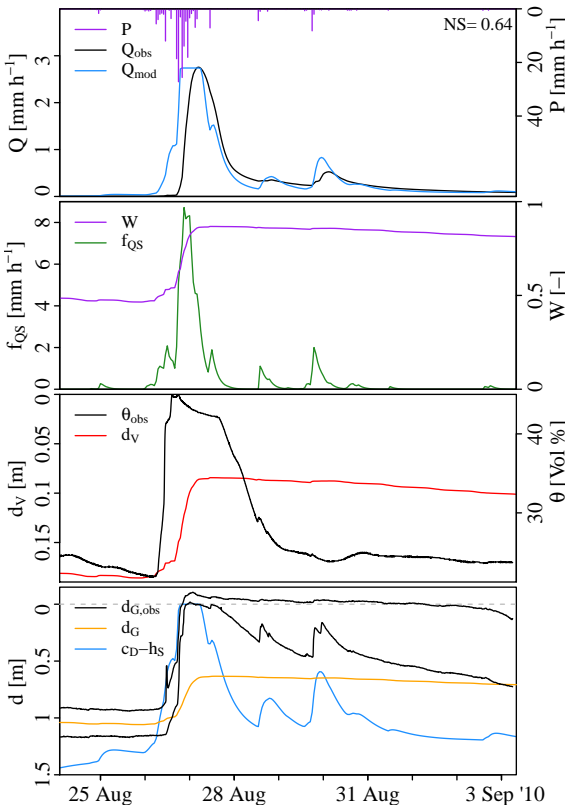

Figure 6.5: Simulation of the flash flood in the Hupsel Brook catchment after the extreme rainfall event in August 2010. Groundwater observations were available from two piezometers near the meteorological station: one in a local depression and one in a local elevation (as shown in Brauer et al., 2011). Soil moisture content was measured in the same field (in a local elevation).
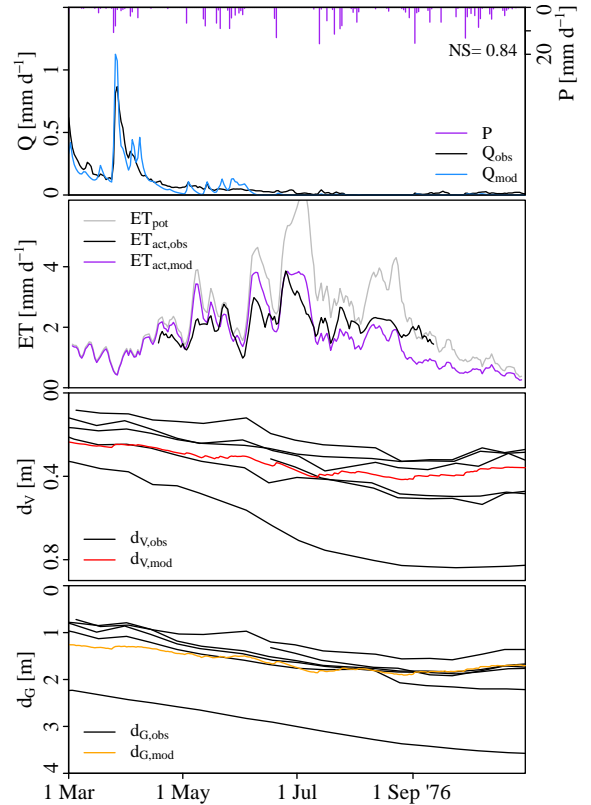

Figure 6.6: Simulation of the extremely dry summer of 1976. Note that in contrast to previous model runs, these model output and rainfall and discharge data are daily, groundwater and soil moisture data are biweekly and evapotranspiration are 5-day moving averages.
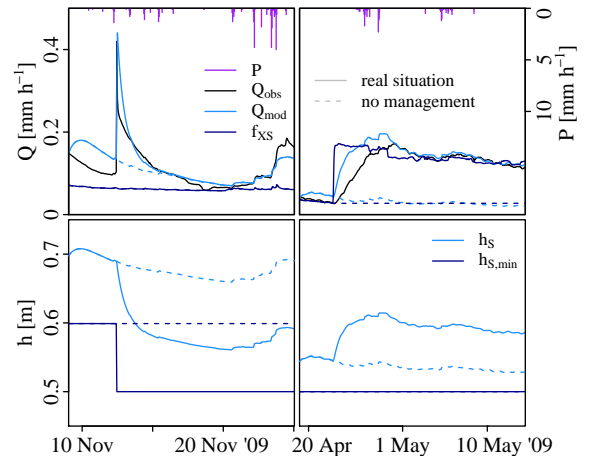

Figure 6.7: Reproduction of the Cabauw polder response to water management interventions: weir level decrease (left panels) and increase in surface water supply (right).

ical Association (NHV), in which teams from Dutch consultancy firms, institutes and universities participated (NHV, 2014).

We used the calibrated model to simulate this extreme event (not part of the calibration period). We used the mean of the observed groundwater depths as initial groundwater level for the simulation, mimicking a real flood forecasting situation, where information about the discharge in the future is not available. This yielded a relatively good discharge response, considering that neither parameters nor initial conditions were fitted to the data of the event (Fig. 6.5). The Nash-Sutcliffe efficiency, however, was relatively low (0.64), mostly because the timing of the peak was slightly off. The total discharge was overestimated by WALRUS: 98 mm, compared to 87 mm observed (runoff ratios of 0.50 and 0.44). The peak discharge was simulated accurately, but the top was flatter than observed, because surface water levels exceeded the soil surface and water flowed overland to the groundwater reservoir. The peak was capped at the bankfull discharge, which has been defined by the stage-discharge relation. In reality, the peak has been capped in many channels at different heights and the combination of many thresholds probably led to the observed smooth curve. Altogether, WALRUS performs better than many models used in the intercomparison study, in which peak discharges were reported ranging from 0.2 to 10 mm h^{-1} (NHV, 2014).

In the model, complete catchment saturation is never reached in the soil reservoir. However, the wetness index reached 0.87, which means that 87 % of the precipitation is led through the quickflow reservoir. So, even though the effective groundwater depth did not reach the soil surface, ponding and overland flow occurred in a large part of the catchment. The wetness index reproduces an increasing fraction of ponding and overland flow in local depressions in the landscape and near the channels, while local elevations in the landscape remain unsaturated. With this technique, this lumped model can account for spatial variability of groundwater depths.

Observations show that groundwater reached the soil surface before overland flow occurred (Fig. 6.5), while according to the model water flowed overland from the surface water to the soil reservoir. Of course, the observations are point measurements and it is likely that areas closer to the channels have flooded before reaching saturation, while local elevations in the landscape remained dry. This example shows that relating modelled (catchment effective) variables to point measurements of groundwater depth and soil moisture content is not trivial.

The satisfactory results indicate that WALRUS can be applied for flood forecasting. The initial storage deficit (and groundwater level) has a large influence on the simulated discharge. It determines when quickflow starts, when the surface water reaches the soil surface and when overland flow towards the groundwater reservoir starts. State updating could reduce the predictive uncertainty resulting from uncertainty in initial conditions when used in an operational flood forecasting/early warning system.

6.3.4 Extreme summer drought

In 1976, much of western Europe including The Netherlands experienced one of the worst summer droughts in recent history (Van Huijgevoort et al., 2013). The annual precipitation sum in the Hupsel Brook catchment was 549 mm for the whole year, compared to 790 mm on average. High evapotranspiration accelerated the development of large storage deficits (Teuling et al., 2013). During this summer, intensive field observations in the Hupsel Brook catchment took place (Stricker and Brutsaert, 1978). Because hourly data were not available, daily data were used as input.

In general, the discharge was simulated well. The simulated initial recession in April and May is too steep and the response to rainfall events in late May and June is too strong, but the limited response to rainfall later on is simulated correctly. It should be noted that extreme drought conditions can temporarily change soil properties and hydrologic response (Seneviratne et al., 2012), which might explain the slight model mismatch in this period. Even during this extremely dry summer, some discharge was observed after rainfall events. This is simulated well by WALRUS, where a small portion of the rainfall is led through the quickflow reservoir, mimicking runoff from paved surfaces or through depressions near the surface water network. This shows the added value of the quickflow reservoir and the surface water reservoir – in models with only a groundwater reservoir, all rainfall would infiltrate into the soil and discharge would remain zero.

No observations of actual evapotranspiration were made before 15 April and after 15 September. It was assumed that it would not deviate much from its potential value in winter, which is confirmed by the data: ET_act is close to ET_pot in late April and early September (Fig. 6.6). Between May and August, a large evapotranspiration reduction is observed. The model simulates the evapotranspiration reduction well, apart from a slight underestimation at the start and a slight overestimation at the end of the period. For the whole period shown in Fig. 6.6, modelled evapotranspiration reduction was 30 % compared to 26 % observed. Depletion of groundwater and soil moisture were slightly under-

estimated, but fall well within the range of observed values.

6.3.5 Effect of water management

WALRUS can incorporate water management operations, which is important if it is to be used in human-influenced lowlands. To investigate if the model can also be used for water management scenario analyses or to separate natural and human effects on the hydrological system (see Van Loon and van Lanen, 2013, and references therein), we simulated the change in the hydrological variables as a result of water management operations in the Cabauw polder. As mentioned in Section 2.2, surface water levels in the Cabauw polder are controlled by adjusting weir elevations and regulating surface water supply.

In Fig. 6.7 model results are shown for situations with and without management operations, being lowering of the weir and increasing surface water supply. Observations of the actual situation (i.e. with management operations) are shown as well. The model reproduces the discharge response to water management operations well, although time delays become visible when we zoom into the short time windows in Fig. 6.7. Lowering the weir causes a discharge peak, as the water stored in the top 10 cm of the surface water is released quickly (left panels). As 5 % of the catchment is covered by surface water, this amounts to $(0.05 \times 100 =)$ 5 mm of water averaged over the catchment area. A sudden increase in surface water supply also leads to a discharge rise, but less rapidly, because first the extra water has to be distributed over the surface water network. This delay represents mostly the response time of the surface water system, which is determined by the surface water area fraction and the stage-discharge relation. This indicates that a surface water reservoir (such as incorporated in WALRUS) is necessary to simulate the effect of the water buffer.

6.4 Sensitivity analyses

We performed three types of analyses to assess the sensitivity of modelled discharge to changes in parameter values: Sect. 6.4.1 focusses on parameter identifiability through a time series analysis, Sect. 6.4.2 focusses on the parameter sensitivity with a novel statistical technique (DELSA) and Sect. 6.4.4 focusses on parameter uncertainty and dependence using an analysis of response surfaces. In addition, we investigate the sensitivity to the choice of objective function for calibration in Sect. 6.4.5 and choice of user-defined parameteriza-

tions in Sect. 6.4.6 (described in Brauer et al., 2014a, and listed in appendix 5.1).

6.4.1 Parameter identifiability

Calibration is improved and the risk of equifinality reduced when the influence of each parameter can be distinguished in the discharge time series. In this section, the derivative of discharge to each of the parameters $(\partial Q/\partial c)$ is determined, keeping the others fixed. This sensitivity is approximated by a numerical difference $\left(\frac{Q(c+\Delta c)-Q(c)}{\Delta c} \right)$, with $\Delta c = 10^{-4}$.

The parameter sensitivity is plotted in Figure 6.8 for all four calibration parameters, focusing on the Hupsel Brook catchment in December 2011 and January 2012 (part of Fig. 6.2). To facilitate comparison, we scaled each sensitivity time series with the parameter value in question.

The sensitivity series of c_W, c_G and c_Q are clearly different enough to make these parameters identifiable. Moreover, the differences can be understood. Sensitivity to the wetness index parameter c_W is large at the start of the period, when wetness index (W) is increasing after the dry summer period and decreases as the winter progresses. With a larger value of c_W, W will be larger at the same value of d_V, leading to more quickflow and higher discharge peaks initially. Because less water is led to the soil reservoir in comparison to the original simulation, d_V decreases less quickly and the same value of W is reached with a different combination of c_W and d_V.

As c_V, c_G and c_Q cause delay and attenuation, an increase in these parameters dampens the discharge signal. The effect of c_Q is easily understood, because there are no direct feedbacks between the quickflow and surface water reservoirs: an increase in c_Q causes a lower and longer discharge peak. The peak decreases (negative $\Delta Q/\Delta c$) and the tail height increases (positive $\Delta Q/\Delta c$). A larger value of c_G causes a decrease of groundwater drainage and lower discharge between peaks. Surface water infiltration during peak flows is limited as well, leading to increased discharge peaks.

Discharge is about 1000 times less sensitive to the vadose zone relaxation time parameter c_V than to the other parameters (see the length of the vertical coloured bars in Fig. 6.8). The time series of sensitivity to c_V in inversely proportional to the sensitivity to c_W. This indicates that it is impossible to distinguish the effect of c_V in the discharge time series and that calibration of this parameter with discharge data alone is impossible.
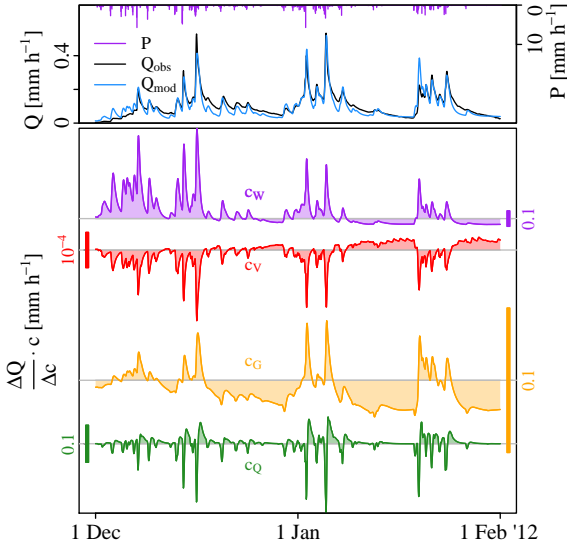
Figure 6.8: Identifiability of model parameters in the discharge time series. Top: observed and modelled discharge. Bottom: sensitivity of discharge to a change in each parameter.
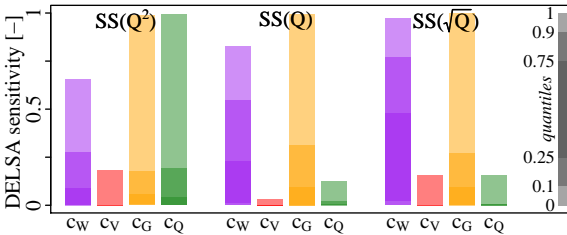

Figure 6.9: Parameter sensitivity computed with the Distributed Evaluation of Local Sensitivity Analysis (Rakovec et al., 2014), obtained for three objective functions ($SS(Q^2)$, $SS(Q)$ and $SS(\sqrt{Q})$). The bars show variation between parameter sets as quantiles. Because there are many realisations with low sensitivity, the lower quantiles are zero for most parameters (except c_W for $SS(Q)$ and $SS(\sqrt{Q})$)
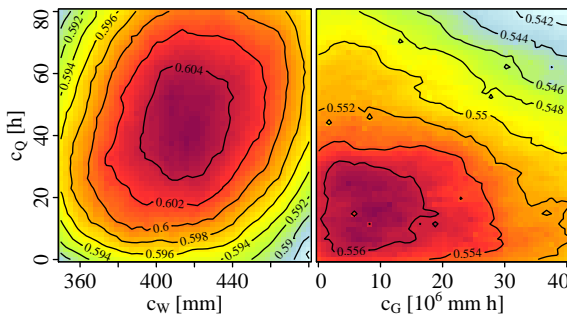

Figure 6.10: Examples of response surfaces showing the dependence between parameters. Colours indicate Nash-Sutcliffe efficiencies obtained with Monte Carlo simulations for the Hupsel Brook catchment.
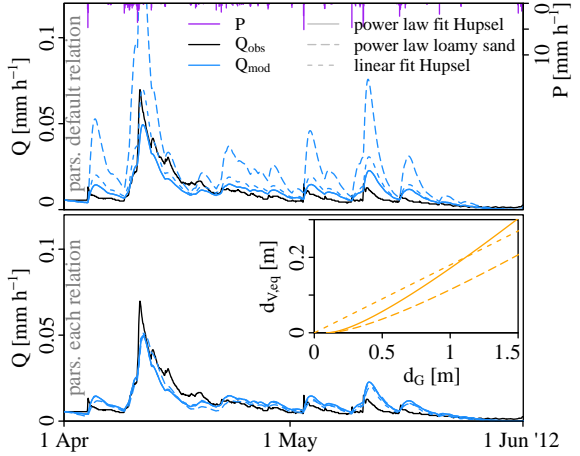

Figure 6.11: Effect of the relation between groundwater depth and equilibrium storage deficit. Three options for this relation are plotted in the inset: the relation based on a power-law soil moisture profile (the default), fitted on soil moisture and groundwater observations in the Hupsel Brook catchment (solid; default), the relation based on the theoretical power-law soil moisture profile for loamy sand (long dashed; Brooks and Corey, 1964) and a linear fit between soil moisture and groundwater observations in the Hupsel Brook catchment (dashed).
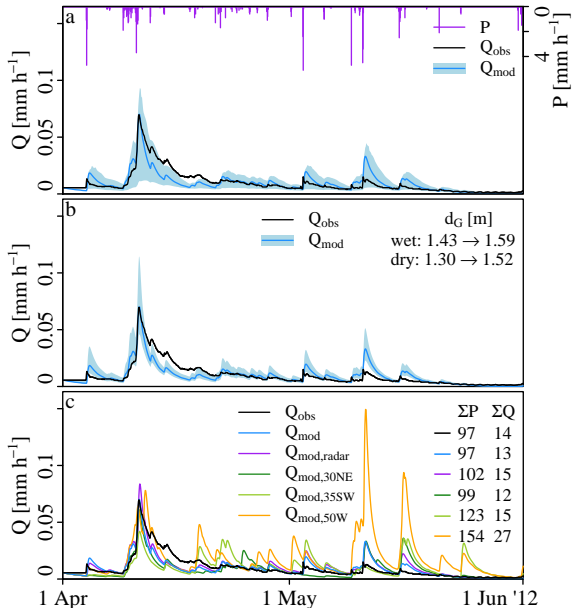
Figure 6.12: Propagation of uncertainty in parameters, initial conditions and forcing. **(a)** Range between the 10th and 90th percentile of discharge computed with 100 parameter sets. **(b)** Range between discharges computed with initial groundwater levels based on 0 % and 100 % of discharge originating from drainage. **(c)** Discharge computed with rainfall from radar and rain gauges in the Hupsel Brook catchment, Twenthe (30 km northeast), Wehl (35 km southwest) and Deelen (50 km west).

6.4.2 Parameter sensitivity

A more sophisticated method to determine the sensitivity of WALRUS to model parameters is the Distributed Evaluation of Local Sensitivity Analysis (DELSA, see Rakovec et al., 2014, for a complete explanation of the method). In short, this hybrid local-global sensitivity method decomposes the variance of a performance measure into contributions from individual parameters using multiple evaluations of local parameter sensitivities, which are distributed throughout the parameter space. The current implementation of the DELSA method provides first-order sensitivities for each of the model parameters. This means that only main effects on the total variance are captured and no parameter interactions are considered. In addition, the DELSA values conveniently scale between 0 and 1 and – when all variance is explained by one parameter, its DELSA sensitivity is 1. Finally, the advantage of DELSA is that a rather small sample size (yielding low computational cost) provides robust results.

To compute the DELSA values, we initially created 100 parameter sets (the base set). Next, we took the base set and perturbed one of the parameters, which we repeated for each of the four parameters. We ran WALRUS with these 500 sets and we evaluated the model output using three performance measures: the sum of squares (SS) of Q, of Q^2 (to focus on peaks) and of $\sqrt{Q}$ (to focus on low flows). For each of the four parameters, the DELSA sensitivity was computed from the difference in parameter value and model performance between the base run and the run with the perturbed parameter.

Figure 6.9 shows boxplots of the obtained DELSA sensitivity for each parameter and each performance measure, in which the ranges indicate the variation between parameter sets. The sensitivity to c_V is again small and the sensitivity to c_Q is only large when extra focus is placed on the peaks ($SS(Q^2)$). These two parameters only change the discharge temporarily, while c_W and c_G have a long-lasting effect through groundwater recharge (c_W) and recession (c_G). WALRUS is sensitive to c_W for many parameter sets (high sensitivity for low quantiles), especially when focussing on low flows ($SS(\sqrt{Q})$). Because c_W determines the amount of water that is led to the soil reservoir, and consequently the starting level of recession periods, a small change in this parameter can lead to overestimation or underestimation of baseflow.

6.4.3 Conclusions of parameter sensitivity analyses

In conclusion, the discharge is most sensitive to parameters c_W, c_G and c_Q. These parameters are iden-tifiable in the discharge time series. This gives confidence that the model is not overparameterized, which facilitates calibration and reduces the risk of equifinality. For c_V, however, an optimum cannot be determined with calibration on discharge data alone for the winter periods in the Hupsel Brook catchment analysed in Sect. 6.4.1. This does not mean that c_V is superfluous — c_V controls the delaying influence of the unsaturated zone, which is not visible unless one zooms in on individual discharge peaks.

6.4.4 Parameter uncertainty

Parameter uncertainty (or the statistics thereof) can be assessed by analysing the surface of the Nash-Sutcliffe efficiency as function of the parameters near the optimum. A first step into this direction is given in Fig. 6.1, where the Nash-Sutcliffe efficiency is plotted as a function of each individual parameter. This Figure was obtained from the Monte Carlo analysis with 10,000 random parameter sets (see Sect. 6.2). Fig. 6.1 shows that the curvature of the Nash-Sutcliffe surface near the optimum clearly differs between parameters, leading to different uncertainties. For example, the optimum of c_Q is clearly defined, while high Nash-Sutcliffe efficiencies appear over the whole range of c_V.

To analyse the simultaneous dependence of the Nash-Sutcliffe efficiency on two parameters, we made response surfaces for all parameter combinations for both catchments using the output from the same Monte Carlo analysis. As illustration, we plotted two response surfaces for the Hupsel Brook catchment in Fig. 6.10. The surfaces were obtained by inverse distance interpolation of the Nash-Sutcliffe efficiencies of the Monte Carlo simulations. The response surfaces are not entirely horizontal or vertical ellipses, indicating some parameter dependence. The c_W-c_Q combination leads to a slightly tilted ellipse, indicating that their optima are positively correlated. The top of the c_G-c_Q response surface is slightly horse-shoe shaped, leading to lower Nash-Sutcliffe efficiencies around $c_G = 5$ h and $c_Q = 15$ mm h. Negative values of c_G and c_Q are not physical and were therefore not chosen in the Monte Carlo analysis. It is also visible that the parameter c_Q has a different optimum in combination with c_W (30–60 h) than with c_G (5–30 h), which hampers calibration. The other parameter combinations lead to similar response surfaces, from which we can conclude that parameters in WALRUS are not independent, but do not show strong dependencies either.

For practical applications of WALRUS this rather computationally expensive Monte Carlo analysis can be replaced with a classical linearisation of the model near the optimum and an analysis of the resulting Hessian.

Table 6.2: Parameter values obtained by optimization with HydroPSO using different objective functions.

fit on:	Q^2	Q	$\sqrt{Q}$	d_{G}
c_{W}	400	380	379	107
c_{V}	1.8	0.8	8.2	0.2
c_{G}	5.3	5.0	5.0	5.0
c_{Q}	1	4	12	87

6.4.5 Sensitivity to calibration objective function

In this Section, we evaluate the effect of the choice of objective function used for calibration on the identified model parameters. We calibrated WALRUS for the Hupsel Brook catchment using 4 performance measures: the sum of squares of (1) the discharge, (2) the square of the discharge to focus on peaks, (3) the square root of the discharge to focus on low flows and (4) the groundwater level measured at the meteorological station. Because all model variables are given as model output and because the calibration does not occur within the model, calibration criteria can be changed easily. We used the longest period for which hourly groundwater data were available and no frost occurred: 1 March 2012 to 20 January 2013.

Fitting on $\sqrt{Q}$ leads to a higher value of the quickflow reservoir constant c_{Q} (12 h) compared to the fit on Q (4 h) and Q^2 (1 h) (Table 6.2). A high c_{Q} causes lower and broader peaks, improving the fit of the recessions (and worsening the fit of the peaks), while a low c_{Q} improves the fit of the peaks. Fitting on Q^2 yields a higher c_{W}, causing more water to be led to the quickflow reservoir. Fitting on d_{G} leads to a very small c_{W} – all water is led to the soil reservoir to mimic the dynamics of the observed groundwater depth. The observed groundwater depth, however, is represented by a combination of the soil reservoir and quickflow reservoir rather than the soil reservoir alone (Sect. 6.3.2). The large value of c_{Q} for the fit on d_{G} is insignificant, because no water is led to the quickflow reservoir.

6.4.6 Sensitivity to default parameterisations

There are four relations between model variables which can be specified by the user and for which defaults have been implemented: (1) the wetness index relation $W(d_{\mathrm{V}})$, (2) the evapotranspiration reduction function $\beta(d_{\mathrm{V}})$, (3) the relation between equilibrium storage deficit and groundwater depth $d_{\mathrm{V,eq}}(d_{\mathrm{G}})$, and (4) the stage-discharge relation $Q(h_{\mathrm{S}})$ (Tab. 5.1). These parameterisations are considered to be identifiable without calibration. Nevertheless, they are also prone to some uncertainty. To examine how sensitive the model is to changes in these relations (i.e. the effect of choices), we ran the model with different options for these functions, with and without recalibrating for each function.

As an example, the results for three options for $d_{\mathrm{V,eq}}(d_{\mathrm{G}})$ are shown in Fig. 6.11. The default option is the relation based on a power law soil moisture profile and data from the Hupsel Brook catchment (Brauer et al., 2014a). We also used the relation based on a power law soil moisture profile of loamy sand (Brooks and Corey, 1964) and a linear fit through observations in the Hupsel Brook catchment. The different relations are shown in the inset of Fig. 6.11.

In the top panel of Fig. 6.11, the same values for the four model parameters (c_{W}, c_{V}, c_{G} and c_{Q}) were used. These were obtained from calibration using the default option for $d_{\mathrm{V,eq}}(d_{\mathrm{G}})$. The initial conditions are computed automatically for each run, assuming stationary groundwater drainage (implemented as default). In the bottom panel, the model parameters were calibrated using the $d_{\mathrm{V,eq}}(d_{\mathrm{G}})$ function in question.

This Figure illustrates that parameters obtained using one function cannot be used directly with another function. The difference between the linear and power-law based fit on the data is limited, but for the theoretical relation peaks are strongly overestimated when the original parameter set is used. However, calibration using this relation yielded similar results.

6.5 Uncertainty propagation

Because WALRUS is computationally efficient, it is feasible to estimate the effect of different types of uncertainty by creating ensembles of model output. In this Section we investigate the consequences of uncertainty in parameter values, initial conditions and forcing data.

6.5.1 Propagation of parameter uncertainty

To examine the effect of parameter uncertainty, we created 10,000 parameter sets randomly by selecting from uniform distributions with ranges displayed in Fig. 6.1. We selected the 100 sets which yielded the highest Nash-Sutcliffe efficiencies for the calibration period used in Sect. 6.2 (Nov. 2011–Oct. 2012). These 100 parameters sets were used for 100 simulations of the period Apr. 2012–May 2012.

The range between the 10th and 90th percentile is shown in Figure 6.12a. Parameter uncertainty

causes the largest deviations during peak flows and decreases to almost zero during recessions. The uncertainty around the large peak of $0.07 \, \mathrm{mm\,h^{-1}}$ is quite large: the range between the 10th and 90th percentile ranges from 0.004 to $0.14 \, \mathrm{mm\,h^{-1}}$.

6.5.2 Propagation of initial condition uncertainty

Initial groundwater depth and quickflow reservoir level can be specified by providing the fraction of discharge at $t = 0$ which originates from groundwater (G_{frac}). The remainder ($1 - G_{\mathrm{frac}}$) is used to compute the quickflow reservoir level. To investigate the effect of these initial conditions, the model calibrated in Section 6.2 is run with an initial groundwater depth based on 0 % and 100 % of discharge originating from drainage (G_{frac} of 0 and 1).

For this catchment and period, uncertainty in initial conditions has less effect on simulated discharge than uncertainty in parameter values (Fig. 6.12b). The range around the large peak is 0.04–$0.07 \, \mathrm{mm\,h^{-1}}$. The difference between the simulations with wet and dry initial conditions decreases in time. During this period, groundwater dropped 22 mm for the wet initial condition (100 % drainage) and 16 mm for the dry initial condition (0 % drainage) and the discharge range decreased slowly as well.

6.5.3 Propagation of forcing uncertainty

Precipitation time series contain errors and uncertainties which can have a large influence on model performance (e.g. Beven, 2012; Pappenberger et al., 2005; Berne et al., 2005; Tetzlaff and Uhlenbrook, 2005; Hazenberg et al., 2011). For many catchments no accurate precipitation data are available and data from rain gauges outside the catchment are used. To investigate the effect of this error, we used precipitation data from the three closest operational Dutch rain gauges with hourly resolution (30–50 km from the Hupsel Brook catchment) to run WALRUS. In addition, we used the operational weather radar of the Royal Netherlands Meteorological Institute. Radar data have been adjusted with rain gauge observations (Overeem et al., 2009b). The spatial resolution was $1 \, \mathrm{km}^2$ (Overeem et al., 2011), leading to 7 pixels for the Hupsel Brook catchment.

The effect of different rainfall inputs on modelled discharges is very large, especially after the first peak in the middle of April (Fig. 6.12c). The rainfall sums over the whole 2-month period measured in Twenthe (30 km northeast of the Hupsel Brook catchment) and Hupsel are similar, leading to similar modelled discharge sums. However, the other two (western) locations experienced up to

60 % more rainfall in Deelen, leading to 100 % more discharge than observed. Between 8 and 11 May 34 mm of rainfall was measured in Deelen, but only 16 mm in Hupsel. This lead to a large overestimation of this discharge peak: $0.15 \, \mathrm{mm\,h^{-1}}$ in stead of $0.013 \, \mathrm{mm\,h^{-1}}$ (observed) and $0.033 \, \mathrm{mm\,h^{-1}}$ (simulated with Hupsel rainfall data).

Precipitation data are the most important forcing data, but not the only ones: observations of potential evapotranspiration, seepage and surface water supply contain errors as well. Potential evapotranspiration estimates obtained at a meteorological station sometimes need preprocessing to become applicable to the whole catchment with its (possible) variety of vegetation. Seepage is difficult to measure and estimates with regional groundwater models are uncertain. Surface water supply is often not measured and modelling decisions of water managers is impossible when changing weir levels and surface water supply are not automated. In the Cabauw polder, surface water supply was measured, but the uncertainty is large, because the measurement weir was often submerged and because two minor inflow routes were not measured continuously. We estimated the seepage term by closing the water budget for one year and assuming a constant seepage flux year-round. With these assumptions we were able to obtain good results for the Cabauw polder.

In summary, forcing uncertainty is found to be more important than parameter uncertainty and much more important than uncertainty in initial conditions.

6.6 Conclusion

We tested the newly developed Wageningen Lowland Runoff Simulator (WALRUS, Brauer et al., 2014a) for two Dutch catchments: the slightly sloping and freely draining Hupsel Brook catchment and the flat Cabauw polder with controlled water levels. In both catchments, WALRUS performed well, with Nash-Sutcliffe efficiencies of 0.87 (Hupsel) and 0.83 (Cabauw) for the calibration periods and 0.74 (Hupsel) and 0.76 (Cabauw) for the validation period. This limited decrease in performance indicates that the model is not overparameterized.

The model is able to reproduce processes which are important in lowland catchments and explicitly included in WALRUS, such as the groundwater influence on the unsaturated zone, activation of different flowroutes at different stages of catchment wetness, feedbacks between groundwater and surface water, and seepage and surface water supply.

The model was also able to simulate discharge in extremely wet (flash flood in August 2010; $\mathrm{NS} = 0.64$) and dry (summer 1976; $\mathrm{NS} = 0.84$) periods in

the Hupsel Brook catchment. Modelled dynamics of groundwater depth, storage deficit and the contribution of quick flow routes are realistic. This indicates that the model is robust and can be used in other climatic conditions than the calibration period and it suggests that the model can also be used to simulate the hydrologic consequences of climate change (assuming that the parameters are not affected by climate change). In addition, it can possibly be used for early warning of floods and droughts.

The effect of water management operations (varying weir elevations and surface water supply) are also simulated well, owing to the explicit modelling of surface water. This indicates that WALRUS is suitable for catchments that are heavily influenced by human activity, that it can be used to separate the effects of natural processes and human actions on the hydrological variables and that WALRUS is suitable to forecast the effect of different water management practices (scenario analyses).

Comparing modelled catchment effective variables to point-measurement is not trivial. Observed groundwater levels are influenced both by slow and quick flowroutes and should therefore be compared to the (spatially varying) combination of modelled groundwater depth and quickflow reservoir level rather than to the groundwater depth alone.

WALRUS is most sensitive to the wetness index parameter c_W and the groundwater reservoir constant c_G, and to a lesser extent to the quickflow reservoir constant c_Q. The effect of these three parameters could be identified in the discharge times series, which suggests that the model is not over-parameterised. The vadose zone relaxation time parameter c_V, however, has a limited effect, cannot be identified in discharge time series alone and may be redundant for most applications. We tested the effect of uncertainty in parameters, initial conditions and forcing and found that the forcing uncertainty was the most important.

In conclusion, the good correspondence between model and observations, identifiability of parameters and computational efficiency are positive characteristics which make WALRUS applicable for research and practice. Recommendations for further research include investigating the possibilities for data assimilation (Liu and Gupta, 2007; Rakovec et al., 2012) and multi-objective calibration (Gupta et al., 1998; Efstratiadis and Koutsoyiannis, 2010), testing the model in catchments with different climates and areas, and regionalisation of model parameters for application in ungauged basins (Merz and Blöschl, 2004).

7 | Synthesis

In this chapter the findings of the previous chapters are combined to answer the research questions posed in the introduction. These findings are discussed and compared to other studies reported in the literature. In addition, recommendations for further research are given and the practical implications for water management in lowland areas are indicated.

7.1 Main findings

The aim of this thesis was to contribute to lowland hydrological science and practice by providing improved understanding of rainfall-runoff processes and a novel parametric model to simulate these processes. The title of this thesis reflects the two-part research question: (1) what are the dominant rainfall-runoff processes in lowland catchments and (2) how can these processes be represented in parametric models? For both of these questions, I focussed on topics which are important for lowland areas: (1) the relation between (catchment) storage and discharge, (2) the coupling between shallow groundwater and the unsaturated zone, (3) the activation of flowroutes at different stages of wetness and (4) the feedback between groundwater and surface water.

In the next sections, I combine findings of the different chapters to describe the contribution of this thesis to process understanding and model developments per topic. The rainfall-runoff model presented in this thesis, the Wageningen Lowland Runoff Simulator (WALRUS), plays a central role in this synthesis. Therefore, a graphical representation of how process understanding of these topics led to the conceptualisation of WALRUS is presented in Fig. 7.1.

7.1.1 Storage-discharge relations

Processes

In Ch. 3 the hydrological response observed during the flash flood of the Hupsel Brook in August 2010 was dissected into a sequence of regimes that characterize the catchment storage and discharge dynamics. The sensitivity of discharge to changes in catchment storage (dQ/dS) varies with catchment wetness (Fig. 3.9), which can be explained from the dominant processes during the four phases of the flood: (1) hardly any sensitivity during soil moisture reservoir filling, (2) limited sensitivity during groundwater response, (3) high sensitivity during surface depression filling and surface runoff and (4) hardly any sensitivity during backwater feedback.

The relation between discharge and storage computed from soil moisture measurements displayed a lot of scatter, which shows that a certain discharge can be achieved at different values of catchment wetness and that the storage-discharge relation is not unique (Fig. 4.3a). In addition, even though the soil moisture observation sites were well distributed over the catchment, storage computed from soil moisture observations showed 2–6 times more variation than storage computed from the catchment water balance (Fig. 4.3b).

Storage-discharge relations are especially non-unique in areas with surface water supply, such as the Cabauw polder area, because a high discharge can occur when the soil is dry and water is supplied upstream (Chs. 2 and 6). In addition, changing weir elevations in order to control the surface water levels, changes the amount of water stored in the catchment, but does not affect the discharge (after the initial step response of settling into the new situation).

Modelling

To investigate if all discharge dynamics can be explained with changes in catchment storage (also during less wet conditions than during the flood in 2010), I investigated whether the Hupsel Brook catchment can be represented by a single nonlinear reservoir with two parameters, following the simple dynamical systems approach (Ch. 4). Considerably different parameter values were found with hydrograph fitting, recession analysis and a direct fit between storage (from soil moisture observations) and discharge (Fig. 4.2). Using this nonlinear reservoir as a hydrological model did not yield satisfactory results, especially in summer (Fig. 4.4), indicating that a single storage-discharge relation cannot describe the rainfall-runoff process completely and that additional processes need to be accounted for.

Even though the discharge at the catchment outlet is not uniquely related to the total catchment storage, internal catchment fluxes might still be modelled adequately with local storage-discharge relations. WALRUS (Ch. 5) contains three reservoirs of which the outflow is completely or partially determined by its contents (Fig. 7.1). The quickflow reservoir is a simple linear reservoir without feedbacks. Flow between the soil reservoir and the surface water reservoir is controlled by the levels of both reservoirs. Discharge depends directly on the surface wa-

ter level and the stage-discharge relation (which can change in time, depending on weir elevations).

7.1.2 Groundwater-unsaturated zone coupling

Processes

Soil moisture contents along different profiles shows a similar temporal variation as groundwater levels (Ch. 2). In Ch. 5 relations between groundwater and storage deficit (based on soil moisture observations) in the Hupsel Brook catchment and the Cabauw polder are investigated (Fig. 5.5). Although some scatter is visible, this analysis points to a strong coupling between groundwater and the unsaturated zone. Plant roots extend to the groundwater table or its capillary fringe and capillary rise is easy, so only in very dry summers a significant evapotranspiration reduction occurs (Fig. 5.2).

Although vadose zone (the unsaturated zone and capillary fringe) and groundwater are strongly linked, the water in the soil column cannot be described completely by a single storage variable. This is illustrated by the flood in 2010 (Ch. 3), which occurred at the end of August when the catchment was dry. The first portion of rain was absorbed by the soil and used to increase soil moisture content. During this phase, groundwater did not rise yet and discharge did not respond to changes in catchment storage. This shows that groundwater rise and discharge peaks were delayed by the unsaturated zone.

Modelling

In the simple dynamical systems approach (Ch. 4), no distinction is made between different types of storage. This assumption may be the cause for the unsatisfactory performance of this model in summer in the Hupsel Brook catchment, when the unsaturated zone is relatively thick and infiltrating rainwater may evaporate before it can influence the groundwater table and the discharge. The unsaturated zone plays a much smaller role in (lowland) catchments with more humid climates than the Hupsel Brook catchment.

WALRUS (Ch. 5) contains one soil reservoir, which is divided effectively by the (dynamic) groundwater table into a groundwater zone and a vadose zone. This prevents the simultaneous occurrence of deep groundwater and a moist unsaturated zone and vice versa. The condition of this soil reservoir is described by two strongly dependent variables: the groundwater depth and the storage deficit (the effective thickness of empty pores). This implementation enables capillary rise when the top soil has dried through evapotranspiration. The groundwater level does not respond directly to changes in the vadose zone, but with a delay.

Groundwater depths and storage deficits (the total amount of air in the unsaturated zone) simulated with WALRUS correspond well to observed ones, although they decrease more quickly than observed in the Cabauw polder (Ch. 6). Because water can flow upwards to replenish water shortage in the top soil created by evapotranspiration, plants are only affected by water stress in dry summers.

7.1.3 Wetness-dependent flowroutes

Processes

In the two field sites (Ch. 2), certain types of flow can only be observed when the local conditions are wet enough. Activation of these flowroutes depends on exceedance of local thresholds: when groundwater levels exceed the drainpipe depth, drainpipes start to discharge water and when groundwater levels reach the soil surface, ponding and overland flow occur.

These thresholds were also observed during the second and third phase of the Hupsel Brook catchment's response to extreme rainfall (Ch. 3). During the second phase, groundwater rose and groundwater started flowing towards the surface water network through the soil and, when levels rose above the level of the drainpipes, through drainpipes. During the third phase, groundwater reached the soil surface, causing ponding and overland flow.

Spatial variability in contribution of quick flow paths can be considerable (Fig. 3.8). In local depressions, ponds remained for a week, while in local elevations no ponds formed at all (Fig. 3.7). Groundwater observations showed the combined effect of quick and slow flow paths (Ch. 6). Piezometers situated far away from surface water or in areas with thick aquifers showed little response to individual rainfall events, but did show a seasonal variation similar to the modelled groundwater depth. Piezometers close to surface water or in areas with thin aquifers reacted quickly to rainfall events, but had a lower groundwater amplitude between seasons (Fig 6.4).

Modelling

In the simple dynamical systems approach (Ch. 4) no distinction is made between different flowroutes: the combination of all flowroutes is modelled jointly. The changing sensitivity of discharge to catchment storage at different stages of wetness could in principle be accounted for in the nonlinear storage-discharge relation, but obtaining this relation becomes difficult when it varies between seasons and events.
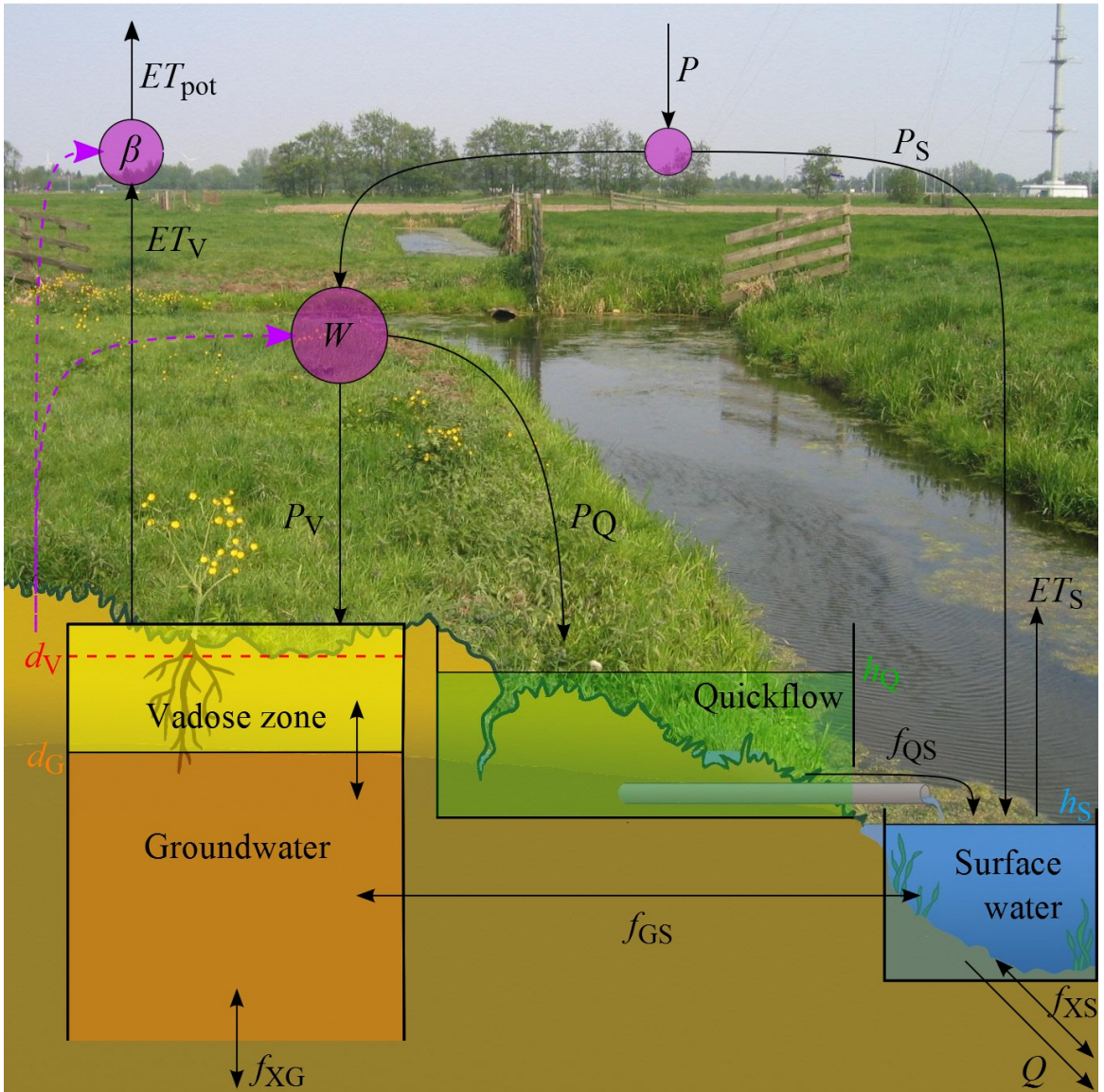
Figure 7.1: Modelling rainfall-runoff processes in lowland catchments: how the different flowpaths and feedbacks are schematised in WALRUS. Compare to Fig. 1.4 showing the research topics of this thesis and Fig. 5.1 showing the model structure of WALRUS. See Tab. 5.1 for abbreviations of variables.

In WALRUS (Ch. 5), the storage deficit determines the division of rain water between the soil reservoir and the quickflow reservoir. This dynamic divider (called wetness index) accounts for the spatial variability in soil wetness and flowpath activation. From the soil reservoir it can evaporate or flow slowly to the surface water reservoir as groundwater flow. The quickflow reservoir is a simple linear reservoir which represents macropore, drainpipe and overland flow. The variable contribution of quickflow has a large effect on all variables (Fig. 5.3) and improves performance and realism of WALRUS

(Ch. 6).

The groundwater depth and quickflow reservoir level in WALRUS are catchment effective values (Ch. 6), while groundwater observations are point measurements which include the effect of both quick and slow flow paths. Groundwater observations can therefore not be directly compared to the modelled groundwater depth, but rather to a combination of modelled groundwater depth and quickflow reservoir level. The contribution of each of these two reservoirs depends on the location of the piezometers (Fig. 6.4).

7.1.4 Groundwater-surface water feedbacks

Processes

When discharge exceeded the design discharge of several culverts in the Hupsel Brook catchment during the flood in 2010, ponds formed upstream of these structures and backwater feedbacks occurred (Ch. 3, Fig. 3.11). Because flow is controlled by head gradients, these high surface water levels limited drainage and even infiltration of surface water into the soil may have occurred.

Groundwater-surface water interactions are especially important in areas with controlled water levels, such as the Cabauw polder (Ch. 2). Surface water level control affects the whole hydrological system through groundwater-surface water feedbacks and groundwater-unsaturated zone coupling. By adjusting weir levels, surface water levels drop or rise independent of discharge. Raising weirs increases surface water levels, leading to less drainage (or, when surface water levels are higher than groundwater levels, more infiltration), higher groundwater levels and soil moisture contents and plants that continue to evaporate at their potential rate.

Modelling

Surface water forms an explicit part of the structure of WALRUS (Ch. 5). Drainage depends on the difference between surface water level and groundwater level (rather than groundwater level alone), allowing for feedbacks and infiltration of surface water into the soil. Groundwater seepage and surface water supply or extraction (pumping) are added to or subtracted from the soil or surface water reservoir. These external fluxes affect the whole system through the surface water level, groundwater drainage (or infiltration) flux, soil moisture deficit and wetness index, which divides rainfall between flowroutes (Fig.5.4).

7.2 Recommendations for further research

7.2.1 Processes

The detailed analysis of the extreme rainfall and flood event (Ch. 3) revealed a lot about the functioning of the Hupsel Brook catchment, not only about rare processes which only occur during extremely wet conditions (e.g. the backwater effect of ponds behind culverts), but also about more general catchment behaviour (e.g. the changing sensitivity of discharge to changes in storage at different stages of catchment wetness). Observations made during (post event) field surveys (as a form of "soft data") are a powerful tool to understand what the main factors in the landscape are that drive runoff generation (Gaume and Borga, 2008; Tetzlaff et al., 2011). The importance of this kind of "soft data" is increasingly being recognised and used in model development, calibration and evaluation (Seibert and McDonnell, 2002; Dunn et al., 2008). In addition to field surveys during or after floods, field surveys during drought episodes can be informative. Soft data about extreme situations are necessary to improve our understanding of catchment behaviour because these events are rare and therefore hard data are often scarce.

Additional measurements can be performed during droughts to investigate for instance plant water stress, evapotranspiration reduction and depletion and recovery of soil moisture and groundwater. During normal and extremely wet conditions, observation techniques beyond the standard groundwater and discharge observations can help to understand streamflow generation. During such intensive measurement campaigns, one could measure for example stream water chemistry (including stable isotopes, see e.g. Uhlenbrook et al., 2008; Tetzlaff and Soulsby, 2008; Soulsby et al., 2008), streamwater temperature with thermal imagery (Pfister et al., 2010) or fibre-optic cables (Westhoff et al., 2011) or habitat-specific algae (Pfister et al., 2009). A collection of portable instruments could be used to analyse one or a few events well during a dedicated field campaign, without needing to build up long time series of many variables for every catchment. These temporary measurements can have additional value, but cannot replace long time series of the main water balance components.

A high density of instruments can provide complementary information, making the whole more than the sum of its parts. The Cabauw Experimental Site for Atmospheric Research is a unique facility which, through its instrument and data density, facilitates instrument development, model intercomparison studies and understanding of processes which cross the boundaries of disciplinary domains (e.g. Chen et al., 1997; Russchenberg et al., 2005; Leijnse et al., 2010). Sites such as CESAR are very valuable, not only for the meteorological scientific community, but also for hydrologists, who need data and understanding about precipitation and land surface-atmosphere interactions for their models and analyses.

A more concrete recommendation concerns some relations which have been established with data from the Hupsel Brook catchment and Cabauw polder (Ch. 5) and used as defaults in Ch. 6. It would be desirable to obtain the relation between storage deficit and evapotranspiration reduction and be-

tween storage deficit and groundwater depth at different sites in different climates and geological settings. A number of sites, ranging from water-limited to energy-limited evaporation conditions (following the curve of Budyko and Miller, 1974) should be chosen, although very water-limited conditions are not likely to occur in areas with shallow groundwater.

Finally, lowland areas are highly affected by human interference and therefore hydrology cannot be investigated separately from society and water management. Interactions between the natural and human system should be considered as well (Wagener et al., 2010; Sivapalan et al., 2012; Montanari et al., 2013). WALRUS can already simulate the effect of control operations, but the effect of changes in runoff processes (and their parameterisation) due to land use change has not been investigated yet.

7.2.2 Modelling

The main recommendations for further research on modelling rainfall-runoff processes in lowland catchments concern WALRUS. A model is never finished and although WALRUS performs well, it can be further improved by iterative model development with experimentalists, modellers and end users, as illustrated by the framework shown in Fig. 7.2, adapted from Dunn et al. (2008). All steps in this framework have been taken during the development of WALRUS. *Data* are described in Ch. 2 and have been used throughout the model development. *Perceptual understanding* of relevant processes is described in Chs. 1, 2 and 3. Hypotheses have been formulated concerning the dominant processes (illustrated in Fig. 1.4). The hypotheses led to the *conceptual model* shown in Figs. 5.1 and 7.1. *Parameterisation* yielded relations between model variables and model parameters in Sect. 5.3, leading to the numerical model: the combination of the equations in Table 5.1. In Ch. 6 the model was *calibrated* (Sect. 6.2). *Sensitivity* to model parameters and functions was analysed in Sect. 6.4 and the effect of different sources of uncertainty in Sect. 6.5. *Model experiments* – simulations of several real situations – were described in Sect. 6.3. Observations and *soft information* were used to assess model performance and realism of the model output from calibration and validation runs in Sects. 6.2 and 6.3. WALRUS has not yet been used to make *predictions* for end-users in an operational setting, but the case studies presented in Sect. 6.3 can be seen as a type of prediction and were also *evaluated* by end-users. Prediction for and evaluation by end-users are the next steps in model development.

WALRUS can be improved through any of the components of the learning framework. New sources of data may demonstrate that key processes are missing in the perceptual model, application to catchments in different climates may require different parameterisations, new sensitivity analyses may point out superfluous model parameters and experience from end users may motivate alteration of the model code.

Some model extensions have already been mentioned in Sect. 5.3.12. Lowland catchments exist all over the world, but in this thesis WALRUS has only been tested in The Netherlands. Since typical lowland processes, such as groundwater-surface water interactions and groundwater control on the unsaturated zone also occur in lowland catchments in other climates, it is likely that WALRUS can be applied outside The Netherlands. For climates where a large portion of the precipitation falls as snow, it will be necessary to include a procedure for snow accumulation and melt as preprocessing step (for instance following Kustas et al., 1994; Seibert, 1997). For climates with high evapotranspiration rates, it may be necessary to pay special attention to the evapotranspiration reduction function. In densely forested catchments, an interception module may be required (Gerrits et al., 2010)

The catchments used for validation are quite small (6.5 and 0.5 km^2) and it may be possible that the simplifications made in WALRUS do not hold in larger catchments. The effect of scale on runoff generation is not trivial, because heterogeneities on smaller scales may either smooth out or transform to nonlinearities on larger scales (Shaman et al., 2004; Sivapalan, 2005; Blöschl, 2006; Laudon et al., 2007; Tetzlaff et al., 2008; Merz et al., 2009). In addition, one stage-discharge relation can determine the average water level in the entire surface water network in a small catchment (with limited slope), but in a larger catchment, this may no longer be the case and an alternative approach may be necessary. Floodwaves are hardly delayed in a small channel network. For application to larger catchments, a routing function may be necessary to mimic the travel time variability in the channels. Convection-diffusion equations as implemented in the old Wageningen Model (Stricker and Warmerdam, 1982) or combined with a width function (Mesa and Mifflin, 1986; Troch, 2008), or simple black-box functions, such as the triangle-shaped routing function implemented in HBV (Seibert, 1997), can be added as post-processing step.

WALRUS has only four states, which have physical connotations and can be compared to field observations. When WALRUS is used for operational forecasting, observations can be used to update model states in a data assimilation framework (Liu and Gupta, 2007; Rakovec, 2013). Remote sensing may provide possibilities for state updating. Satellite soil moisture data can be used to update the
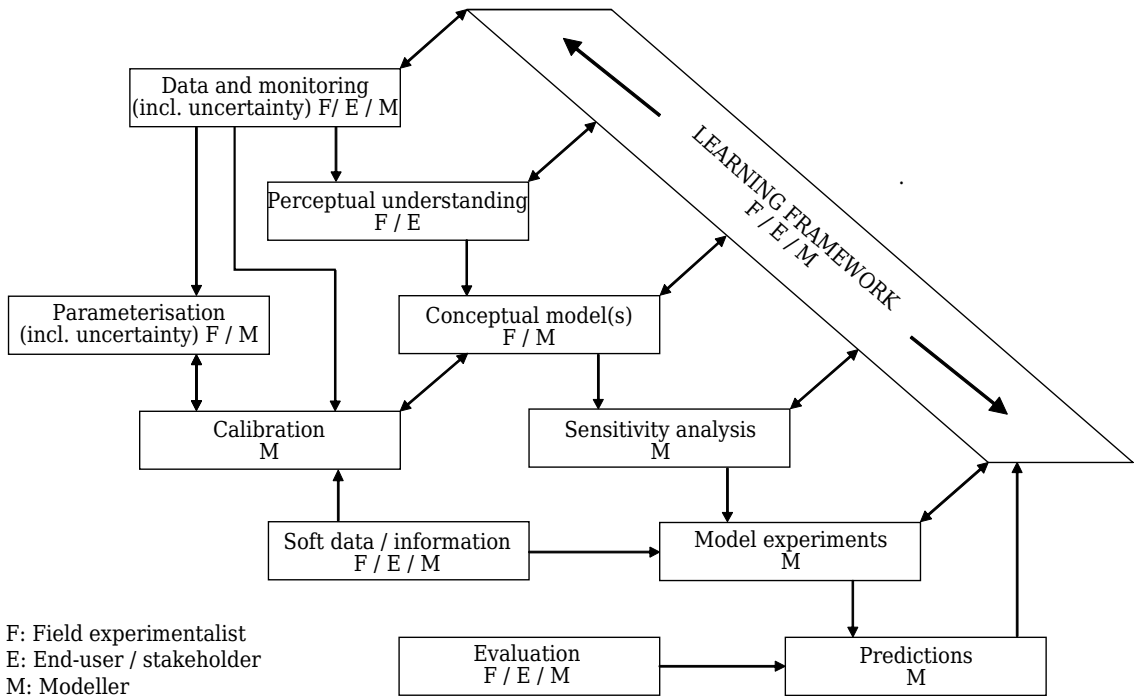
Figure 7.2: Learning framework for model development (adapted from Dunn et al., 2008).

storage deficit (e.g. Houser et al., 1998; Pauwels et al., 2001; Reichle et al., 2004). In areas with heavy clay, swelling and shrinkage caused by wetting and drying can be observed from space as elevation changes. In these areas, radar interferometry from satellites may provide possibilities for updating the storage deficit in the future (Te Brake et al., 2012).

Many lowland catchments or polders are ungauged, not only in developing countries, but also in The Netherlands. Prediction in ungauged basins has been a major research topic during the PUB-decade of the International Association of Hydrological Sciences (Blöschl et al., 2013; Hrachowitz et al., 2013). For prediction in ungauged basins, model parameters have to be determined without calibration. This may be achieved by calibrating WALRUS for a large number of gauged basins and investigating similarities between catchments (Wagener et al., 2007). Relations between catchment characteristics and parameter values can be determined and used for simulations in ungauged basins (Seibert, 1999b; Merz and Blöschl, 2004; Parajka et al., 2005).

For calibration, I only used discharge data (except for one sensitivity analysis, where I used groundwater data as well). Multi-objective calibration, possibly including soft data, could improve model performance and reduce the risk of overfitting even further (Madsen, 2000; Seibert and Mc-

Donnell, 2002; Wagener, 2003). More advanced calibration algorithms (such as DREAM by Vrugt and ter Braak, 2011) may also lead to better parameter estimates.

It is assumed that the model parameters do not change in time. However, it may be possible that they vary seasonally or show multi-year trends (Kuczera et al., 2006). Systematically fitting model parameters on part of the time series by applying a moving window may reveal parameter dependence or errors in the model structure (Merz et al., 2011).

WALRUS performs well in the Hupsel Brook catchment and the Cabauw polder, but other parametric rainfall-runoff models have not been tested under the same circumstances. Rainfall-runoff models have been used for other periods in the Hupsel Brook catchment (the most well-known experimental catchment in The Netherlands). The old Wageningen Model (Stricker and Warmerdam, 1982), SWAP (Van Dam et al., 2008), SIMGRO (Van Walsum and Veldhuizen, 2011) and LGSI-model (Van der Velde et al., 2009) have all been developed using data from the Hupsel Brook catchment. The flood in August 2010 has resulted in a model intercomparison study (without WALRUS) initiated by the Dutch Hydrological Association (NHV), in which teams from Dutch engineering firms, institutes and universities participated (NHV, 2014). In addition, Kloosterman (2012) compared the perfor-

mance of five lumped models for this extreme event: the old Wageningen Model, HBV, the Sacramento Model, the LGSI-model and SWAP. For an independent judgement of quality, a model intercomparison study including WALRUS and other widely used rainfall-runoff models (e.g. HBV, The Sacramento Model, SWAT) is recommended (e.g. Refsgaard and Knudsen, 1996).

7.3 Contribution to water management

7.3.1 Processes

The flood in 2010 (Ch. 3) showed that initial conditions are an important factor in determining the response of a catchment to (heavy) rainfall. It is therefore important to have an accurate monitoring network with groundwater (and preferably also soil moisture) measurements to predict the response. This is even more important in controlled catchments, where the discharge measured at the catchment outlet is not a proxy for the catchment's wetness. Actual groundwater and soil moisture data can also be used for data assimilation in operational forecasting.

Another lesson learnt from the flood in the Hupsel Brook catchment in August 2010 is the importance of hydraulic structures during extremely high discharges (confirmed by Hailemariam et al., 2013). Because the design discharge of the culverts was exceeded, the discharge peak was topped off at different locations within the catchment, causing local flooding upstream of the culvert. Topping off discharge peaks in headwaters such as the Hupsel Brook likely reduced peak water levels further downstream. Through unintended effects of these structures, large floods downstream may have been avoided. The Dutch national strategy of "retaining-storing-discharging" (in Dutch: vasthouden-bergen-afvoeren), which prescribes that during flood events, water should first be retained locally in the soil or surface water, then stored regionally in storage reservoirs and then discharged, was followed accidentally.

7.3.2 Modelling

The validation study of WALRUS (Ch. 6) included several test cases, suggesting that the model can be used for simulation (forecasting) of floods and droughts and to investigate the effect of different water management practices. The learning framework in Fig. 7.2 assigns an important role for the end users of the model (Dunn et al., 2008). End users have already been involved in the development of

WALRUS and their experience and ideas for application will likely lead to further improvement.

Advantages

WALRUS has several advantages for practical implementation:

Applicable to both freely draining and polder areas. This allows water authorities to use (for examples of applications, see further in this Section) the same model for their entire management area. In addition, many catchments have characteristics of both freely draining and controlled areas. For example, headwaters that are naturally freely draining are often managed by weirs. Many models can only be used in one of the two types of catchments and it is difficult to couple them.

Computational efficiency is a large advantage even though computer power increases continuously. In The Netherlands, most water authorities do not have supercomputers (in contrast to the KNMI). Creating ensembles of output to quantify predictive uncertainty is therefore not feasible for computationally demanding models, but can be achieved relatively easily with WALRUS.

Few parameters. This facilitates calibration. For many catchments, only discharge data are available and, as a consequence, only 3–5 parameters can be identified using one objective function (Jakeman and Hornberger, 1993). In WALRUS, only four parameters need calibration and the three most important ones can be identified using the discharge time series.

A clear (qualitative) relation between model states and measurable variables. This allows for state updating when WALRUS is used for early warning in operational flood forecasting. In addition, the simple model structure allows end-users to evaluate the model performance by comparing the output to their perception of the catchment functioning.

Default options for initial conditions are implemented. These are based on a stationary situation, thereby avoiding long burn-in periods. The output of WALRUS can be saved at any moment and used as input for a next run. This facilitates scenario analyses to investigate the effect of different management operations or rainfall events after an initial period which is the same for all scenarios.

Open source and freeware. Currently, WALRUS is implemented in R. It generates plots of the main diagnostic variables of model output automatically, which helps to understand quickly how the

model works and performs. WALRUS can easily be implemented in other programming languages and environments to increase computational efficiency and to facilitate coupling to other models, data bases or forecasting environments.

Applicability

In a practical setting, WALRUS can be used for several applications:

Operational forecasting of floods and droughts and early warning systems. Operational forecasting can be improved with data assimilation and state updating. Predictive uncertainty can be quantified by generating ensembles of model output.

Real-time control. With forecasts from WALRUS, water managers can give advice to their colleagues in the field. When floods are predicted (early warning), weirs or pumps can be adjusted (manually or automatically) or maintenance of the surface water network can be performed to increase discharge capacity.

Input for a hydraulic model, which can then be used to estimate flow division at bifurcations (natural or man-made), flow velocity in large channels or sediment transport.

Risk assessment of floods, droughts or (indirectly) deterioration of water quality. These assessments are often imposed by national or European legislature, such as the Water Framework Directive. For example, presently Dutch water authorities have to prove that their water system is (to a certain degree) safe from flooding, according to the National Administrative Agreement Water (in Dutch: Nationaal Bestuursakkoord Water).

Infrastructure design. Estimates of discharge ranges are necessary for many types of design

projects. For example, for stream restoration, the variation in discharge (and consequently flow velocities) partly determines where vegetation will develop and how much sediment will be eroded and deposited (Eekhout and Hoitink, 2013; Eekhout, 2013). Estimates of the height and duration of discharge peaks are necessary to design water retention basins. For design of by-pass channels to allow migration of fish around hydraulic structures, the discharge needs to be known in order to construct the channels such that flow velocities and elevation gradients are appropriate (Boersema et al., 2011).

Gap filling in measured discharge time series or for validation of measurements. One should take care, however, that simulations and measurements can always be separated, lest conclusions about observations are based on simulations.

7.4 Outlook

Of the recommendations presented in Sect. 7.2, some are more concrete than others and will be carried out in the near future. First the model code of WALRUS will be documented and published online, such that everyone can access it easily. Then, WALRUS will be applied to several (freely draining and polder) catchments in The Netherlands with different sizes, slopes, land use and soils/geology. The outcomes will be evaluated together with end-users and may lead to a study on parameter regionalisation. For some of these catchments, a model intercomparison study will be carried out. Investigating possibilities for operational (flood) forecasting and data assimilation are other topics which will be investigated in the near future. During all of these steps, acquiring new knowledge and gaining more experience will probably lead to a continuous improvement of WALRUS.

Bibliography

Abbott, M. B., Bathurst, J. C., Cunge, J. A., O'Connell, P. E., Rasmussen, J., 1986. An introduction to the European Hydrological System-Système Hydrologique Européen, "SHE", 1: History and philosophy of a physically-based, distributed modelling system. J. Hydrol. 87 (1), 45–59.

Alley, W. M., Healy, R. W., LaBaugh, J. W., Reilly, T. E., 2002. Flow and storage in groundwater systems. science 296 (5575), 1985–1990.

Appels, W. M., 2013. Water redistribution at the soil surface: ponding and surface runoff in flat areas. Ph.D. thesis, Wageningen University.

Appels, W. M., Bogaart, P. W., van der Zee, S. E. A. T. M., 2011. Influence of spatial variations of microtopography and infiltration on surface runoff and field scale hydrological connectivity. Adv. Water Resour. 34 (2), 303–313.

Arnold, J. G., Srinivasan, R., Muttiah, R. S., Williams, J. R., 1998. Large area hydrologic modeling and assessment part I: Model development. J. Am. Water Resour. As. 34 (1), 73–89.

Azous, A., Horner, R. R., 2010. Wetlands and urbanization: Implications for the future. CRC Press.

Baldocchi, D., Falge, E., Gu, L., Olson, R., Hollinger, D., Running, S., Anthoni, P., Bernhofer, C., Davis, K., Evans, R., Fuentes, J., Goldstein, A., Katul, G., Law, B., Lee, X., Malhi, Y., Meyers, T., Munger, W., Oechel, W., Paw, K., Pilegaard, K., Schmid, H., Valentini, R., Verma, S., Vesala, T., Wilson, K., Wofsy, S., 2001. Fluxnet: A new tool to study the temporal and spatial variability of ecosystem-scale carbon dioxide, water vapor, and energy flux densities. Bulletin of the American Meteorological Society 82 (11), 2415–2434.

Beljaars, A. C. M., Bosveld, F. C., 1997. Cabauw data for the validation of land surface parameterization schemes. J. Climate 10 (6), 1172–1193.

Bergström, S., Forsman, A., 1973. Development of a conceptual deterministic rainfall-runoff model. Nord. hydrol. 4 (3), 147–170.

Berne, A., ten Heggeler, M., Uijlenhoet, R., Delobbe, M., Dierickx, P., de Wit, M., 2005. A preliminary investigation of radar rainfall estimation in the Ardennes region and a first hydrological application for the Ourthe catchment. Nat. Hazard. Earth Sys.. 5, 267–274.

Beven, K., 1989. Changing ideas in hydrology–the case of physically-based models. J. Hydrol. 105 (1), 157–172.

Beven, K., 1995. Linking parameters across scales: subgrid parameterizations and scale dependent hydrological models. Hydrol. Process. 9 (5-6), 507–525.

Beven, K., 2007. Towards integrated environmental models of everywhere: uncertainty, data and modelling as a learning process. Hydrol. Earth Syst. Sci. 11 (1), 460–467.

Beven, K., Freer, J., 2001a. A dynamic topmodel. Hydrol. Process. 15 (10), 1993–2011.

Beven, K., Freer, J., 2001b. Equifinality, data assimilation, and uncertainty estimation in mechanistic modelling of complex environmental systems using the GLUE methodology. J. Hydrol. 249 (1), 11–29.

Beven, K., Germann, P., 1982. Macropores and water flow in soils. Water Resour. Res. 18 (5), 1311–1325.

Beven, K., Germann, P., 2013. Macropores and water flow in soils revisited. Water Resour. Res. 49 (6), 3071–3092.

Beven, K., Young, P., 2013. A guide to good practice in modeling semantics for authors and referees. Water Resour. Res. 49 (8), 5092–5098.

Beven, K. J., 2012. Rainfall-runoff modelling: the primer, 2nd Edition. John Wiley & Sons, LTD, Chichester, UK.

Beven, K. J., Binley, A. M., 1992. The future of distributed models: model calibration and uncertainty prediction. Hydrol. Process. 6, 297–298.

Beven, K. J., Kirkby, M. J., 1979. A physically based, variable contributing area model of basin hydrology. Hydrolog. Sci. J. 24 (1), 43–69.

Bierkens, M. F. P., Puente, C. E., 1990. Analytically derived runoff models based on rainfall point processes. Water Resour. Res. 26, 2653–2659.

Bierkens, M. F. P., van den Hurk, B. J. J. M., 2007. Groundwater convergence as a possible mechanism for multi-year persistence in rainfall. Geophys. Res. Lett. 34 (2), L02402.

Bishop, C. M., 1995. Neural networks for pattern recognition. Oxford university press.

Blöschl, G., 2006. Hydrologic synthesis: Across processes, places, and scales. Water Resour. Res. 42 (3).

Blöschl, G., Sivapalan, M., Wagener, T., Viglione, A., Savenije, H. (Eds.), 2013. Runoff Prediction

in Ungauged Basins: Synthesis Across Processes, Places and Scales. Cambridge University Press.

Boersema, M. P., Vermeulen, B., Torfs, P. J. J. F., Hoitink, A. J. F., Roelofs, G. W. M., van den Houten, G. J., 2011. Hydraulic functioning of fish-passable cascades. Tech. Rep. 22, STOWA.

Bogaart, P. W., Teuling, A. J., Troch, P. A., 2008. A state-dependent parameterization of saturated-unsaturated zone interaction. Water Resour. Res. 44 (11), W11423.

Bonnifait, L., Delrieu, G., le Lay, M., Boudevillain, B., Masson, A., Belleudy, P., Gaume, E., Saulnier, G., 2009. Distributed hydrologic and hydraulic modelling with radar rainfall input: Reconstruction of the 8–9 September 2002 catastrophic flood event in the Gard region, France. Adv. Water Resour. 32, 1077–1089.

Borga, M., Anagnostou, E., Blöschl, G., Creutin, J.-D., 2011. Flash flood forecasting, warning and risk management: the HYDRATE project. Environmental Science & Policy 14 (7), 834–844.

Borga, M., Boscolo, P., Zanon, F., Sangati, M., 2007. Hydrometeorological analysis of the 29 August 2003 flash flood in the Eastern Italian Alps. J. Hydrometeorol. 8, 1049–1067.

Bormann, H., Ahlhorn, F., Klenke, T., 2012. Adaptation of water management to regional climate change in a coastal region–hydrological change vs. community perception and strategies. J. Hydrol. 454, 64–75.

Bormann, H., Elfert, S., 2010. Application of WaSiM-ETH model to Northern German lowland catchments: model performance in relation to catchment characteristics and sensitivity to land use change. Adv. Geosci. 27 (27), 1–10.

Bouwer, L. M., Bubeck, P., Aerts, J. C. J. H., 2010. Changes in future flood risk due to climate and development in a Dutch polder area. Global Environmental Change 20 (3), 463–471.

Brakensiek, D., Osborn, H., Rawls, W., 1979. Field manual for research in agricultural hydrology. Vol. 224 of Agricultural Handbook. U.S. Department of Agriculture.

Brauer, C. C., Teuling, A. J., Overeem, A., Van der Velde, Y., Hazenberg, P., Warmerdam, P. M. M., Uijlenhoet, R., 2011. Anatomy of extraordinary rainfall and flash flood in a Dutch lowland catchment. Hydrol. Earth Syst. Sci. 15, 1991–2005.

Brauer, C. C., Teuling, A. J., Torfs, P. J. J. F., Uijlenhoet, R., 2013. Investigating storage-discharge relations in a lowland catchment using hydrograph fitting, recession analysis, and soil moisture data.

Water Resour. Res. 49, 4257–4264.

Brauer, C. C., Teuling, A. J., Torfs, P. J. J. F., Uijlenhoet, R., 2014a. The Wageningen Lowland Runoff Simulator (WALRUS): a lumped rainfall-runoff model for catchments with shallow groundwater. Geosci. Model Dev. Discuss. 7, 1357–1411.

Brauer, C. C., Torfs, P. J. J. F., Teuling, A. J., Uijlenhoet, R., 2014b. The Wageningen Lowland Runoff Simulator (WALRUS): application to the Hupsel Brook catchment and Cabauw polder. Hydrol. Earth Syst. Sci. Discuss. 11, 2091–2148.

Brooks, R. H., Corey, A. . T., 1964. Hydraulic properties of porous media. Hydrology Paper 3, Colorado State University, Fort Collins, CO, 27 pp.

Brunner, G. W., 1995. HEC-RAS River Analysis System. Hydraulic Reference Manual. Version 1.0. DTIC Document, US Army Corps of Engineers.

Brutsaert, W., 1994. The unit response of groundwater outflow from a hillslope. Water Resour. Res. 30, 2759–2763.

Brutsaert, W., Nieber, J. L., 1977. Regionalized drought flow hydrographs from a mature glaciated plateau. Water Resour. Res. 13, 637–643.

Budyko, M. I., Miller, D. H., 1974. Climate and life. Vol. 508. Academic press New York.

Burnash, R. J. C., 1995. The NWS river forecast system – catchment modeling. In: Singh, V. P. (Ed.), Computer Models of Watershed Hydrology. Water Resour. Publ., Highlands Ranch, Colorado, USA, pp. 311–366.

Byrd, R. H., Lu, P, Nocedal, J., Zhu, C., 1995. A limited memory algorithm for bound constrained optimization. SIAM J. Sci. Stat. Comp. 16, 1190–1208.

Canadell, J., Jackson, R. B., Ehleringer, J. B., Mooney, H. A., Sala, O. E., Schulze, E. D., 1996. Maximum rooting depth of vegetation types at the global scale. Oecologia 108 (4), 583–595.

Chen, T. H., Henderson-Sellers, A., Milly, P. C. D., Pitman, A. J., Beljaars, A. C. M., Polcher, J., Abramopoulos, F., Boone, A., Chang, S., Chen, F., Dai, Y., Desborough, C. E., Dickinson, R. E., Dümenil, L., Ek, M., Garratt, J. R., Gedney, N., Gusev, Y. M., Kim, J., Koster, R., Kowalczyk, E. A., Laval, K., Lean, J., Lettenmaier, D., Liang, X., Mahfouf, J.-F., Mengelkamp, H.-T., Mitchell, K., Nasonova, O. N., Noilhan, J., Robock, A., Rosenzweig, C., Schaake, J., Schlosser, C. A., Schulz, J.-P., Shao, Y., Shmakin, A. B., Verseghy, D. L., Wetzel, P., Wood, E. F., Xue, Y., Yang, Z.-L., Zengi, Q., 1997. Cabauw experimental results from the

Project for Intercomparison of Land-Surface Parameterization Schemes. J. Climate 10 (6), 1194–1215.

Chen, X., Hu, Q., 2004. Groundwater influences on soil moisture and surface evaporation. J. Hydrol. 297 (1), 285–300.

Clapp, R. B., Hornberger, G. M., 1978. Empirical equations for some hydraulic properties. Water Resour. Res. 14, 601–604.

Clark, C. O., 1945. Storage and the unit hydrograph. Transactions of the American Society of Civil Engineers 110 (1), 1419–1446.

Clark, M. P., Slater, A. G., Rupp, D. E., Woods, R. A., Vrugt, J. A., Gupta, H. V., Wagener, T., Hay, L. E., 2008. Framework for Understanding Structural Errors (FUSE): A modular framework to diagnose differences between hydrological models. Water Resour. Res. 44 (12), W00B02.

Cosby, B. J., Hornberger, G. M., Clapp, R. B., Ginn, T. R., 1984. A statistical exploration of the relationships of soil moisture characteristics to the physical properties of soils. Water Resour. Res. 20 (6), 682–690.

Day, J. W., Boesch, D. F., Clairain, E. J., Kemp, G. P., Laska, S. B., Mitsch, W. J., Orth, K., Mashriqui, H., Reed, D. J., Shabman, L., et al., 2007. Restoration of the Mississippi Delta: lessons from hurricanes Katrina and Rita. Science 315 (5819), 1679–1684.

De Roode, S. R., Bosveld, F. C., Kroon, P. S., 2010. Dew formation, eddy-correlation latent heat fluxes, and the surface energy imbalance at Cabauw during stable conditions. Bound.-Lay. Meteorol. 135 (3), 369–383.

Delrieu, G., Ducrocq, V., Gaume, E., Nicol, J., Payrastre, O., Yates, E., Kirstetter, P.-E., Andrieu, H., Ayral, P.-A., Bouvier, C., Creutin, J.-D., Livet, M., Anquetin, S., Lang, M., Neppel, L., Obled, C., Parent-du-Châtelet, J., Saulnier, G.-M., Walpersdorf, A., Wobrock, W., 2005. The catastrophic flash-flood event of 8–9 September 2002 in the Gard region, France: A first case study for the Cévennes-Vivarais Mediterranean Hydrometeorological Observatory. J. Hydrometeorol. 6, 34–52.

Delsman, J. R., Oude Essink, G. H. P., Beven, K. J., Stuyfzand, P. J., 2013. Uncertainty estimation of end-member mixing using generalized likelihood uncertainty estimation (GLUE), applied in a lowland catchment. Water Resour. Res. 49, 4792–4806.

Deltares, December 2013. SOBEK, 1D/2D modelling suite for integral water solutions: Hydrodynamics, rainfall runoff and real-time control. Deltares, Delft, www.deltares.nl.

Demeritt, D., Nobert, S., Cloke, H. L., Pappenberger, F., 2013. The European Flood Alert System and the communication, perception, and use of ensemble predictions for operational flood risk management. Hydrol. Process. 27 (1), 147–157.

Devonec, E., Barros, A. P., 2002. Exploring the transferability of a land-surface hydrology model. J. Hydrol. 265 (1), 258–282.

Dunn, S. M., Freer, J., Weiler, M., Kirkby, M. J., Seibert, J., Quinn, P. F., Lischeid, G., Tetzlaff, D., Soulsby, C., 2008. Conceptualization in catchment modelling: simply learning? Hydrol. Process. 22 (13), 2389–2393.

Dunne, T., Black, R. D., 1970. Partial area contributions to storm runoff in a small New England watershed. Water Resour. Res. 6 (5), 1296–1311.

Edijatno, de Oliveira Nascimento, N., Yang, X., Makhlouf, Z., Michel, C., 1999. GR3J: a daily watershed model with three free parameters. Hydrol. Sci. J. 44(2), 263–277.

Eekhout, J. P. C., 2013. Morphological processes in lowland streams: Implications for stream restoration. Ph.D. thesis, Wageningen University, in preparation.

Eekhout, J. P. C., Hoitink, A. J. F., 2013. Morphodynamic regime change induced by riparian vegetation in a restored lowland stream. Earth Surf. Dynam. Discuss. 1, 711–743.

Efron, B., Tibshirani, R., 1993. An introduction to the bootstrap. Chapman and Hall / CRC, London.

Efstratiadis, A., Koutsoyiannis, D., 2010. One decade of multi-objective calibration approaches in hydrological modelling: a review. Hydrolog. Sci. J. 55 (1), 58–78.

Elfert, S., Bormann, H., 2010. Simulated impact of past and possible future land use changes on the hydrological response of the northern german lowland ŚhunteŠcatchment. Journal of Hydrology 383 (3), 245–255.

Ericson, J. P., Vörösmarty, C. J., Dingman, S. L., Ward, L. G., Meybeck, M., 2006. Effective sea-level rise and deltas: causes of change and human dimension implications. Global Planet. Change 50 (1), 63–82.

Fan, Y., Li, H., Miguez-Macho, G., 2013. Global patterns of groundwater table depth. Science 339, 940–943.

Fenicia, F., Kavetski, D., Savenije, H. H. G., 2011. Elements of a flexible approach for conceptual hydrological modeling: 1. Motivation and theo-

retical development. Water Resour. Res. 47 (11), W11510.

Fenicia, F., Savenije, H. H. G., Matgen, P., Pfister, L., 2006. Is the groundwater reservoir linear? Learning from data in hydrological modelling. Hydrol. Earth Syst. Sci. 10 (1), 139–150.

Field, C. B., Barros, V., Stocker, T. F., Qin, D., Dokken, D. J., Ebi, K. L.and Mastrandrea, M. D., Mach, K. J., Plattner, G.-K., Allen, S. K., Tignor, M., Midgley, P. M. (Eds.), 2012. Managing the risks of extreme events and disasters to advance climate change adaptation (SREX): A Special Report of Working Groups I and II of the Intergovernmental Panel on Climate Change. Cambridge University Press, Cambridge, UK, and New York, NY, USA, pp. 1-19.

Foken, T., 2008. The energy balance closure problem: An overview. Ecol. Appl. 18 (6), 1351–1367.

Gambolati, G., Putti, M., Teatini, P., Stori, G. G., 2003. Subsidence due to peat oxidation and its impact on drainage infrastructures in a farmland catchment south of the Venice Lagoon. Materials and Geoenvironment 50, 125–128.

Gaume, E., Borga, M., 2008. Post-flood field investigations in upland catchments after major flash floods: proposal of a methodology and illustrations. J. Flood Risk Manage. 1, 175–189.

Gaume, E., Livet, M., Desbordes, M., 2003. Study of the hydrological processes during the Avène River extraordinary flood (south of France): 6–7 October 1997. Phys. Chem. Earth 28, 263–267.

Gaume, E., Livet, M., Desbordes, M., Villeneuve, J. P., 2004. Hydrological analysis of the river Aude, France, flash flood on 12 and 13 November 1999. J. Hydrol. 286, 135–154.

Gerrits, A. M. J., Pfister, L., Savenije, H. H. G., 2010. Spatial and temporal variability of canopy and forest floor interception in a beech forest. Hydrol. Process. 24 (21), 3011–3025.

Gilfedder, M., Rassam, D., Stenson, M., Jolly, I., Walker, G., Littleboy, M., 2012. Incorporating land-use changes and surface–groundwater interactions in a simple catchment water yield model. Environmental Modelling & Software 38, 62–73.

Gillham, R. W., 1984. The capillary fringe and its effect on water-table response. J. Hydrol. 67 (1), 307–324.

Gupta, H. V., Sorooshian, S., Yapo, P. O., 1998. Toward improved calibration of hydrologic models: Multiple and noncommensurable measures of information. Water Resour. Res. 34 (4), 751–763.

Gusev, Y. M., Nasonova, O. N., 1998. The land surface parameterization scheme SWAP: Description and partial validation. Global Planet. Change 19 (1), 63–86.

Hailemariam, F. M., Brandimarte, L., Dottori, F., 2013. Investigating the influence of minor hydraulic structures on modeling flood events in lowland areas. Hydrol. Process.

Hall, F. R., 1968. Base-flow recessions – a review. Water Resour. Res. 4 (5), 973–983.

Hansen, A. L., Refsgaard, J. C., Christensen, B. S. B., Jensen, K. H., 2013. Importance of including small-scale tile drain discharge in the calibration of a coupled groundwater-surface water catchment model. Water Resour. Res. 49 (1), 585–603.

Haylock, M., Hofstra, N., Klein Tank, A., Klok, E., Jones, P., New, M., 2008. A european daily high-resolution gridded dataset of surface temperature and precipitation. J. Geophys. Res (Atmospheres) 113.

Hazenberg, P., Leijnse, H., Uijlenhoet, R., 2011. Radar rainfall estimation of stratiform winter precipitation in the Belgian Ardennes. Water Resour. Res. 47, W02507.

Heimovaara, T., Bouten, W., 1990. A computer-controlled 36-channel time domain reflectometry system for monitoring soil water contents. Water Recour. Res. 26, 2311–2316.

Herrmann, A., Duncker, D., 2008. Runoff formation in a tile-drained agricultural basin of the Harz Mountain foreland, Northern Germany. Soil Water Res. 3 (3), 83–97.

Hidayat, 2013. Runoff, discharge and flood occurrence in a poorly gauged tropical basin. Ph.D. thesis, Wageningen University.

Hooghart, J., 1984. Vergelijking van modellen voor het onverzadigd grondwatersysteem en de verdamping. Verslag van de 4e CHO-studiebijeenkomst in samenwerking met de Studiegroep Hupselse Beek comparison of models for the unsaturated groundwater system and evapotranspiration. Report of the 4th CHO-study meeting in cooperation with the Study Group Hupsel Brook. Tech. Rep. 13, Commissie voor Hydrologisch Onderzoek TNO, (in Dutch).

Hopmans, J., van Immerzeel, C., 1988. Variation in evapotranspiration and capillary rise with changing soil profile characteristics. Agr. Water Manage. 13, 295–305.

Hopmans, J. W., Stricker, J. N. M., 1989. Stochastic analysis of soil water regime in a watershed. J. Hydrol. 105, 57–84.

Hosking, J., Wallis, J., 1997. Regional Frequency Analysis: an Approach Based on L-moments. Cambridge University Press, Cambridge.

Houser, P. R., Shuttleworth, W. J., Famiglietti, J. S., Gupta, H. V., Syed, K. H., Goodrich, D. C., 1998. Integration of soil moisture remote sensing and hydrologic modeling using data assimilation. Water Resour. Res. 34 (12), 3405–3420.

Howden, N. J. K., Bowes, M. J., Clark, A. D. J., Humphries, N., Neal, C., 2009. Water quality, nutrients and the European union's Water Framework Directive in a lowland agricultural region: Suffolk, south-east England. Sci. Total Environ. 407 (8), 2966–2979.

Hrachowitz, M., Savenije, H., Blöschl, G., McDonnell, J. J., Sivapalan, M., Pomeroy, J. W., Arheimer, B., Blume, T., Clark, M. P., Ehret, U., Fenicia, A., Freer, J. E., Gelfan, A., Gupta, H. V., Hughes, D. A., Hut, R. W., Montanari, A., Pande, S., Tetzlaff, D., Troch, P. A., Uhlenbrook, S., Wagener, T., Winsemius, H. C., Woods, R. A., Zehe, E., Cudennec, C., 2013. A decade of predictions in ungauged basins (PUB)–a review. Hydrol. Sci. J. 58 (6), 1198–1255.

IPCC, 2013. Climate Change 2013: The Physical Science Base. Cambridge University Press.

Jacobs, A. F. G., Heusinkveld, B. G., Holtslag, A. A. M., 2010. Eighty years of meteorological observations at Wageningen, the Netherlands: precipitation and evapotranspiration. Int. J. Climatol. 30 (9), 1315–1321.

Jacobs, A. F. G., Heusinkveld, B. G., Kruit, R. J. W., Berkowicz, S. M., 2006. Contribution of dew to the water budget of a grassland area in The Netherlands. Water Resour. Res. 42 (3), W03415.

Jakeman, A. J., Hornberger, G. M., 1993. How much complexity is warranted in a rainfall-runoff model? Water Resour. Res. 29 (8), 2637–2649.

Jarvis, N. J., 1989. A simple empirical model of root water uptake. J. Hydrol. 107 (1), 57–72.

Jonkman, S. N., Bočkarjova, M., Kok, M., Bernardini, P., 2008. Integrated hydrodynamic and economic modelling of flood damage in the netherlands. Ecological Economics 66 (1), 77–90.

Kao, S.-C., Kume, T., Komatsu, H., Liang, W.-L., 2012. Spatial and temporal variations in rainfall characteristics in mountainous and lowland areas in Taiwan. Hydrol. Process.

Kavetski, D., Fenicia, F., 2011. Elements of a flexible approach for conceptual hydrological modeling: 2. Application and experimental insights. Water Resour. Res. 47 (11), W11511.

Kew, S., Selten, F., Lenderink, G., 2011. Storm surges and high discharge: A joint probabilities study. Scientific Report WR 2011-05, Royal Netherlands Meteorological Institute (KNMI).

Kew, S. F., Selten, F. M., Lenderink, G., Hazeleger, W., 2010. Robust assessment of future changes in extreme precipitation over the rhine basin using a gcm. Hydrol. Earth Syst. Sci. 15, 1157–1166.

Kilpatrick, F., Schneider, V., 1983. Use of flumes in measuring discharge. Vol. 3 of U.S. Geological Survey Techniques of Water-Resources Investigations. U.S. Department of the Interior, Ch. A14, p. 46 p.

Kirchner, J., 2006. Getting the right answers for the right reasons: Linking measurements, analyses, and models to advance the science of hydrology. Water Resour. Res. 42, W03S04.

Kirchner, J. W., 2009. Catchments as simple dynamical systems: catchment characterization, rainfall - runoff modeling, and doing hydrology backwards. Water Resour. Res. 45, W02429.

Klemeš, V., 1986. Operational testing of hydrological simulation models. Hydrol. Sci. J. 31 (1), 13–24.

Kloosterman, P., 2012. A comparison of the performance of lumped hydrological models in modelling a flash flood in the Hupsel Brook catchment. Master's thesis, Wageningen University.

Koch, S., Bauwe, A., Lennartz, B., 2013. Application of the SWAT Model for a tile-drained lowland catchment in North-Eastern Germany on subbasin scale. Water Resour. Manage. 27 (3), 791–805.

Kollet, S. J., Maxwell, R. M., 2006. Integrated surface–groundwater flow modeling: A free-surface overland flow boundary condition in a parallel groundwater flow model. Adv. Water Resour. 29 (7), 945–958.

Koster, R. D., Suarez, M. J., Ducharne, A., Stieglitz, M., Kumar, P., 2000. A catchment-based approach to modeling land surface processes in a general circulation model: 1. Model structure. J. Geophys. Res.: Atmospheres (1984–2012) 105 (D20), 24,809–24,822.

Krause, S., Bronstert, A., 2007. The impact of groundwater–surface water interactions on the water balance of a mesoscale lowland river catchment in northeastern Germany. Hydrol. Process. 21 (2), 169–184.

Krause, S., Bronstert, A., Zehe, E., 2007. Groundwater–surface water interactions in a North German lowland floodplain–Implications for the river discharge dynamics and riparian water balance. J. Hydrol. 347 (3), 404–417.

Krzysztofowicz, R., 2001. The case for probabilistic forecasting in hydrology. J. Hydrol. 249 (1), 2–9.

Kuczera, G., Kavetski, D., Franks, S., Thyer, M., 2006. Towards a Bayesian total error analysis of conceptual rainfall-runoff models: Characterising model error using storm-dependent parameters. J. Hydrol. 331 (1), 161–177.

Kustas, W. P., Rango, A., Uijlenhoet, R., 1994. A simple energy budget algorithm for the Snowmelt Runoff Model. Water Resour. Res. 30, 1515–1527.

Kwadijk, J. C. J., Haasnoot, M., Mulder, J. P. M., Hoogvliet, M., Jeuken, A., van der Krogt, R. A. A., van Oostrom, N. G. C., Schelfhout, H. A., van Velzen, E. H., van Waveren, H., de Wit, M. J. M., 2010. Using adaptation tipping points to prepare for climate change and sea level rise: a case study in the netherlands. Wiley Interdisciplinary Reviews: Climate Change 1 (5), 729–740.

Lam, Q. D., Schmalz, B., Fohrer, N., 2012. Assessing the spatial and temporal variations of water quality in lowland areas, Northern Germany. J. Hydrol. 438, 137–147.

Lasserre, F., Razack, M., Banton, O., 1999. A GIS-linked model for the assessment of nitrate contamination in groundwater. J. Hydrol. 224 (3), 81–90.

Laudon, H., Sjöblom, V., Buffam, I., Seibert, J., Mörth, M., 2007. The role of catchment scale and landscape characteristics for runoff generation of boreal streams. J. Hydrol. 344 (3), 198–209.

Leijnse, H., Uijlenhoet, R., Stricker, J. N. M., 2007. Rainfall measurement using radio links from cellular communication networks. Water Resour. Res. 43.

Leijnse, H., Uijlenhoet, R., van de Beek, C. Z., Overeem, A., Otto, T., Unal, C. M. H., Dufournet, Y., Russchenberg, H. W. J., Figueras i Ventura, J., Klein Baltink, H., Holleman, I., 2010. Precipitation measurement at CESAR, the Netherlands. J. Hydrometeorol. 11, 1322–1329.

Liang, X., Lettenmaier, D. P., Wood, E. F., 1996. One-dimensional statistical dynamic representation of subgrid spatial variability of precipitation in the two-layer variable infiltration capacity model. J. Geophys. Res. 101 (D16), 21403–21.

Liu, Y., Gupta, H. V., 2007. Uncertainty in hydrologic modeling: Toward an integrated data assimilation framework. Water Resour. Res. 43 (7), W07401.

Liu, Y., Weerts, A. H., Clark, M., Hendricks Franssen, H.-J., Kumar, S., Moradkhani, H., Seo, D.-J., Schwanenberg, D., Smith, P., van Dijk, A. I. J. M., He, M., Lee, H., Noh, S. J., Rakovec, O., Restrepo, P., 2012. Advancing data assimilation in

operational hydrologic forecasting: progresses, challenges, and emerging opportunities. Hydrol. Earth Syst. Sci.. 16 (10), 3863–3887.

Madsen, H., 2000. Automatic calibration of a conceptual rainfall–runoff model using multiple objectives. J. Hydrol. 235 (3), 276–288.

Makkink, G. F., 1957. Testing the Penman formula by means of lysimeters. Int. J. Water. Eng. 11, 277–288.

Manning, R., 1889. On the flow of water in open channels and pipes. Trans. Inst. Civ. Eng. Ireland 20, 161–207.

Marchi, L., Boraga, M., Preciso, E., Gaume, E., 2010. Characterisation of selected extreme flash floods in Europe and implications for flood risk management. J. Hydrol. 394, 118–133.

Marchi, L., Borga, M., Preciso, E., Sangati, M., Gaume, E., Bain, V., Delrieu, G., Bonnifait, L., Pogačnik, N., 2009. Comprehensive post-event survey of a flash flood in Western Slovenia: observation strategy and lessons learned. Hydrol. Process. 23, 3761–3770.

Maréchal, J., Ladouche, B., Dorfliger, N., 2009. Hydrogeological analysis of groundwater contribution to the 6-8 september 2005 flash flood in Nîmes (in French). Houile Blanche, 88–93.

Maxwell, R. M., Kollet, S. J., 2008. Interdependence of groundwater dynamics and land-energy feedbacks under climate change. Nature Geoscience 1 (10), 665–669.

Maxwell, R. M., Miller, N. L., 2005. Development of a coupled land surface and groundwater model. J. Hydrometeorol. 6 (3), 233–247.

McDonald, M. G., Harbaugh, A. W., 1984. A modular three-dimensional finite-difference ground-water flow model. USGS Numbered Series 83–875, U.S. Geological Survey.

McDonnell, J. J., 2003. Where does water go when it rains? Moving beyond the variable source area concept of rainfall-runoff response. Hydrol. Process 17 (9), 1869–1875.

McDonnell, J. J., Sivapalan, M., Vaché, K., Dunn, S., Grant, G., Haggerty, R., Hinz, C., Hooper, R., Kirchner, J., Roderick, M. L., 2007. Moving beyond heterogeneity and process complexity: A new vision for watershed hydrology. Water Resour. Res. 43 (7), W07301.

Melsen, L. A., Teuling, A. J., van Berkum, S. W., Torfs, P. J. J. F., Uijlenhoet, R., 2013. Catchments as simple dynamical systems: A case study on methods and data requirements for parameter identifica-

tion. Water Resour. Res., under review.

Merz, B., Kreibich, H., Thieken, A., Schmidtke, R., 2004. Estimation uncertainty of direct monetary flood damage to buildings. Natural Hazards and Earth System Science 4 (1), 153–163.

Merz, R., Blöschl, G., 2004. Regionalisation of catchment model parameters. J. Hydrol. 287 (1), 95–123.

Merz, R., Parajka, J., Blöschl, G., 2009. Scale effects in conceptual hydrological modeling. Water Resour. Res. 45 (9), W09405.

Merz, R., Parajka, J., Blöschl, G., 2011. Time stability of catchment model parameters: Implications for climate impact analyses. Water Resour. Res. 47 (2), W02531.

Mesa, O. J., Mifflin, E. R., 1986. On the relative role of hillslope and network geometry in hydrologic response. In: Gupta, V. K., Rodriguez-Iturbe, I., Wood, E. F. (Eds.), Scale Problems in Hydrology. D. Reidel, Dordrecht, pp. 1–17.

Messer, H., Zinevich, A., Alpert, P., 2006. Environmental monitoring by wireless communication networks. Science 312, 713.

Messner, F., Meyer, V., 2006. Flood damage, vulnerability and risk perception–challenges for flood damage research. Springer.

Miglietta, M., Regano, A., 2008. An observational and numerical study of a flash-flood event over south-eastern italy. Nat. Hazard Earth Sys. 8, 1417–1430.

Monincx, S., Termes, P., Tromp, G., 2006. Regie afvoerpieken noodzakelijk om problemen op overijsselse vecht te voorkomen direction discharge peaks necessary to avoid problems with Overijsselse Vecht. H_2O 23, 44–47, (in Dutch).

Montanari, A., Young, G., Savenije, H. H. G., Hughes, D., Wagener, T., Ren, L. L., Koutsoyiannis, D., Cudennec, C., Toth, E., Grimaldi, S., Blöschl, G., Sivapalan, M., Beven, K., Gupta, H., Hipsey, M., Schaefli, B., Arheimer, B., Boegh, E., Schymanski, S., Di Baldassarre, G., Yu, B., Hubert, P., Huang, Y., Schumann, A., Post, D., Srinivasan, V., Harman, C., Thompson, S., Rogger, M., Viglione, A., McMillan, H., Characklis, G., Pang, Z., Belyaev, V., 2013. Panta rhei–everything flows: Change in hydrology and society–The IAHS Scientific Decade 2013–2022. Hydrolog. Sci. J. 58 (6), 1256–1275.

Moore, R. J., 1985. The probability-distributed principle and runoff production at point and basin scales. Hydrol. Sci. J. 30(2), 273–297.

Moore, R. J., 2007. The PDM rainfall-runoff model.

Hydrol. Earth Syst. Sci. 11 (1), 483–499.

Mosley, M. P., 1979. Streamflow generation in a forested watershed, New Zealand. Water Resour. Res. 15 (4), 795–806.

Nash, J. E., Sutcliffe, J. V., 1970. River flow forecasting through conceptual models, Part I - A discussion of principles. J. Hydrol. 10, 282–290.

National Institute for Drinking Water Supply, 1982. Possible locations for deep groundwater extraction in West-Utrecht (in Dutch). Tech. rep.

Neal, C., Bowes, M., Jarvie, H. P., Scholefield, P., Leeks, G., Neal, M., Rowland, P., Wickham, H., Harman, S., Armstrong, L., et al., 2012. Lowland river water quality: a new uk data resource for process and environmental management analysis. Hydrol. Process. 26 (6), 949–960.

NHV, 2014. Modelling the Hupsel Brook catchment (in Dutch) – contributions from E. Querner, W. Klutman, P. Droogers, W. Terink, A. Schuphof, B. van Meekeren, F. Verhagen, H. Vermue, B. van der Wal, C. Brauer, P. Kloosterman, R. Teuling, R. Uijlenhoet, H. Pavelková, W. Swierstra, A. Veldhuizen and G. Willems. Stromingen, in press.

Nicholls, R. J., Hoozemans, F. M. J., Marchand, M., 1999. Increasing flood risk and wetland losses due to global sea-level rise: regional and global analyses. Global Environmental Change 9, S69–S87.

Ogden, F. L., Sharif, H. O., Senarath, S. U. S., Smith, J. A., Baeck, M. L., Richardson, J. R., 2000. Hydrologic analysis of the Fort Collins, Colorado flash flood of 1997. J. Hydrol. 228, 82–100.

Oreskes, N., Shrader-Frechette, K., Belitz, K., 1994. Verification, validation, and confirmation of numerical models in the earth sciences. Science 263 (5147), 641–646.

Oude Essink, G. H. P., 2001. Salt water intrusion in a three-dimensional groundwater system in the Netherlands: a numerical study. Transport Porous Med. 43 (1), 137–158.

Overeem, A., , Buishand, A. Holleman, I., Uijlenhoet, R., 2010. Extreme value modeling of areal rainfall from weather radar. Water Resour. Res. 46.

Overeem, A., Buishand, A., Holleman, I., 2008. Rainfall depth-duration-frequency curves and their uncertainties. J. Hydrol. 348, 124–134.

Overeem, A., Buishand, A., Holleman, I., 2009a. Extreme rainfall analysis and estimation of depth-duration-frequency curves using weather radar. Water Resour. Res. 45.

Overeem, A., Holleman, I., Buishand, A., 2009b. Derivation of a 10-year radar-based climatology of

rainfall. J. Appl. Meteor. Climatol. 48, 1448–1463.

Overeem, A., Leijnse, H., Uijlenhoet, R., 2011. Measuring urban rainfall using microwave links from commercial cellular communication networks. Water Resour. Res. 47 (12), W12505.

Pappenberger, F., Beven, K. J., Hunter, N. M., Bates, P. D., Gouweleeuw, B. T., Thielen, J., de Roo, A. P. J., 2005. Cascading model uncertainty from medium range weather forecasts (10 days) through a rainfall-runoff model to flood inundation predictions within the European Flood Forecasting System (EFFS). Hydrol. Earth Syst. Sci. 9 (4), 381–393.

Parajka, J., Merz, R., Blöschl, G., 2005. A comparison of regionalisation methods for catchment model parameters. Hydrol. Earth Syst. Sci. 9, 157–171.

Pauwels, V., Hoeben, R., Verhoest, N. E. C., De Troch, F. P., 2001. The importance of the spatial patterns of remotely sensed soil moisture in the improvement of discharge predictions for small-scale basins through data assimilation. J. Hydrol. 251 (1), 88–102.

Perrin, C., Michel, C., Andréassian, V., 2001. Does a large number of parameters enhance model performance? Comparative assessment of common catchment model structures on 429 catchments. J. Hydrol. 242 (3), 275–301.

Perrin, C., Michel, C., Andréassian, V., 2003. Improvement of a parsimonious model for streamflow simulation. J. Hydrol. 279 (1), 275–289.

Pfister, L., McDonnell, J. J., Hissler, C., Hoffmann, L., 2010. Ground-based thermal imagery as a simple, practical tool for mapping saturated area connectivity and dynamics. Hydrol. Process. 24 (21), 3123–3132.

Pfister, L., McDonnell, J. J., Wrede, S., Hlúbiková, D., Matgen, P., Fenicia, F., Ector, L., Hoffmann, L., 2009. The rivers are alive: on the potential for diatoms as a tracer of water source and hydrological connectivity. Hydrol. Process. 23 (19), 2841–2845.

Prinsen, G. F., Becker, B. P. J., 2011. Application of Sobek hydraulic surface water models in the Netherlands Hydrological Modelling Instrument. Irrig. Drain. 60 (S1), 35–41.

Querner, E. P., 1988. Description of a regional groundwater flow model SIMGRO and some applications. Agr. Water Manage. 14 (1), 209–218.

Rakovec, O., 2013. Improving operational flood forecasting using data assimilation. Ph.D. thesis, Wageningen University, submitted.

Rakovec, O., Hill, M. C., Clark, M. P., Weerts, A. H.,

Teuling, A. J., Uijlenhoet, R., 2014. Distributed Evaluation of Local Sensitivity Analysis (DELSA), with application to hydrologic models. Water Resour. Res. 50, 1–18.

Rakovec, O., Weerts, A. H., Hazenberg, P., Torfs, P. J. J. F., Uijlenhoet, R., 2012. State updating of a distributed hydrological model with Ensemble Kalman Filtering: effects of updating frequency and observation network density on forecast accuracy. Hydrol. Earth Syst. Sci. 16, 3435–3449.

Reed, R. D., Marks, R. J., 1998. Neural smithing: supervised learning in feedforward artificial neural networks. MIT Press.

Refsgaard, J. C., Knudsen, J., 1996. Operational validation and intercomparison of different types of hydrological models. Water Resour. Res. 32 (7), 2189–2202.

Refsgaard, J. C., Storm, B., 1995. Mike she. In: Singh, V. (Ed.), Computer models of watershed hydrology. Water Resources Publications, Colorado, USA, pp. 809–846.

Reichle, R. H., Koster, R. D., Dong, J., Berg, A. A., 2004. Global soil moisture from satellite observations, land surface models, and ground data: Implications for data assimilation. J. Hydrometeorol. 5 (3), 430–442.

Rozemeijer, J. C., van der Velde, Y., van Geer, F. C., Bierkens, M. F. P., Broers, H. P., 2010a. Direct measurements of the tile drain and groundwater flow route contributions to surface water contamination: From field-scale concentration patterns in groundwater to catchment-scale surface water quality. Environ. Pollut. 158, 3571–3579.

Rozemeijer, J. C., van der Velde, Y., van Geer, F. C., de Rooij, G. H., Torfs, P. J. J. F., Broers, H. P., 2010b. Improving load estimates for NO3 and P in surface waters by characterizing the concentration response to rainfall events. Environ. Sci. Technol. 44 (16), 6305–6312.

Rupp, D., Owens, J., Warren, K., Selker, J., 2004. Analytical methods for estimating saturated hydraulic conductivity in a tile-drained field. J. Hydrol. 289, 111–127.

Rupp, D., Selker, J. S., 2006a. Information, artifacts, and noise in dq/dt-q recession analysis. Adv. Water Resour. 29, 154–160.

Rupp, D. E., Schmidt, J., Woods, R. A., Bidwell., V. J., 2009. Analytical assessment and parameter estimation of a low-dimensional groundwater model. J. Hydrol. 377, 143–154.

Rupp, D. E., Selker, J. S., 2006b. On the use of the Boussinesq equation for interpreting reces-

sion hydrographs from sloping aquifers. Water Resour. Res. 42, W12241.

Russchenberg, H., Bosveld, F., Swart, D., ten Brink, H., de Leeuw, G., Uijlenhoet, R., Arbesser-Rastburg, B., van der Marel, H., Ligthart, L., Boers, R., Apituley, A., 2005. Ground-based atmospheric remote sensing in the Netherlands: European outlook. IEICE Trans. Commun. E88-B, 2252–2258.

Schenk, H. J., Jackson, R. B., 2002. The global biogeography of roots. Ecol. Monogr. 72 (3), 311–328.

Schulla, J., Jasper, K., 2007. Model description WaSiM-ETH. Institute for Atmospheric and Climate Science, Swiss Federal Institute of Technology, Zürich.

Schumacher, R., Johnson, R., 2005. Organization and environmental properties of extreme-rain-producing mesoscale convective systems. Mon. Wea. Rev. 133, 961–976.

Schumacher, R., Johnson, R., 2008. Mesoscale processes contributing to extreme rainfall in a mid-latitude warm-season flash flood. Mon. Wea. Rev. 136, 3964–3986.

Schuurmans, J. M., Bierkens, M. F. P., 2007. Effect of spatial distribution of daily rainfall on interior catchment response of a distributed hydrological model. Hydrol. Earth Syst. Sci. 11 (2), 677–693.

Seibert, J., 1997. Estimation of parameter uncertainty in the HBV model. Nordic Hydrol. 28, 247–262.

Seibert, J., 1999a. Multi-criteria calibration of a conceptual runoff model using a genetic algorithm. Hydrol. Earth Syst. Sci. 4 (2), 215–224.

Seibert, J., 1999b. Regionalisation of parameters for a conceptual rainfall-runoff model. Agr. Forest Meteorol. 98, 279–293.

Seibert, J., McDonnell, J. J., 2002. On the dialog between experimentalist and modeler in catchment hydrology: Use of soft data for multicriteria model calibration. Water Resour. Res. 38 (11), 1241.

Seneviratne, S. I., Lehner, I., Gurtz, J., Teuling, A. J., Lang, H., Moser, U., Grebner, D., Menzel, L., Schroff, K., Vitvar, T., Zappa, M., 2012. Swiss prealpine Rietholzbach research catchment and lysimeter: 32 year time series and 2003 drought event. Water Resour. Res. 48 (6), W06526.

Shaman, J., Stieglitz, M., Burns, D., 2004. Are big basins just the sum of small catchments? Hydrol. Process. 18 (16), 3195–3206.

Simůnek, J., van Genuchten, M. T., Šejna, M., 2008. The HYDRUS-1D software package for simulating the one-dimensional movement of water, heat, and multiple solutes in variably-saturated media. Tech. Rep. 3, KNMI.

Sivapalan, M., 2005. Pattern, process and function: elements of a unified theory of hydrology at the catchment scale. Encyclopedia of Hydrological Sciences.

Sivapalan, M., Savenije, H. H., Blöschl, G., 2012. Socio-hydrology: A new science of people and water. Hydrol. Process. 26 (8), 1270–1276.

Smith, J. A., Baeck, M. L., Steiner, M., Miller, A. J., 1996. Catastrophic rainfall from an upslope thunderstorm in the central Appalachians: The Rapidan storm of June 27, 1995. Water Resour. Res. 32, 3099–3113.

Sophocleous, M., Perkins, S. P., 2000. Methodology and application of combined watershed and ground-water models in Kansas. J. Hydrol. 236 (3), 185–201.

Soulsby, C., Neal, C., Laudon, H., Burns, D. A., Merot, P., Bonell, M., Dunn, S. M., Tetzlaff, D., 2008. Catchment data for process conceptualization: simply not enough? Hydrol. Process. 22 (12), 2057–2061.

Soulsby, C., Rodgers, P. J., Petry, J., Hannah, D. M., Malcolm, I. A., Dunn, S. M., 2004. Using tracers to upscale flow path understanding in mesoscale mountainous catchments: two examples from Scotland. J. Hydrol. 291 (3), 174–196.

Stenitzer, E., Diestel, H., Zenker, T., Schwartengräber, R., 2007. Assessment of capillary rise from shallow groundwater by the simulation model SIMWASER using either estimated pedotransfer functions or measured hydraulic parameters. Water Resour. Manage. 21 (9), 1567–1584.

Stricker, J. N. M., Brutsaert, W., 1978. Actual evapotranspiration over a summer in the Hupsel Catchment. J. Hydrol. 39, 139–157.

Stricker, J. N. M., Warmerdam, P. M. M., 1982. Estimation of the water balance in the Hupselse Beek basin over a period of three years and a first effort to simulate the rainfall-runoff process for a complete year. In: Proceedings of the International symposium on hydrological research basins and their use in water resources planning. Bern, Switzerland, pp. 379–388.

Sugawara, M., Ozaki, E., Watanabe, I., Katsuyama, Y., 1974. Tank model and its application to Bird Creek, Wollombi Brook, Bikin River, Kitsu River, Sanaga River and Nam Mune. Vol. 11. National Research Center for Disaster Prevention.

Te Brake, B., Hanssen, R. F., van der Ploeg, M. J.,

de Rooij, G. H., 2012. Satellite-based radar interferometry to estimate large-scale soil water depletion from clay shrinkage: Possibilities and limitations. Vadose Zone J. 12 (8).

Te Brake, B., van der Ploeg, M. J., de Rooij, G. H., 2013. Water storage change estimation from in situ shrinkage measurements of clay soils. Hydrol. Earth Syst. Sci. 17 (5), 1933–1949.

Tetzlaff, D., McDonnell, J. J., Uhlenbrook, S., McGuire, K. J., Bogaart, P. W., Naef, F., Baird, A. J., Dunn, S. M., Soulsby, C., 2008. Conceptualizing catchment processes: simply too complex? Hydrol. Process. 22 (11), 1727–1730.

Tetzlaff, D., Soulsby, C., 2008. Sources of baseflow in larger catchments–Using tracers to develop a holistic understanding of runoff generation. J. Hydrol. 359 (3), 287–302.

Tetzlaff, D., Soulsby, C., Hrachowitz, M., Speed, M., 2011. Relative influence of upland and lowland headwaters on the isotope hydrology and transit times of larger catchments. J. Hydrol. 400 (3), 438–447.

Tetzlaff, D., Soulsby, C., Waldron, S., Malcolm, I. A., Bacon, P. J., Dunn, S. M., Lilly, A., Youngson, A. F., 2007. Conceptualization of runoff processes using a geographical information system and tracers in a nested mesoscale catchment. Hydrol. Process. 21 (10), 1289–1307.

Tetzlaff, D., Uhlenbrook, S., 2005. Significance of spatial variability in precipitation for process-oriented modelling: results from two nested catchments using radar and ground station data. Hydrol. Earth Syst. Sci. 9, 29–41.

Teuling, A. J., Lehner, I., Kirchner, J. W., Seneviratne, S. I., 2010. Catchments as simple dynamical systems: Experience from a Swiss prealpine catchment. Water Resour. Res. 46, W10502.

Teuling, A. J., Troch, P. A., 2005. Improved understanding of soil moisture variability dynamics. Geophys. Res. Lett. 32 (5), L05404.

Teuling, A. J., Uijlenhoet, R., Hupet, F., Troch, P. A., 2006. Impact of plant water uptake strategy on soil moisture and evapotranspiration dynamics during drydown. Geophys. Res. Lett. 33 (3), L03401.

Teuling, A. J., van Loon, A. F., Seneviratne, S. I., Lehner, I., Aubinet, M., Heinesch, B., Bernhofer, C., Grünwald, T., Prasse, H., Spank, U., 2013. Evapotranspiration amplifies European summer drought. Geophys. Res. Lett. 40, 2071Ű2075.

Therrien, R., McLaren, R. G., Sudicky, E. A., Panday, S. M., 2006. Hydrogeosphere: A three-dimensional numerical model describing fully-integrated subsurface and surface flow and solute transport. Groundwater Simul. Group, Waterloo, Ont., Canada.

Thom, A., Oliver, H., 1977. On Penman's equation for estimating regional evaporation. Q. J. Roy. Meteor. Soc. 103, 345–357.

Thompson, J. R., Gavin, H., Refsgaard, A., Sørenson, H. R., Gowing, D. J., 2009. Modelling the hydrological impacts of climate change on UK lowland wet grassland. Wetl. Ecol. and Manag. 17 (5), 503–523.

Tiemeyer, B., Moussa, R., Lennartz, B., Voltz, M., 2007. MHYDAS-DRAIN: A spatially distributed model for small, artificially drained lowland catchments. Ecological modelling 209 (1), 2–20.

Todini, E., 1996. The ARNO rainfall-runoff model. J. Hydrol. 175 (1), 339–382.

Troch, P., 2008. Land surface hydrology. In: Bierkens, M., Troch, P., Dolman, H. (Eds.), Climate and the Hydrological Cycle. No. 8 in IAHS Special Publications. IAHS Press, Wallingford, UK, pp. 99–115.

Troch, P., de Troch, F., Brutsaert, W., 1993. Effective water table depth to describe initial conditions prior to storm rainfall in humid regions. Water Recour. Res. 29, 427–434.

Troch, P. A., Berne, A., Bogaart, P., Harman, C., Hilberts, A. G. J., Lyon, S. W., Paniconi, C., Pauwels, V. R. N., Rupp, D. E., Selker, J. S., Teuling, A. J., Uijlenhoet, R., C, V. N. E., 2013. The importance of hydraulic groundwater theory in catchment hydrology: The legacy of Wilfried Brutsaert and Jean-Yves Parlange. Water Resour. Res. 49 (9), 5099–5116, submitted.

Tromp-van Meerveld, H. J., McDonnell, J. J., 2006. Threshold relations in subsurface stormflow: 2. The fill and spill hypothesis. Water Resour. Res. 42 (2), W02411.

Turunen, M., Warsta, L., Paasonen-Kivekäs, M., Nurminen, J., Myllys, M., Alakukku, L., Äijö, H., Puustinen, M., Koivusalo, H., 2013. Modeling water balance and effects of different subsurface drainage methods on water outflow components in a clayey agricultural field in boreal conditions. Agr. Water Manage. 121, 135–148.

Twine, T. E., Kustas, W. P., Norman, J. M., Cook, D. R., Houser, P. R., Meyers, T. P., Prueger, J. H., Starks, P. J., Wesely, M. L., 2000. Correcting eddy-covariance flux underestimates over a grassland. Agr. Forest Meteorol. 103 (3), 279–300.

Uhlenbrook, S., Didszun, J., Wenninger, J., 2008.

Source areas and mixing of runoff components at the hillslope scale–a multi-technical approach. Hydrol. Sci. J. 53 (4), 741–753.

Uhlenbrook, S., Seibert, J., Leibundgut, C., Rodhe, A., 1999. Prediction uncertainty of conceptual rainfall-runoff models caused by problems in identifying model parameters and structure. Hydrol. Sci. J. 44 (5), 779–797.

Van Andel, S. J., Price, R., Lobbrecht, A., van Kruiningen, F., 2010. Modeling controlled water systems. J. Irrig. Drain. E-ASCE 136 (6), 392–404.

Van Dam, J. C., Groenendijk, P., Hendriks, R. F. A., Kroes, J. G., 2008. Advances of modeling water flow in variably saturated soils with SWAP. Vadose Zone J. 7 (2), 640–653.

Van den Eertwegh, G. A. P. H., 2002. Water and nutrient budgets at field and regional scale: travel times of drainage water and nutrient loads to surface water. Ph.D. thesis, Wageningen University.

Van den Eertwegh, G. A. P. H., Nieber, J. L., de Louw, P. G. B., van Hardeveld, H. A., Bakkum, R., 2006. Impacts of drainage activities for clay soils on hydrology and solute loads to surface water. Irrig. Drain. 55 (3), 235–245.

Van der Ploeg, M. J., Appels, W. M., Cirkel, D. G., Oosterwoud, M. R., Witte, J.-P. M., van der Zee, S. E. A. T. M., 2012. Microtopography as a driving mechanism for ecohydrological processes in shallow groundwater systems. Vadose Zone J. 11 (3).

Van der Velde, Y., 2011. Dynamics in groundwater and surface water quality: From field-scale processes to catchment-scale models. Ph.D. thesis, Wageningen University.

Van der Velde, Y., de Rooij, G. H., Rozemeijer, J. C., van Geer, F. C., Broers, H. P., 2010a. Nitrate response of a lowland catchment: On the relation between stream concentration and travel time distribution dynamics. Water Resour. Res. 46 (11), W11534.

Van der Velde, Y., de Rooij, G. H., Torfs, P. J. J. F., 2009. Catchment-scale non-linear groundwater-surface water interactions in densely drained lowland catchments. Hydrol. Earth Syst. Sci. 13, 1867–1885.

Van der Velde, Y., Rozemeijer, J. C., de Rooij, G. H., van Geer, F. C., Broers, H. P., 2010b. Field-scale measurements for separation of catchment discharge into flow route contributions. Vadose Zone J. 9 (1), 25–35.

Van der Velde, Y., Rozemeijer, J. C., de Rooij, G. H., van Geer, F. C., Broers, H. P., 2010. Field scale measurements for separation of catchment dis-

charge into flow route contributions. Vadose Zone J. 9, 25–35.

Van der Velde, Y., Rozemeijer, J. C., de Rooij, G. H., van Geer, F. C., Torfs, P. J. J. F., de Louw, P. G. B., 2011. Improving catchment discharge predictions by inferring flow route contributions from a nested-scale monitoring and model setup. Hydrol. Earth Syst. Sci. 15, 913–930.

Van der Velde, Y., Torfs, P. J. J. F., van der Zee, S. E. A. T. M., Uijlenhoet, R., 2012. Quantifying catchment-scale mixing and its effect on time-varying travel time distributions. Water Resour. Res. 48, W06536.

Van Genuchten, 1980. A closed-form equation for predicting the hydraulic conductivity of unsaturated soils. Soil Sci. Soc. Am. J. 44, 892–898.

Van Huijgevoort, M. H. J., Hazenberg, P., van Lanen, H. A. J., Teuling, A. J., Clark, D. B., Folwell, S., Gosling, S. N., Hanasaki, N., Heinke, J., Koirala, S., Stacke, T., Voss, F., Sheffield, J., Uijlenhoet, R., 2013. Global multimodel analysis of drought in runoff for the second half of the twentieth century. J. Hydrometeorol. 14 (5), 1535–1552.

Van Loon, A. F., van Lanen, H. A. J., 2013. Making the distinction between water scarcity and drought using an observation-modeling framework. Water Resour. Res. 49, 1483–1502.

Van Ulden, A. P., Wieringa, J., 1996. Atmospheric boundary layer research at Cabauw. Bound.-Lay. Meteorol. 78 (1-2), 39–69.

Van Walsum, P. E. V., Groenendijk, P., 2008. Quasi steady-state simulation of the unsaturated zone in groundwater modeling of lowland regions. Vadose Zone J. 7 (2), 769–781.

Van Walsum, P. E. V., Veldhuizen, A. A., 2011. Integration of models using shared state variables: Implementation in the regional hydrologic modelling system SIMGRO. J. Hydrol. 409, 363–370.

Vellinga, P., Katsman, C., Sterl, A., Beersma, J. J., Hazeleger, W., Church, J., Kopp, R., Kroon, D., Oppenheimer, M., Plag, H. P., Rahmstorf, S., Lowe, J., Ridley, J., van Storch, H., Vaughan, D., van de Wal, R., Weisse, R., Kwadijk, J., Lammersen, R., Marinova, N., 2009. Exploring high-end climate change scenarios for flood protection of the Netherlands. Tech. Rep. WR 2009-05, Royal Netherlands Meteorological Institute.

Vrugt, J. A., Diks, C. G., Gupta, H. V., Bouten, W., Verstraten, J. M., 2005. Improved treatment of uncertainty in hydrologic modeling: Combining the strengths of global optimization and data assimilation. Water Resour. Res. 41 (1), W01017.

Vrugt, J. A., ter Braak, C. J. F., 2011. DREAM(D): an adaptive Markov Chain Monte Carlo simulation algorithm to solve discrete, noncontinuous, and combinatorial posterior parameter estimation problems. Hydrol. Earth Syst. Sci. 15 (12), 3701–3713.

Vrugt, J. A., ter Braak, C. J. F., Clark, M. P., Hyman, J. M., Robinson, B. A., 2008. Treatment of input uncertainty in hydrologic modeling: Doing hydrology backward with Markov chain Monte Carlo simulation. Water Resour. Res. 44 (12), W00B09.

Wagener, T., 2003. Evaluation of catchment models. Hydrol. Process. 17 (16), 3375–3378.

Wagener, T., Boyle, D. P., Lees, M. J., Wheater, H. S., Gupta, H. V., Sorooshian, S., 2001. A framework for development and application of hydrological models. Hydrol. Earth Syst. Sci. 5 (1), 13–26.

Wagener, T., Sivapalan, M., Troch, P., Woods, R., 2007. Catchment classification and hydrologic similarity. Geogr. Compass 1 (4), 901–931.

Wagener, T., Sivapalan, M., Troch, P. A., McGlynn, B. L., Harman, C. J., Gupta, H. V., Kumar, P., Rao, P. S. C., Basu, N. B., Wilson, J. S., 2010. The future of hydrology: An evolving science for a changing world. Water Resour. Res. 46 (5), W05301.

Wagener, T., Wheater, H. S., 2004. Rainfall-runoff modelling in gauged and ungauged catchments. Imperial College Press.

Wand, M., Jones, M., 1995. Kernel Smoothing. Chapman and Hall, London.

Wandee, P., 2013. Optimization of water management in polder areas. Ph.D. thesis, Wageningen University and UNSECO-IHE.

Wassmann, R., Hien, N. X., Hoanh, C. T., Tuong, T. P., 2004. Sea level rise affecting the Vietnamese Mekong Delta: water elevation in the flood season and implications for rice production. Climatic Change 66 (1-2), 89–107.

Weiler, M., McDonnell, J., 2004. Virtual experiments: a new approach for improving process conceptualization in hillslope hydrology. J. Hydrol. 285 (1), 3–18.

Weir, A. H., Barraclough, P. B., 1986. The effect of drought on the root growth of winter wheat and on its water uptake from a deep loam. Soil Use Manage. 2 (3), 91–96.

Westhoff, M. C., Bogaard, T. A., Savenije, H. H. G., 2011. Quantifying spatial and temporal discharge dynamics of an event in a first order stream, using distributed temperature sensing. Hydrol. Earth Syst. Sci. 15, 1945–1957.

Witte, J. P. M., Runhaar, J., van Ek, R., van der Hoek, D. C. J., Bartholomeus, R., Batelaan, O., van Bodegom, P. M., Wassen, M. J., van der Zee, S. E. A. T. M., 2012. An ecohydrological sketch of climate change impacts on water and natural ecosystems for the netherlands: bridging the gap between science and society. Hydrol. Earth Syst. Sci. 16, 3945–3957.

Wösten, J. H. M., Ismail, A. B., Van Wijk, A. L. M., 1997. Peat subsidence and its practical implications: a case study in Malaysia. Geoderma 78 (1-2), 25–36.

Younis, J., Anquetin, S., Thielen, J., 2008. The benefit of high-resolution operational weather forecasts for flash flood warning. Hydrol. Earth Syst. Sci. 12, 1039–1051.

Zambrano-Bigarini, M., Rojas, R., 2013. A model-independent particle swarm optimisation software for model calibration. Environ. Modell. Softw. 43, 5–25.

Zampieri, M., Serpetzoglou, E., Anagnostou, E. N., Nikolopoulos, E. I., Papadopoulos, A., 2012. Improving the representation of river–groundwater interactions in land surface modeling at the regional scale: Observational evidence and parameterization applied in the Community Land Model. J. Hydrol. 420, 72–86.

Zencich, S. J., Froend, R. H., Turner, J. V., Gailitis, V., 2002. Influence of groundwater depth on the seasonal sources of water accessed by Banksia tree species on a shallow, sandy coastal aquifer. Oecologia 131 (1), 8–19.

Zeng, F., Song, C., Guo, H., Liu, B., Luo, W., Gui, D., Arndt, S., Guo, D., 2013. Responses of root growth of Alhagi sparsifolia Shap.(Fabaceae) to different simulated groundwater depths in the southern fringe of the Taklimakan Desert, China. J. Arid Land 5 (2), 220–232.

Zhang, Q., Gemmer, M., Chen, J., 2008. Climate changes and flood/drought risk in the Yangtze Delta, China, during the past millennium. Quaternary International 176, 62–69.

Summary

Around the world, lowland areas are often densely populated and centers of economic activity and transport. The lack of topography, however, makes them vulnerable to flooding, climate change, and deterioration of water quality. Hydrological models can be used by water managers as a tool for early warning, risk assessment and infrastructure design. However, the models that are commonly used in lowland areas are often high-dimensional (groundwater or hydraulic) models. Low-dimensional models have typically been designed for use in mountainous catchments. The title of this thesis reflects the two-part research question: (1) what are the dominant catchment processes determining a lowland river's response to rainfall and (2) how can these processes be represented in simple hydrological models? For both of these questions, I focussed on topics which are important for lowland areas: (1) the relation between catchment storage and discharge, (2) the coupling between shallow groundwater and unsaturated zone, (3) activation of flowroutes at different stages of wetness and (4) the feedback between groundwater and surface water.

Lowland catchments can be divided into mildly sloping, freely draining catchments and flat areas with managed surface water levels. In this thesis, data from two Dutch field sites are used. The mildly sloping, freely draining Hupsel Brook catchment is located in the east of The Netherlands, with elevations ranging from 22 to 35 m above sea level. This catchment has been an experimental catchment since the 1960s. The flat Cabauw polder is located in the west of The Netherlands at an "elevation" of 1 meter below sea level. This area is part of the Cabauw Experimental Site for Atmospheric Research (CESAR).

On 26 August 2010 the eastern part of The Netherlands and the bordering part of Germany were struck by a series of rainfall events lasting for more than a day. Over an area of $740\,\mathrm{km}^2$ more than $120\,\mathrm{mm}$ of rainfall was observed in $24\,\mathrm{h}$. This extreme event resulted in local flooding of city centres, highways and agricultural fields, and considerable financial loss. In Chapter 3 we report on the unprecedented flash flood triggered by this exceptionally heavy rainfall event in the $6.5\,\mathrm{km}^2$ Hupsel Brook catchment. This study aims to improve our understanding of the dynamics of such lowland flash floods. We present a detailed hydrometeorological analysis of this extreme event, focusing on its synoptic meteorological characteristics, its space-time rainfall dynamics as observed with rain gauges, weather radar and a microwave link, as well as the measured soil moisture, groundwater and discharge response of the catchment. At the Hupsel Brook catchment $160\,\mathrm{mm}$ of rainfall was observed in $24\,\mathrm{h}$, corresponding to an estimated return period of well over 1000 years. As a result, discharge at the catchment outlet increased from 4.4×10^{-3} to nearly $5\,\mathrm{m}^3\,\mathrm{s}^{-1}$. Within $7\,\mathrm{h}$ discharge rose from 5×10^{-2} to $4.5\,\mathrm{m}^3\,\mathrm{s}^{-1}$. The catchment response can be divided into four phases: (1) soil moisture reservoir filling, (2) groundwater response, (3) surface depression filling and surface runoff and (4) backwater feedback. The first $35\,\mathrm{mm}$ of rainfall were stored in the soil without a significant increase in discharge. Relatively dry initial conditions (in comparison to those for past discharge extremes) prevented an even faster and more extreme hydrological response.

Relations between storage and discharge are essential characteristics of many rainfall-runoff models. The simple dynamical systems approach, in which a rainfall-runoff model is constructed from a single storage-discharge relation, has been successfully applied to humid catchments. In Chapter 4, we investigate (1) if and when the less humid lowland Hupsel Brook catchment also behaves like a simple dynamical system by hydrograph fitting, and (2) if system parameters can be inferred from streamflow recession rates or more directly from soil moisture storage observations. Only 39 % of the fitted hydrographs yielded Nash-Sutcliffe efficiencies above 0.5, from which we can conclude that the Hupsel Brook catchment does not always behave like a simple dynamical system. Model results were especially poor in summer, when evapotranspiration is high and the thick unsaturated zone attenuates the rainfall input. Using soil moisture data to obtain system parameters is not trivial, mainly because there is a discrepancy between local and catchment storage. Parameters obtained with direct storage-discharge fitting led to a strong underestimation of the response of runoff to rainfall, while recession analysis led to an overestimation.

The Wageningen Lowland Runoff Simulator (WALRUS) is presented in Chapter 5. WALRUS is a novel rainfall-runoff model to fill the gap between complex, spatially distributed models which are often used in lowland catchments and simple, parametric models which have mostly been developed for mountainous catchments. WALRUS explicitly accounts for processes that are important in lowland areas, notably (1) groundwater-unsaturated zone coupling, (2) wetness-dependent flow routes, (3) groundwater-surface water feedbacks and (4) seepage and surface water supply. WALRUS consists of a coupled groundwater-vadose zone reservoir, a quickflow reservoir and a surface water reservoir. WALRUS is suitable for operational use because it
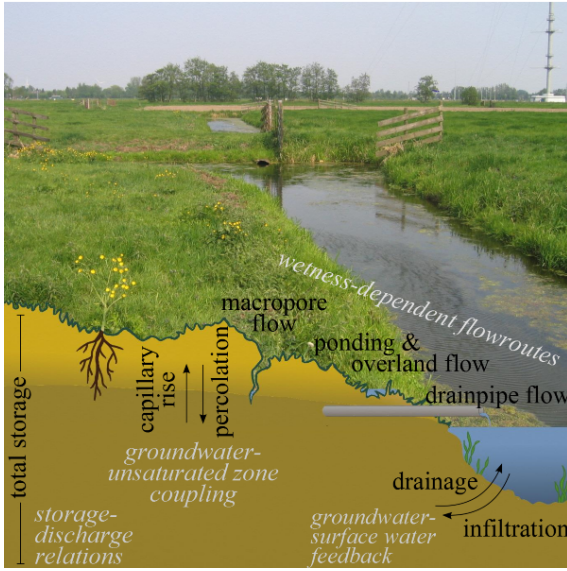
Schematic representation of the topics of this thesis (see Fig. 1.4): (1) storage-discharge relations, (2) groundwater-unsaturated zone coupling, (3) wetness-dependent flowroutes and (4) groundwater-surface water feedback.
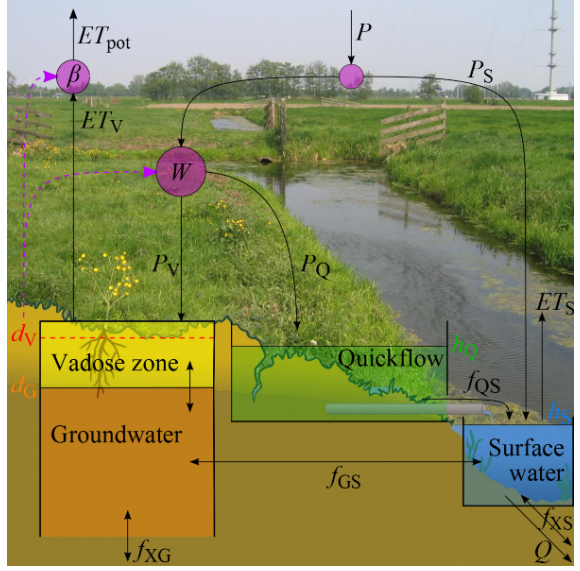
Modelling rainfall-runoff processes in lowland catchments (see Fig. 7.1): how the different flowpaths and feedbacks are schematised in WALRUS (see Tab. 5.1 for abbreviations of variables).

is computationally efficient and numerically stable (achieved with a flexible time step approach). In the open source model code default relations have been implemented, leaving only four parameters which require calibration. For research purposes, these defaults can easily be changed. Numerical experiments show that the implemented feedbacks have the desired effect on the system variables.

In Chapter 6, WALRUS is applied to two contrasting Dutch catchments: the Hupsel Brook catchment and Cabauw polder. In both catchments, WALRUS performs well: Nash-Sutcliffe efficiencies obtained after calibration on one year of discharge observations are 0.87 for the Hupsel Brook catchment and 0.83 for the Cabauw polder, with values of 0.74 and 0.76 for validation. The model also performs well during floods and droughts and can forecast the effect of control operations. Through the dynamic division between quick and slow flowroutes controlled by a wetness index, temporal and spatial variability in groundwater depths can be accounted for, which results in adequate simulation of discharge peaks as well as low flows. The performance of WALRUS is most sensitive to the parameters controlling the wetness index and the groundwater reservoir constant,

and to a lesser extent to the quickflow reservoir constant. The effects of these three parameters can be identified in the discharge time series, which indicates that the model is not overparameterised (parsimonious). Forcing uncertainty was found to have a larger effect on modelled discharge than parameter uncertainty and uncertainty in initial conditions.

Finally, in Chapter 7, the findings are combined to answer the research questions posed in the introduction. Although discharge is not uniquely related to the total catchment storage, internal catchment fluxes might still be understood and modelled adequately with local storage-discharge relations. Observations in the Hupsel Brook catchment and Cabauw polder show that shallow groundwater causes moist unsaturated zones and limits evapotranspiration reduction, that certain types of flow (e.g. drainpipe flow, overland flow) only occur when the catchment is wet enough and that high surface water levels reduce groundwater drainage during flood peaks. These findings are incorporated in the Wageningen Lowland Runoff Simulator (WALRUS), which can be used by water managers and researchers in lowland areas all over the world.

Samenvatting

Laaglandgebieden wereldwijd zijn vaak dichtbevolkt en centra van economische activiteit en transport. Door het gebrek aan topografie zijn laaglandgebieden gevoelig voor overstromingen, klimaatverandering en waterkwaliteitsproblemen. Hydrologische modellen kunnen worden gebruikt door waterbeheerders voor waarschuwingen, risicoinschattingen en ontwerp van infrastructuur. Helaas zijn de modellen die gewoonlijk gebruikt worden in laaglandgebieden vaak complexe (grondwater- of hydraulische) modellen, terwijl eenvoudige modellen meestal zijn ontworpen voor berggebieden. De titel van dit proefschrift slaat op de tweeledige onderzoeksvraag: (1) wat zijn de dominante stroomgebiedsprocessen die de respons van een laaglandrivier op regen bepalen en (2) hoe kunnen deze processen worden gerepresenteerd in simpele hydrologische modellen? Voor beide vragen is gefocust op onderwerpen die belangrijk zijn voor laaglandgebieden: (1) de relatie tussen (stroomgebiedsgemiddelde) berging en afvoer, (2) de koppeling tussen ondiep grondwater en de onverzadigde zone, (3) de activatie van stroomroutes bij verschillende vochttoestanden en (4) de terugkoppeling tussen grondwater en oppervlaktewater.

Laaglandgebieden kunnen worden ingedeeld in licht hellende, vrij afwaterende stroomgebieden en vlakke gebieden met beheerste oppervlaktewaterpeilen. In dit proefschrift wordt data gebruikt van twee Nederlandse proefgebieden. Het licht hellende, vrij afwaterende stroomgebied van de Hupselse Beek ligt in Oost-Nederland (tussen Eibergen en Groenlo), tussen 22 en 35 m boven zeeniveau, en wordt sinds de jaren '60 gebruikt als experimenteel stroomgebied. De vlakke polder Cabauw ligt in West-Nederland (bij Lopik), op 1 meter beneden zeeniveau, en is deel van een observatorium met meetinstrumenten voor atmosferisch onderzoek.

Op 26 Augustus 2010 werden het oosten van Nederland en het Duitse grensgebied getroffen door een reeks regenbuien die meer dan een dag aanhield. Over een oppervlakte van $740\,\mathrm{km}^2$ is meer dan $120\,\mathrm{mm}$ regen gemeten in 24 uur. Deze extreme gebeurtenis leidde tot lokale overstromingen van stedelijk gebied, snelwegen en bouwland en aanzienlijke financiële schade. In hoofdstuk 3 doen we verslag van de stortvloed die door deze uitzonderlijk hevige regen is veroorzaakt in het stroomgebied van de Hupselse Beek ($6{,}5\,\mathrm{km}^2$). Het doel van dit onderzoek is om ons begrip van de processen die spelen tijdens zulke laaglandstortvloeden te verbeteren. We presenteren een gedetailleerde hydrometeorlogische analyse van deze extreme gebeurtenis, waarbij we ons richten op de synop-tische meteorologische eigenschappen, de neerslagvariatie in ruimte en tijd gemeten met regenmeters, weerradar en een radiostraalverbinding, evenals de gemeten bodemvocht-, grondwater- en afvoerrespons van het stroomgebied. In het stroomgebied van de Hupselse Beek is $160\,\mathrm{mm}$ regen gemeten in 24 uur, wat overeenkomt met een herhalingstijd van aanzienlijk meer dan 1000 jaar. Hierdoor steeg de afvoer bij het lozingspunt van het stroomgebied van $4{,}4 \times 10^{-3}$ tot bijna $5\,\mathrm{m}^3\,\mathrm{s}^{-1}$. Binnen 7 uur steeg de afvoer van 5×10^{-2} tot $4{,}5\,\mathrm{m}^3\,\mathrm{s}^{-1}$. De respons van het stroomgebied kon worden ingedeeld in vier fasen: (1) bodemvochtaanvulling, (2) grondwaterrespons, (3) plasvorming en oppervlakte-afvoer en (4) oppervlaktewaterterugkoppeling. De eerste $35\,\mathrm{mm}$ regen zijn opgeslagen in de bodem zonder significante stijging in afvoer. Een relatief droge uitgangssituatie (in vergelijking met eerdere afvoerextremen) voorkwam een nog extremere respons.

Relaties tussen berging en afvoer zijn essentiële onderdelen van veel neerslag-afvoermodellen. De eenvoudige dynamische systeemaanpak, waarin een neerslag-afvoermodel wordt geconstrueerd op basis van een enkele berging-afvoerrelatie, is succesvol toegepast op vochtige stroomgebieden. In hoofdstuk 4 onderzoeken we (1) of en, zo ja, wanneer het minder vochtige stroomgebied van de Hupselse Beek zich ook gedraagt als een eenvoudig dynamisch systeem, en (2) of systeemparameters kunnen worden afgeleid uit afvoerrecessiesnelheden of direct uit bodemvochtmetingen. Slechts 39 % van de gemodelleerde hydrogrammen leidde tot Nash-Sutcliffe-efficiënties boven de 0.5, waarmee we kunnen concluderen dat het stroomgebied van de Hupselse Beek zich niet altijd gedraagt als een eenvoudig dynamisch systeem. De modelresultaten waren vooral slecht in de zomer, wanneer verdamping hoog is en regen wordt gedempt door de dikke onverzadigde zone. Het gebruiken van bodemvocht-data om systeemparameters te verkrijgen is niet triviaal, voornamelijk doordat er een discrepantie is tussen lokale en stroomgebiedsgemiddelde berging. Parameters verkregen met een directe relatie tussen berging en afvoer leidden tot een sterke onderschatting van de afvoerrespons op regen, terwijl recessieanalyse leidde tot een overschatting.

De Wageningse Laagland Afvoer Simulator (WALRUS) wordt gepresenteerd in hoofdstuk 5. WALRUS is een nieuw neerslag-afvoermodel dat het gat moet vullen tussen complexe, ruimtelijk gedistribueerde modellen die vaak gebruikt worden in laaglandgebieden en simpele, ruimtelijk geïntegreerde parametrische modellen die voornamelijk zijn ontwikkeld voor berggebieden. WALRUS houdt expliciet rekening met processen die belangrijk zijn in laaglandgebieden, in het bijzonder (1) de kop-
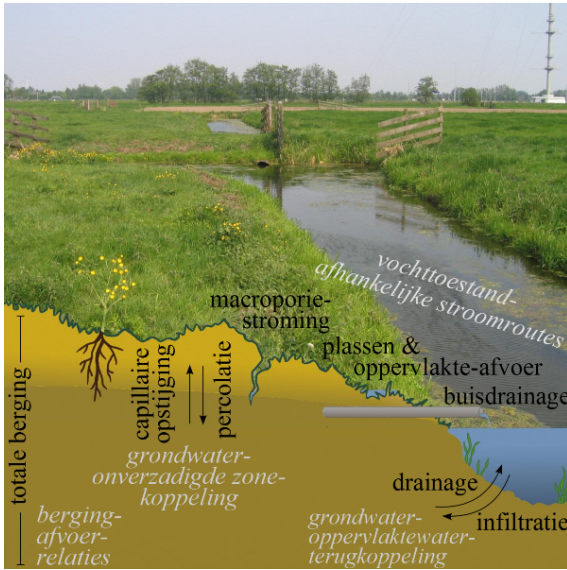
De onderwerpen van dit proefschrift (zie fig. 1.4): (1) berging-afvoerrelaties, (2) koppeling tussen grondwater en onverzadigde zone, (3) vochttoestandafhankelijke stroomroutes en (4) grondwater-oppervlaktewaterterugkoppeling.
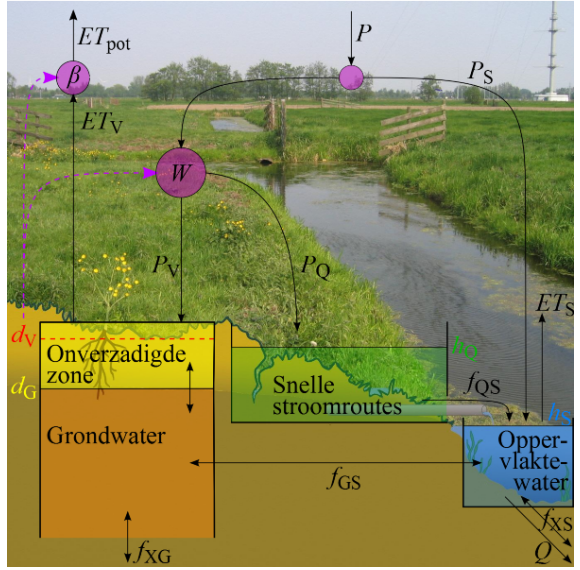
Het modelleren van neerslag-afvoerprocessen in laaglandgebieden (zie fig. 7.1): hoe de verschillende stroomroutes zijn geschematiseerd in WALRUS (zie Tab. 5.1 voor afkortingen van de variabelen).

peling tussen grondwater en onverzadigde zone, (2) vochttoestandafhankelijke stroomroutes, (3) grondwater-oppervlaktewaterterugkoppeling en (4) kwel, wegzijging en het inlaten of wegpompen van oppervlaktewater. WALRUS bestaat uit een gekoppeld reservoir voor grondwater en onverzadigde zone, een reservoir voor snelle stroomroutes en een oppervlaktewaterreservoir. WALRUS is geschikt voor operationele toepassingen omdat het efficiënt rekent en numeriek stabiel is (bereikt met een aanpak voor flexibele tijdstappen). In de vrij toegankelijke modelcode zijn standaardrelaties geïmplementeerd, zodat er slechts vier parameters overblijven die gekalibreerd moeten worden. Voor onderzoeksdoeleinden kunnen deze standaardrelaties gemakkelijk worden aangepast. Numerieke experimenten laten zien dat de geïmplementeerde terugkoppelingen het gewenste effect hebben op systeemvariabelen.

In hoofdstuk 6 is WALRUS toegepast op twee contrasterende Nederlandse stroomgebieden: het stroomgebied van de Hupselse Beek en de polder Cabauw. In beide stroomgebieden presteert WALRUS goed: Nash-Sutcliffe-efficiënties verkregen na kalibratie op één jaar aan afvoermetingen zijn 0.87 voor het stroomgebied van de Hupselse Beek en 0.83 voor de polder Cabauw, met waarden van 0.74 en 0.76 voor de validatie. Het model simuleert overstromingen en droogtes ook goed en kan het effect van waterbeheer nabootsen. Door de dynamische verdeling tussen snelle en langzame stroomroutes die bepaald wordt door een natheidsin-

dex, kunnen temporele en ruimtelijke variatie in grondwaterdieptes worden meegenomen, wat resulteert in een adequate simulatie van zowel hoge als lage afvoeren. WALRUS is het meest gevoelig voor de parameter die de natheidsindex bepaalt en de grondwaterreservoirconstante, en in mindere mate voor de reservoirconstante van het reservoir voor snelle stroomroutes. De effecten van deze drie parameters kunnen worden onderscheiden in de afvoerreeks, wat aangeeft dat het model niet overgeparametriseerd is. Onzekerheid in de invoervariabelen heeft een groter effect op de gemodelleerde afvoer dan parameteronzekerheid en onzekerheid in de uitgangssituatie.

In hoofdstuk 7 worden de bevindingen gecombineerd om de onderzoeksvragen te beantwoorden. Hoewel afvoer niet direct gekoppeld is aan de totale stroomgebiedsberging, kunnen interne fluxen nog steeds begrepen en gemodelleerd worden met lokale berging-afvoerrelaties. Waarnemingen in het stroomgebied van de Hupselse Beek en de polder Cabauw laten zien dat ondiep grondwater zorgt voor een vochtige onverzadigde zone en beperkte verdampingsreductie, dat bepaalde typen stroming (bijv. buisdrainage of oppervlakteafvoer) alleen optreden als het stroomgebied nat genoeg is en dat hoge oppervlaktewaterpeilen grondwaterdrainage beperken. Deze bevindingen zijn meegenomen bij de ontwikkeling van de Wageningse Laagland Afvoersimulator (WALRUS), die gebruikt kan worden door waterbeheerders en onderzoekers in laaglandgebieden wereldwijd.

Acknowledgements

Dankwoord

Eigenlijk is het dankwoord het moeilijkste stuk van het proefschrift om te schrijven: veel mensen slaan de rest van het proefschrift over, maar lezen dit wel. Bovendien ben ik nooit zo goed in het bedenken wat ik op zo'n plek moet schrijven. Maar er moeten mensen genoemd worden die hebben bijgedragen aan de totstandkoming van dit proefschrift, dus hier gaan we. De opbouw van dit dankwoord is de klassieke dankwoordopbouw: in alinea 2 bespreek in de aanleiding van het onderzoek, in alinea's 3–5 bedank ik mijn (co)promotoren, daarna volgen andere collega's, vrienden en tot slot familie.

Het is alweer zeven jaar geleden dat ik bezig was met een afstudeeronderzoek bij Piet Warmerdam (over het simuleren van de Oude IJssel met het Wageningen Model, overigens na een afstudeeronderzoek bij Aart Overeem over extreme neerslag – de parallellen met verschillende hoofdstukken van dit proefschrift zijn opvallend gemakkelijk te trekken) en Remko aan mij vroeg of het mij niet wat leek om een promotieonderzoek te doen. Aanvankelijk hield ik de boot af; ik moest na de afstudeerscriptie nog een stage doen en het onderwerp sprak mij eigenlijk niet zo aan (dat neerslag-afvoermodelleren in laaglandgebieden had ik inmiddels wel gezien dacht ik). Bijna een jaar later was ik afgestudeerd en de positie nog niet gevuld en dacht ik "ach, laten wij het maar proberen". Daar heb ik zeker geen spijt van gehad, want ik heb het prima naar mijn zin gehad (en nu nog overigens).

In de eerste plaats is dat een verdienste van Remko Uijlenhoet, die mij als promotor en dagelijks begeleider gesteund en gestuurd heeft om mijn onderzoek in goede banen te leiden en tegelijkertijd de vrijheid gaf om soms keuzes te maken die uit het oogpunt van "een proefschrift schrijven binnen de tijd" onverstandig waren, maar die voor mijn werkplezier heel belangrijk zijn geweest (zoals bijvoorbeeld ongeveer 2700 uur aan onderwijs besteden). Dat het uiteindelijk toch gelukt is om het boekje af te krijgen, komt mede doordat Remko steeds tijd vrijmaakte om snel en gedetailleerd commentaar te leveren op stukken die ik veel te laat had opgestuurd.

Mijn begeleider Paul Torfs wil ik als tweede noemen. Ik vind het nog steeds erg jammer dat de regels het niet toelaten om hem te vermelden als co-promotor op de tweede bladzijde van dit proefschrift, want die plek heeft hij echt verdiend. Niet alleen als vraagbaak voor wiskundig/statistische problemen of doordat zijn enthousiasme voor R en LaTeX aanstekelijk heeft gewerkt (wat heeft geleid tot onze meest gelezen publicatie: "a (very) short introduction to R"), maar vooral omdat ik veel heb geleerd van zijn vermogen om ingewikkelde dingen goed uit te leggen.

Ryan Teuling, mijn co-promotor, heeft mij erg geholpen doordat hij vaak wél door de bomen het bos kon zien en heel goed is in het identificeren van de kern en toegevoegde waarde van een stuk onderzoek. Dat we met zijn allen op de overstroming in Hupsel zijn gedoken, bleek achteraf een goede boost voor mijn onderzoek. De inhoudelijke discussies met Remko, Paul en Ryan waren cruciaal voor de ontwikkeling van dit proefschrift.

Ook Han Stricker en Piet Warmerdam, die, vooral in het begin, nauw betrokken zijn geweest bij het onderzoek, moet ik expliciet bedanken. Han heeft mij geholpen bij het veldwerk in Cabauw en bij het uitpluizen en interpreteren van de oude Hupsel-data voor de recessieanalyse (hoofdstuk 4). Piets ervaring met het Wageningen Model was erg nuttig bij de ontwikkeling van WALRUS en zijn eindeloze verzameling anekdotes hielp om mijn onderzoek, de metingen in het stroomgebied van de Hupselse Beek, het Wageningen Model en de leerstoelgroep in een historisch perspectief te zetten.

Marjolein en Anne, mijn kamergenootjes en paranimfen, zorgden ervoor dat de werkdagen zowel gezellig als productief waren. Je kan heel lang naar je scherm gaan staren, maar het is toch vaak effectiever (en leuker) om de hoe-programmeer-ik-dat-nou-, hoe-vertaal-ik-dat-nou- en hoe-pak-ik-dat-nou-aan-vragen óver je scherm te roepen. Soms hadden ze meteen een antwoord klaar, maar de discussies als dat niet het geval was, waren vaak net zo nuttig.

En dan natuurlijk de rest van HWM – een prettige club mensen met wie het zeker geen straf is om samen te werken. Wat ook erg hielp is de hechte band tussen een vrij grote groep aio's van HWM en SEG (nu SLM) die min of meer tegelijkertijd zijn begonnen. Van deze "generatie" zijn de meesten inmiddels uitgevlogen, maar ik zal altijd goede herinneringen hebben aan de congressen, koffiepauzes en schrijfweken waar wij bij elkaar te rade konden gaan over onderzoek, hydrologie en andere zaken.

Verder wil ik alle studenten bedanken waar ik ooit mee heb samengewerkt – vooral degenen die ik begeleid heb bij hun BSc- en MSc-scripties, maar ook degenen die ik tijdens vakken ben tegengekomen. Het is echt waar dat je het meest leert door dingen aan anderen uit te leggen. Een student die doorvraagt zorgt vaak voor meer inzicht dan de gemiddelde onderzoekspresentatie op een internationaal congres.

Ik heb het promotieonderzoek als heel leuk ervaren, maar er zijn altijd dingen die niet meezitten (planningen die te strak bleken, tegenvallende reviews, geen inspiratie voor stellingen). Ik moet daarom ook Dieuwke en Miranda, en Christel en Julitta bedanken voor de luisterende oren en het

meedenken over oplossingen. Waar moeten we het nu nog over hebben tijdens onze wandelingen nu al onze proefschriften af zijn?

Tot slot bedank ik mijn familie. Met name mijn mamma, my pappa en mijn grote broer, die mij altijd een veilig nest hebben geboden, mij hebben gestimuleerd om door te leren en hun best hebben gedaan om mij goed uit te rusten met kennis en vaardigheden. Alle andere familie, zowel van mijzelf als van Tim, wil ik bedanken voor hun interesse voor mijn onderzoek, waardoor ik kon oefenen met het uitleggen van mijn werk aan niet-hydrologen. En natuurlijk Tim (volgens de dankwoord-opbouw-regels komen vriendjes altijd aan het einde), die een grote bijdrage heeft geleverd door het aanvoeren van thee en chocola. Want zonder die twee "principal components" was dit proefschrift natuurlijk nooit af gekomen.

List of publications

Peer-reviewed publications

- Brauer, C. C., Teuling, A. J., Torfs, P. J. J. F. and Uijlenhoet, R., 2013. Investigating storage-discharge relations in a lowland catchment using hydrograph fitting, recession analysis, and soil moisture data. Water Resources Research 49, 4257–4264, DOI: 10.1002/wrcr.20320.

- Brauer, C. C., Teuling, A. J., Overeem, A., van der Velde, Y., Hazenberg, P., Warmerdam, P. M. M. and Uijlenhoet, R., 2011. Anatomy of extraordinary rainfall and flash flood in a Dutch lowland catchment. Hydrology and Earth System Sciences 15, 1991–2005, 2011, DOI: 10.5194/hess-15-1991-2011.

Pubications under review

- Brauer, C. C., Teuling, A. J., Torfs, P. J. J. F. and Uijlenhoet, R. (2014a): The Wageningen Lowland Runoff Simulator (WALRUS): a lumped rainfall-runoff model for catchments with shallow groundwater. Geoscientific Model Development Discussions 7, 1357–1411, http://www.geosci-model-dev-discuss.net/7/1357/2014/gmdd-7-1357-2014.html

- Brauer, C. C., Torfs, P. J. J. F., Teuling, A. J. and Uijlenhoet, R. (2014b): The Wageningen Lowland Runoff Simulator (WALRUS): application to the Hupsel Brook catchment and Cabauw polder. Hydrology and Earth System Sciences Discussions 11, 2091–2148, http://www.hydrol-earth-syst-sci-discuss.net/11/2091/2014/hessd-11-2091-2014.html

Other publications

- Torfs, P. J. J. F. and Brauer, C. C., 2014. A (very) short introduction to R. http://cran.r-project.org/doc/contrib/Torfs+Brauer-Short-R-Intro.pdf.

- Brauer, C. C., Teuling, A. J., Overeem, A. and Uijlenhoet, R., 2011. Extreme regenval en overstromingen in het stroomgebied van de Hupselse Beek. H2O 18, 23–26 (in Dutch).

Conference abstracts

- Brauer, C. C., Torfs, P. J. J. F., Teuling, A. J. and Uijlenhoet, R., 2014. The Wageningen Lowland Runoff Simulator (WALRUS): implementation and application to the freely draining Hupsel Brook catchment and controlled Cabauw polder. EGU General Assembly, 27 Apr.–2 May, Vienna, Austria.

- Brauer, C. C., Torfs, P. J. J. F., Teuling, A. J. and Uijlenhoet, R., 2014. The Wageningen Lowland Runoff Simulator (WALRUS): development of a novel parametric rainfall-runoff model using field experience. EGU General Assembly, 27 Apr.–2 May, Vienna, Austria.

- Brauer, C. C., Teuling, A. J., Torfs, P. J. J. F., Hobbelt, L. G., Jansen, F. A., Melsen, L. A. and Uijlenhoet, R., 2013. Understanding lowland (flash) floods: analysis of the 2010 flash flood in the Hupsel Brook catchment and comparison with other recent lowland floods. 11th International Precipitation Conference, 30 June–3 July, Ede, The Netherlands.

- Brauer, C. C., Teuling, A. J., Torfs, P. J. J. F., Hobbelt, L. G., Jansen, F. A., Melsen, L. A. and Uijlenhoet, R., 2012. Looking for similarities between lowland (flash) floods. AGU Fall Meeting, 3–7 Dec., San Francisco, USA.

- Uijlenhoet, R., Brauer, C. C., Stricker, J. N. M., 2012. Water budget of the Cabauw Experimental Site for Atmospheric Research (CESAR), The Netherlands. AGU Fall Meeting, 3–7 Dec., San Francisco, USA.

- Teuling, A. J., Brauer, C. C., Stricker, J. N. M. and Uijlenhoet, R., 2012. Storage-discharge relationships in a lowland catchment in The Netherlands. AGU Fall Meeting, 3–7 Dec., San Francisco, USA.

- Torfs, P. J. J. F., Brauer, C. C., Teuling, A. J., Kloosterman, P., Willems, G. J., Verkooijen, B. L. M. T. and Uijlenhoet, R. (2012), Simulating a lowland flash flood in a long-term experimental watershed with 7 standard hydrological models. AGU Fall Meeting, 3–7 Dec., San Francisco, USA.

- Brauer, C. C., Teuling, A. J., Overeem, A., van der Velde, Y., Hazenberg, P., Warmerdam, P. M. M., Kloosterman, P. and Uijlenhoet, R., 2012. Analyzing and modelling a lowland flash flood. IMPRINTS Final Workshop, 27 Sep., Brussels, Belgium.

- Brauer, C. C., Kloosterman, P., Teuling, A. J., Overeem, A., van der Velde, Y., Hazenberg, P., Warmerdam, P. M. M. and Uijlenhoet, R., 2012. Analysis and modelling of the 2010 flood in the Hupsel Brook catchment, The Netherlands.

14th Biennial Conference ERB — Studies of Hydrological Processes in Research Basins: Current Challenges and Prospects, 17–20 Sept., St Petersburg (extended abstract).

- Brauer, C. C., Teuling, A. J., Overeem, A., van der Velde, Y., Hazenberg, P., Warmerdam, P. M. M., Kloosterman, P. and Uijlenhoet, R., 2012. Modelling (flash) floods in a Dutch lowland catchment. Hydrologic Discovery Through Physical Analysis — Honoring the Scientific Legacies of Wilfried H. Brutsaert and Jean-Yves Parlange, 14–15 Apr., Ithaca, USA.

- Brauer, C. C., Stricker, J. N. M. and Uijlenhoet, R., 2012. Hydrology in a Dutch polder catchment: natural processes in a man-made landscape. Hydrologic Discovery Through Physical Analysis — Honoring the Scientific Legacies of Wilfried H. Brutsaert and Jean-Yves Parlange, 14–15 Apr., Ithaca, USA.

- Brauer, C. C., Teuling, A. J., Overeem, A., van der Velde, Y., Hazenberg. P., Warmerdam, P. M. M., Kloosterman, P. and Uijlenhoet, R., 2012. Modelling (flash) floods in a Dutch lowland catchment. EGU General Assembly, 22–27 Apr., Vienna, Austria.

- Brauer, C. C., Stricker, J. N. M. and Uijlenhoet, R., 2012. Hydrology in a Dutch polder catchment: natural processes in a man-made landscape. EGU General Assembly, 22–27 Apr., Vienna, Austria.

- Brauer, C. C., Teuling, A. J., Overeem, A., van der Velde, Y., Hazenberg. P., Warmerdam, P. M. M. and Uijlenhoet, R., 2011. Soil buffer limits flash flood response to extraordinary rainfall in a Dutch lowland catchment. EGU General Assembly, 3–8 Apr., Vienna, Austria.

- Brauer, C. C., Teuling, A. J., Overeem, A. van der Velde, Y., Hazenberg. P., Warmerdam, P. M. M., Hobbelt, L. G. and Uijlenhoet, R., 2010. (Flash) Floods on 27 Augustus 2010 in lowland catchments in The Netherlands and Germany. EGU Leonardo Conference Series on the Hydrological Cycle, 23–25 Nov., Bratislava, Slovakia.

- Brauer, C. C., Stricker, J. N. M. and Uijlenhoet, R., 2011. Water balance and dynamics of a Dutch polder catchment. EGU Leonardo Conference Series on the Hydrological Cycle — Looking at catchment in colors, 10–12 Nov., Luxembourg City, Luxembourg.

- Brauer, C. C., Stricker, J. N. M. and Uijlenhoet, R., 2010. Does the Hupselse Beek catchment (Netherlands) behave like a simple dynamical system? EGU Leonardo Conference Series on the Hydrological Cycle — Looking at catchment in colors, 10–12 Nov., Luxembourg City, Luxembourg.

- Brauer, C. C., Stricker, J. N. M. and Uijlenhoet, R., 2010. Linking hydrology and meteorology: measuring water balance terms in Cabauw, the Netherlands. 13th Biennial Conference ERB 2010 — Hydrological Responses of Small Basins to a Changing Environment, 5–8 Sep., Seggau Castle, Austria (extended abstract).

- Brauer, C. C., Stricker, J. N. M., Warmerdam, P. M. M. and Uijlenhoet, R., 2010. Recession analysis and hydrograph simulation of the Hupselse Beek catchment, the Netherlands. 13th Biennial Conference ERB 2010 on Hydrological Responses of Small Basins to a Changing Environment, 5–8 Sep., Seggau Castle, Austria (extended abstract)

- Brauer, C. C., Stricker, J. N. M. and Uijlenhoet, R., 2009. Linking meteorology and hydrology: measuring water balance terms in Cabauw, the Netherlands. 8th International Symposium on Tropospheric Profiling 19–23 Oct., Delft, The Netherlands (extended abstract).

- Brauer, C. C., Stricker, J. N. M., Warmerdam, P. M. M. and Uijlenhoet, R., 2009. Recession analysis of the Hupselse Beek catchment, The Netherlands. EGU General Assembly, 19–24 Apr., Vienna, Austria.

SENSE

Netherlands Research School for the
Socio-Economic and Natural Sciences of the Environment

C E R T I F I C A T E

The Netherlands Research School for the
Socio-Economic and Natural Sciences of the Environment
(SENSE), declares that

Claudia Catharina Brauer

born on 23 September 1984 in Rotterdam, The Netherlands

has successfully fulfilled all requirements of the
Educational Programme of SENSE.

Wageningen, 11 April 2014

the Chairman of the SENSE board

Prof.dr.ir. Huub Rijnaarts

the SENSE Director of Education

Dr. Ad van Dommelen

The SENSE Research School has been accredited by the Royal Netherlands Academy of Arts and Sciences (KNAW)

K O N I N K L I J K E   N E D E R L A N D S E
A K A D E M I E   V A N   W E T E N S C H A P P E N

The SENSE Research School declares that **Ms. Brauer** has successfully fulfilled all requirements of the Educational PhD Programme of SENSE with a work load of 60.4 EC, including the following activities:

SENSE PhD Courses
- o Environmental research in context
- o Research context activity: 'Co-organising WIMEK Water Cycle Symposium, 29 January 2009, Wageningen'

Other PhD and Advanced MSc Courses
- o Techniques for writing and presenting a scientific paper, 2009
- o Uncertainty analysis, 2010
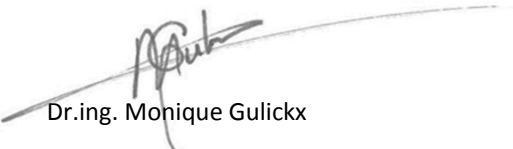- o Catchment science summer school, University of Aberdeen, 2011

Management and Didactic Skills Training
- o Project and time management, 2009
- o Teaching methodology and skills for PhD students, 2011
- o Supervising and organising MSc theses, 2011
- o Brain based teaching, 2012
- o Teaching in five BSc and MSc courses (e.g. designing and supervising computer and field practicals), 2009-2013
- o Supervising six MSc theses and four BSc Theses, 2009-2013

Oral Presentations
- o *Linking hydrology and meteorology: measuring water balance terms in Cabauw, the Netherlands*. 13th Biennial Conference ERB, 5-8 September 2010, Leibnitz, Austria
- o *Does the Hupsel Brook catchment (Netherlands) behave like a simple dynamical system?* EGU Leonardo Conference Series on the Hydrological Cycle, 10-12 November 2011, Luxembourg City, Luxembourg
- o *(Flash) Floods on 27 Augustus 2010 in lowland catchments in The Netherlands and Germany*. EGU Leonardo Conference Series on the Hydrological Cycle, 23-25 November 2011, Bratislava, Slovakia
- o *Understanding lowland (flash) floods: analysis of the 2010 flash flood in the Hupsel Brook catchment and comparison with other recent lowland floods*. 11th International Precipitation, 30 June–3 July 2013, Ede, The Netherlands

SENSE Coordinator PhD Education

Dr.ing. Monique Gulickx